Monitoring of the fixation of orthopaedic implants by vibration analysis

Leonard Cezar PASTRAV

Promoters:
Prof. Georges Van der Perre
Prof. Remy Van Audekercke

Members of the Examination Committee:
Prof. Guy Fabry
Prof. Jos Vander Sloten
Prof. Ward Heylen
Prof. Johan Bellemans
Prof. Michiel Mulier
Prof. James L. Cunningham

Chair
Prof. Ann Haegemans

Dissertation presented in partial fulfillment of the requirements for the degree of Doctor in Engineering

October 2010

ISBN 978-94-6018-267-9
D/2010/7515/106

Acknowledgements

The path towards this thesis spans several years of work at the Division of Biomechanics and Engineering Design, K.U.Leuven, Belgium. During this time I have met many people that, in different ways, have helped me in getting to this point. I am very grateful to all of them.

In particular, I wish to express my gratitude to my promoters, Professor Georges Van der Perre and Professor Remy Van Audekercke for their scientific advice and for continuous encouragement and support.

I would especially like to thank all the members of the Examination Committee, Professor Guy Fabry, Professor Jos Vander Sloten, Professor Ward Heylen, Professor Johan Bellemans, Professor Michiel Mulier, Professor James L. Cunningham, and Professor Ann Haegemans, for analysing so carefully my work and for their useful comments.

I am deeply indebted to my colleagues at the Division of Biomechanics and Engineering Design and to all the collaborators that I have met during my work at K.U.Leuven and Group T.

I would also like to thank all the friends that I found in Belgium for adding so much joy to my life.

And at last, but not least, I would like to thank my family for all their support and love.

The studies included in this paper were partially funded by the K.U.Leuven research council (project OT/03/31 “Hip Hub”), Biomet Orthopedics, and Group T.

Custom made prostheses provided by courtesy of Advanced Custom Made Implants S.A./N.V.

Hip resurfacing femoral and acetabular implants provided by courtesy of Biomet Orthopedics.

Reverse shoulder glenoidal implants provided by courtesy of DePuy International Ltd.

Thank you all !!!

Abstract

(Dutch language)

Jaarlijks wordt een groot aantal gewrichtsprothesen geplaatst, meer dan één miljoen heupprothesen alleen al. Het succes van deze implantaten hangt in belangrijke mate af van hun initiële bevestiging. Het is niet eenvoudig om de primaire stabiliteit van niet-gecementeerde implantaten objectief te beoordelen, chirurgen kunnen hiervoor slechts steunen op hun klinische ervaring. Bovendien is het zo dat wanneer het femorale implantaat te diep in het bot wordt gedreven, dit aanleiding kan geven tot intra-operatieve breuk van het femur.

Trillingsanalyse kent reeds succesvolle biomechanische toepassingen: bij het bepalen van mechanische eigenschappen van bot, om het herstel van breuken na te gaan, en om de stabiliteit te beoordelen van dentale implantaten, en van femurimplantaten in vitro en in vivo.

Het hoofddoel van het hier gepresenteerde onderzoek was de ontwikkeling van een methode, gebaseerd op trillingsanalyse, voor het intra-operatief beoordelen van de stabiliteit van op maat gemaakte femorale prothesecomponenten, alsook het bijhorende meettoestel.

In een reeks in vitro experimenten werd de verandering in de transferfunctie (FRF, frequency response function) van de implantaat/femur structuur tijdens de verschillende stappen van het inbrengen van het implantaat onderzocht. Om het verschil tussen de FRF-spectra horende bij opeenvolgende insertiestappen te kwantificeren, werden de Pearson correlatiecoëfficiënt en de kruiscorrelatiefunctie gebruikt. De stijfheid van het implantaat-botsysteem verandert tijdens de insertie. Dit resulteert in een verandering in FRF, vooral bij de hogere frequenties. Als het FRF-spectrum naar rechts verschuift, neemt de stijfheid van het implantaat-botsysteem toe, en bijgevolg verbetert de bevestiging van het implantaat. Als de FRF niet meer verandert tussen twee opeenvolgende insertiestappen, dan is de implantaat-botverbinding stabiel en zou de insertie beëindigd moeten worden om intra-operatieve breuken te vermijden.

Om de invloed van de veranderende contactomstandigheden op de resonantiefrequenties na te gaan, werden eindige elementen analyses uitgevoerd. Modale analyses werden uitgevoerd op het implantaat-botsysteem onder verschillende omstandigheden. De resultaten komen overeen met de voorgaande vaststellingen: een toename in contactoppervlak leidt tot een positieve verschuiving van de resonantiefrequenties en in het algemeen zijn de hogere modes gevoeliger voor deze toename. Deze vaststelling kan als volgt uitgelegd worden: bij de lagere modes gedraagt de prothese zich als een

onvervormbaar voorwerp en voegt dus enkel extra massa toe, terwijl bij de hogere modes de interactie tussen de prothese en het bot ingewikkelder wordt en de interfacetoestand ook de resonantiefrequenties zal beïnvloeden.

Vervolgens werd een per-operatief protocol opgesteld, gebaseerd op FRF-analyse, en werd dit getest bij 83 patiënten die een op maat gemaakte, intra-operatief vervaardigde femorale prothese kregen. Twee groepen werden onderzocht: een groep met niet-gecementeerde femorale componenten (n = 30) en een groep met hybride steelfixatie (n = 53). FRF's van het implantaat-botsysteem overeenkomend met opeenvolgende insertiestappen werden vergeleken. De correlatiecoëfficiënt tussen de laatste twee FRF's was hoger dan 0,99 bij 86,7% van de niet-gecementeerde implantaten. Lagere waarden van de finale correlatiecoëfficiënt en afwijkingen in het patroon van de transferfunctie kwamen overeen met instabiliteit of dreigende breuk. Bij de hybride gecementeerde implantaten werd in 84,9% van de gevallen een aanzienlijk verschil gevonden tussen de FRF horende bij de laatste stap van niet-gecementeerde proefinsertie en de FRF van de uiteindelijke gecementeerde prothese. Bovendien varieerde de FRF naargelang de uitharding van de cement.

Omdat de resultaten van de studies op steelachtige implantaten veelbelovend waren, werd deze methode aangepast en uitgebreid tot bolvormige implantaten in een eerste reeks van in-vitro onderzoeken. Een onderzoek op omgekeerde schouderprothesen focust op metaal-metaal fixatie terwijl onderzoeken op heup resurfacing implantaten focussen op metaal-bot fixatie. FRF's werden gemeten met de implantaten onder verschillende gecontroleerde omstandigheden. Gewoonlijk duidt een verhoging van de resonatiefrequenties op een verhoging in stijfheid, en dus op een betere fixatie, terwijl een verlaging van de resonantiefrequenties geïnterpreteerd wordt als een verlies aan stabiliteit. Er werd een reeks destructieve testen uitgevoerd om de kracht te meten die nodig is om een implantaat te verwijderen, en de resultaten werden vergeleken met de resultaten verkregen bij trillingsanalyse onder vergelijkbare omstandigheden.

Tot besluit, de resultaten bewijzen duidelijk de gevoeligheid van trillingsanalyse voor het beoordelen van implantaatfixatie. De verandering in FRF verschaft betrouwbare informatie over de evolutie van de stabiliteit van het implantaat-botsysteem tijdens het inbrengen. Het protocol beschreven in dit werk kan gebruikt worden om op nauwkeurige wijze de laatste stap in de insertieprocedure te bepalen en om het risico op intra-operatieve breuk te verminderen bij totale heuparthroplastie. De trillingsmethode gebaseerd op FRF analyse kan aangepast en uitgebreid worden naar andere orthopedische implantaten.

Een mogelijke toekomstige ontwikkeling is het aanwenden van trillingsanalyse om de stabiliteit van een orthopedisch implantaat te beoordelen en om vroegtijdig loskomen te detecteren tijdens de postoperatieve follow-up.

(Translated from English by dr.ir. Kathleen Denis)

Abstract

A large number of orthopaedic joint replacements are performed every year in the world (i.e. more than one million hip replacements) and the rate of success is strongly dependent on the initial fixation of the implants. Objective intra-operative assessment of primary stability of cementless implants is a challenge, since surgeons have to rely mainly on their clinical experience. Moreover, excessive press-fitting of an implant into the bone can cause intraoperative fractures.

Vibration analysis has been successfully applied in biomechanics to determine bone mechanical properties, to monitor fracture healing, and to assess the stability of dental implants and femoral stems in vitro and in vivo as well.

The main objective of the research work presented in this paper was the developing of a vibrational method and the corresponding measuring device for the intra-operatively assessment of the stability of custom made femoral stems.

In a series of in vitro experiments the change in the frequency response function (FRF) of the hip stem/femur structure during implant insertion was studied. To quantify the difference between the FRF spectra corresponding to successive insertion stages, the Pearson's correlation coefficient and the cross correlation function were used. The stiffness of the implant - bone system varies during insertion, which results in a change in FRF, especially in the range of higher frequencies. If the FRF spectrum shifts to the right, then the stiffness of the implant/bone connection increases and, consequently, the fixation of the implant increases as well. If the FRF does not change between two successive insertion stages, then the stem-bone connection is stable and the insertion should stop to avoid intra-operative fractures.

To better understand the influence of changing contact conditions on the resonance frequencies a finite element analysis (FEA) was set up. Modal analyses on the hip stem–femur system were performed in various contact situations. The results are in agreement with previous observations: contact increase causes positive resonance frequency shifts and, in general, the higher modes are more sensitive to the contact change. This phenomenon can be understood from the fact that in the lower modes the prosthesis moves as a rigid body and only exerts an added mass effect whereas in the higher modes the interaction between the stem and the femur becomes more complicated and the interface conditions also affect the resonance frequencies.

In the next research stage, a per-operative protocol based on FRF analysis was designed and tested in 83 patients receiving a custom-made, intra-operatively manufactured

femoral stem. Two groups were studied: one (n = 30) with non cemented and one (n = 53) with hybrid stem fixation. FRFs of the stem-femur system corresponding to successive insertion stages were compared.

The correlation coefficient between the last two FRF curves was above 0.99 in 86.7% of the non cemented cases. Lower values of the final correlation coefficient and deviations in the frequency response pattern were associated with instability or impending bone fracture. In the cases with a hybrid cemented stem an important difference in FRF between the final stage of non cemented trial insertion and the final cemented stage was found in 84.9% of the cases. Furthermore, the frequency response function varied with the degree of cement curing.

Since the results obtained during the studies on stem-like implants were very promising, the vibrational method was adapted and extended to spherical implants in a series of preliminary in vitro studies. A study on reverse shoulder prosthesis focuses on metal-on-metal fixation whereas the studies on hip resurfacing implants focus on metal-on-bone fixation.

FRFs were obtained for the implants in different controlled conditions. Usually, an increase of resonance frequencies indicates an increasing stiffness, thus a better fixation, while a decrease of resonance frequencies is interpreted as a stability loss. A series of destructive tests to measure the force needed to extract the implant were performed and the results were correlated with the results obtained by vibration analysis in similar conditions.

In conclusion, the results clearly prove the sensitivity of vibration analysis in assessing the implant fixation. The FRF change provides reliable information regarding the stability evolution of the implant-bone system during the insertion. The protocol described in this paper can be used to accurately detect the insertion end point and to reduce the risk for intraoperative fracture in total hip arthroplasty. The vibrational method based on FRF analysis can be adapted and extended to other kind of orthopaedic implants.

A future possible development is a vibrational method to assess the stability and to detect the early loosening of an orthopaedic implant during the post-operative follow-up.

Abbreviations

ABG	Anatomical Benoist-Girard
BMD	Bone Mineral Density
CMP	Custom Made Prosthesis
CT	Computer Tomograph
DFT	Discrete Fourier Transform
DIRSA	Digital Interactive RSA
DXA	Dual X-ray Absorptiometry
FEA	Finite Element Analysis
FEM	Finite Element Model
FFT	Fast Fourier Transform
FRF	Frequency Response Function
HA	Hydroxyapatite
HRA	Hip Resurfacing Arthroplasty
IMP	Intra-operatively Manufactured Prosthesis
NCCF	Normalised Cross Correlation Function
PMMA	Polymethylmethacrylate
RSA	Roentgen Stereophotogrammetric Analysis
THR	Total Hip Replacement

Symbols

E	Young's modulus
GPa	gigapascal (pressure unit 1 GPa = 10^6 Pa)
Hz	hertz (frequency unit)
kHz	kilohertz (frequency unit 1 kHz = 10^3 Hz)
I	Second moment of inertia
m	meter (length unit)
mm	milimeter (length unit 1mm = 10^{-3} m)
μm	micrometer (length unit 1 μm = 10^{-6} m)
m^3	cubic meter (volume unit)
N	newton (force unit)
R	Pearson's correlation coefficient
W	watt (power unit)
Ø	diameter
ν	Poisson's ratio
ρ	mass density

The symbols used in appendices are defined in their corresponding sections.

Contents

1. Introduction

Section 1.1 of the introductory chapter presents a short overview on the orthopaedic implants and their specific problems: fixation methods, osseointegration, failure causes, importance of primary fixation.

Different methods used to assess the stability of orthopaedic implants are described in section 1.2, while section 1.3 focuses on vibrational techniques applied on bone implants.

The research hypotheses and objectives are formulated in section 1.4.

1.1. Orthopaedic implants

An implant is a medical device manufactured to replace a missing biological structure, support a damaged biological structure, or enhance an existing biological structure (Williams 1999). Medical implants are man-made devices, in contrast to a transplant, which is a transplanted biological tissue. Implants can be made of soft tissues, synthetics, ceramics, or metals that are relatively inert and compatible with body tissues.

In orthopaedic surgery, implants may refer to devices that are placed over or within bones to hold a fracture reduction or to replace a part or whole of an irreversible damaged joint (figure 1.1).

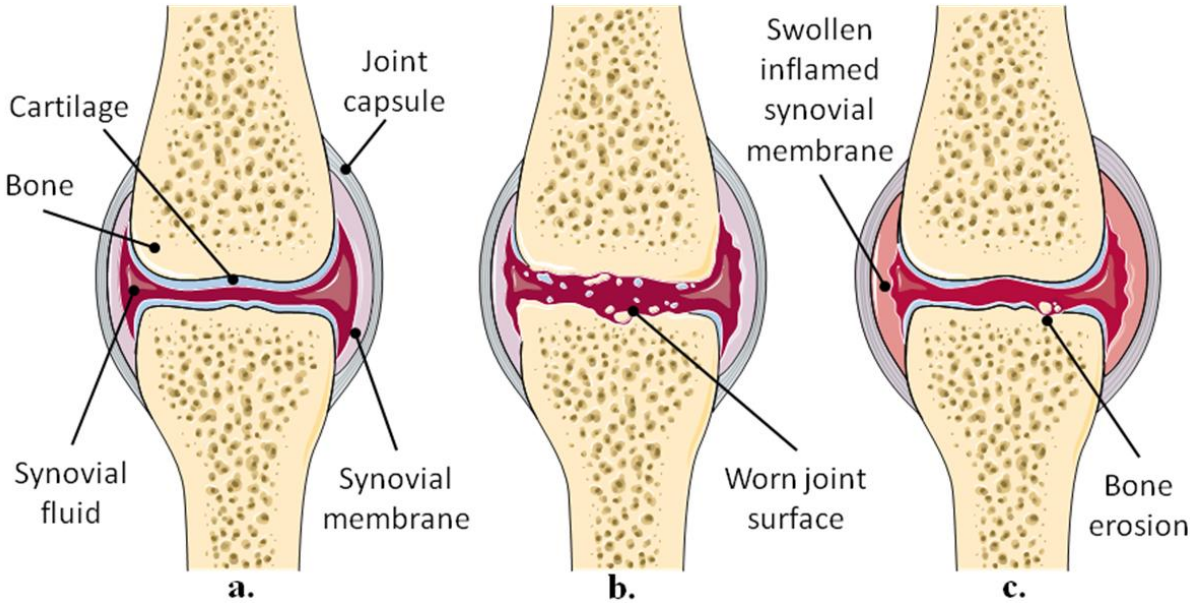

Figure 1.1. Damaged joints

a. Normal joint, b. Osteoarthritis, c. Rheumatoid arthritis

(Figures were produced using Servier Medical Art)

There are many types of orthopaedic implants and each of them is designed to correct the affected joint so that it supports the movement and stress associated and to enhance mobility and decrease pain. Used on a larger scale, orthopaedic implants are available for the hip (figure 1.2.a), knee (figure 1.2.b), shoulder (figure 1.2.c), elbow, and ankle. They are also known as prosthetic implants.

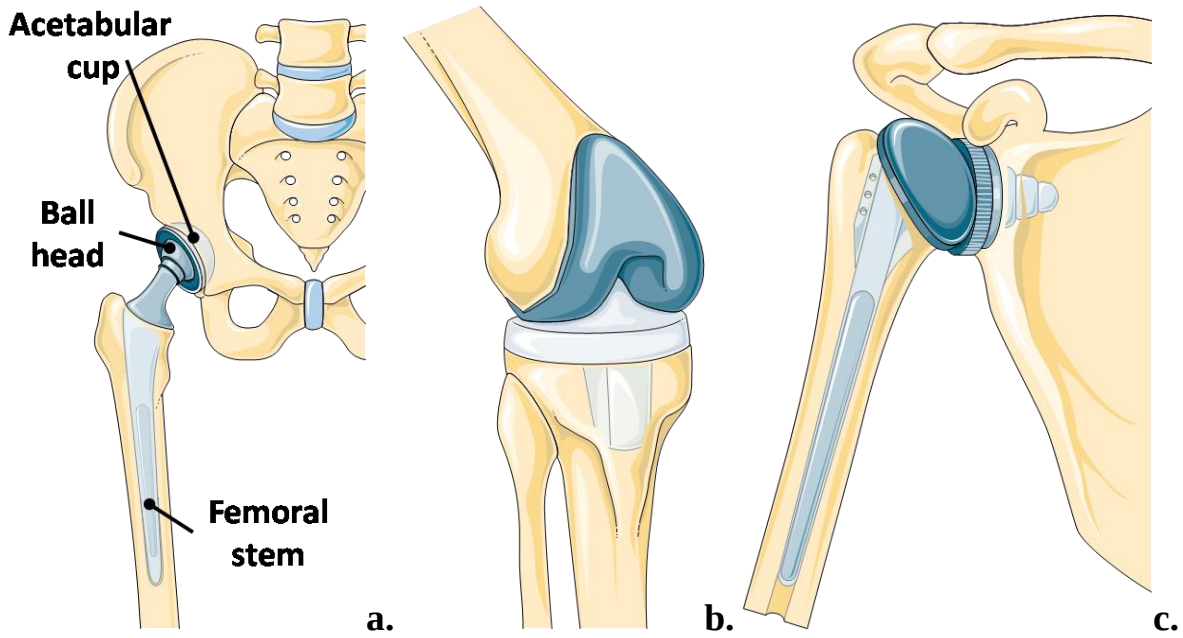

Figure 1.2. Joint replacement surgery

a. Total hip replacement, b. Total knee replacement, c. Shoulder replacement

(Figures were produced using Servier Medical Art)

For long-term performance orthopaedic implants must be stable to physiological loads.

The stability of an implant may be accomplished by using cemented or cementless techniques. The fixation of a cemented implant within bone is obtained by using an intermediary filling material such as polymethylmethacrylate (PMMA) bone cement that has no adhesive properties and functions as a grout. The cementless fixation is achieved by preparing a slightly undersized bone bed so that the implant is forcefully inserted into the bone with a press fit. Hybrid fixation is possible as well. In this case a part of the joint prosthesis is directly supported by the surrounding bone while another part is supported by an intermediary layer of PMMA cement.

If a stable long-term fixation is not achieved early in the lifetime of an implant, the migration phenomenon occurs. Migration, the progressive displacement of an implant within the surrounding bone, generates pain and compromises the normal biomechanics of the prosthetic joint, predicting probable future failure. (Goodman et al. 2008, Mulier et al. 2010).

Another phenomenon that may adversely affect the stability of the implant is micromotion i.e. implant–bone relative micro-movements of the order of 100 or 200 μm induced by physiological loads (Viceconti et al. 2000).

The lifetime of a cementless implant and, as a consequence, the success rate of an implantation surgical procedure depend to a large extent upon the osseointegration process. Brånemark (1977) defined osseointegration as a direct structural and functional connection between ordered living bone and the surface of a load-carrying implant. An implant is also regarded as osseointegrated when there is no progressive relative movement between the implant and the bone with which it has direct contact (Albrektsson et al. 1981, Brånemark 1983). In practice, this means that in osseointegration there is a fixation mechanism whereby implants can be reliably and predictably incorporated into living bone and that this fixation can persist under all normal conditions of loading (Worthington 1997).

The most important cause of late fixation failure is aseptic loosening (Harris 1991, Kobayashi et al. 1997, Lombardi 1989). The causes of this severe complication are not very well understood, but the experience of the past decades has suggested a number of possible scenarios (Huiskes, 1993):

1) The accumulated damage scenario: gradual accumulation of damage from repetitive dynamic loading leads to failure of interfaces and loosening.
2) The failed bonding scenario: failure of bone ingrowth due to gaps or excessive micromotion.
3) The particulate reaction scenario: bone resorption caused by the presence of wear particles.
4) The destructive wear scenario: mechanical failure of prosthesis components due to excessive wear.
5) The stress shielding scenario.
6) The stress bypass scenario: bone resorption around prosthesis components due to subnormal stresses in bone.

From this list can be derived that induced displacements might trigger the loosening process (as in scenarios 1 and 2) or at least contribute to it (as in scenarios 3 and 4). Similar conclusions were obtained by Bauer and Schils (1999).

A more recent study suggests that high-velocity (20 mm/s) fluid flow caused by implant instability (micromotions) induces an osteolytic process in the surrounding bone that may contribute to prosthetic loosening (Fahlgren et al. 2010).

Experiments on animals have shown that excessive micromotion can prevent or even reverse bone ingrowth (Søballe 1992, Goodman 1994). Prendergast used a bi-phasic finite element model to explain this biological behaviour of connective tissues and, in a simulation of this implant-bone system, found results that corresponded reasonably well with the experimental results (Prendergast 1997). It is generally argued that, to obtain bone ingrowth, the induced displacements should not exceed 150 μm (Pilliar et al. 1986).

The design of a cementless prosthesis and the corresponding surgical procedure should respect this upper limit of 150μm for induced displacements and, during the rehabilitation after joint arthroplasty, an adequate loading of the implant-bone interface should be respected whilst restoring the weightbearing capacity of the limb.

The amount of induced displacement (also referred to as relative motion) can be accurately predicted by means of finite element models that make use of contact elements (Viceconti et al. 2000, 2001).

Therefore, the fixation of orthopaedic implants in bone relies strongly upon the initial stability of the implant. When the initial stability is not achieved, micromotions occur at the bone implant interface (Mandell et al. 2004, Ramaniraka et al. 2000). The micromotions then activate an osteoclastic response (Stadelmann et al. 2008), which results in periprosthetic osteolysis and later implant migration and wear (Karrholm et al. 1994). Both debris formation from implant wear and implant migration have been shown to be associated with increased implant failure rate (Clarke et al. 1992, Horikoshi et al. 1994).

With an estimated number of more than one million operations each year worldwide the total hip replacement (THR) is considered the operation of the century (Learmonth et al. 2007). This implies that, despite survival rates of 97% at 3 years (Lucht 2000) and 92% to 97% at 10 years follow-up (Britton et al. 1996) for some prosthesis types, a large number of revision operations are needed every year, most of them because of aseptic loosening. Revision operations are more difficult to perform, carry more risk for complications and have a poorer prognosis than primary THR (Kavanagh et al. 1985).

As for the other bone implants, the survival rate is directly related to the long term fixation stability of the prosthesis stem (Mjöberg 1997). Beside the design, material composition and surface characteristics of the implant, the initial per-operative fixation of the stem in the femoral bone has a critical influence on its long term fixation stability. This is

especially the case for non cemented, press-fit fixated stems. The insertion procedure results in well-defined contact areas and interface pre-stresses between the stem and the femoral bone. Femoral stress distribution has a crucial influence on bone remodelling and therefore on the final strength of the bone-implant structure.

Under actual loading, the hip stem displacement and the femoral stress distribution will strongly depend upon these initial contact conditions. Primary hip stem fixation is not only important regarding prosthesis migration, but also regarding micro movements that must be limited in order to allow interfacial bone formation and in-growth (Ramamurti et al. 1997, Søballe et al. 1992).

1.2. Stability measurements on orthopaedic implants

For clinicians, implant designers, and implant manufacturers the measurement of the stability of orthopaedic implants in vitro and in vivo is a research topic for many years.

Both the migration of the implant in time and the implant relative movements (micromotion) induced by load are important for the stability assessment and for loosening detection and prediction.

A complete evaluation of implant micromotion is by no means trivial and many published studies suffer from shortcomings. For example, in a number of studies muscle loads are limited or even absent (Maloney et al. 1989, Schneider et al. 1989). Although more recent studies include active simulation of muscle forces (Kassi et al. 2005) and despite considerable research efforts, the matter of implant micromotion has not yet been settled and there remains a great deal of work to be done in this field.

Up till now the diagnosis of loosening of orthopaedic implants is mainly based on parameters that are all either qualitative, subjective or non-standardised. Usually, orthopaedic surgeons combine qualitative information from X-rays (Gruen 1987, Zhang et al. 2002), patient complaints about pain, and functionality assessments to decide about a revision.

The magnitude of the migration of the implant is a more direct measure of the quality of the interface between implant and bone. Kärrholm (1994) has shown that early migration (after one year) has predictive value for the long-term success of an implant. Therefore, quantifying the migration of implants in vivo can be considered as a diagnostic technique to objectively assess the condition of the implant-bone system (Freeman, Plante-Bordeneuve 1994, Kärrholm 1994, Malchau 1995, Walker 1995). If such a diagnostic tool were available

and sufficiently accurate and precise, the clinician could decide to revise the prosthesis, before the loosening process affected the implant bed too severely, or take other measures.

Roentgen stereophotogrammetric analysis (RSA) is an imaging technique that enables precise measurements of implant migration in the order of a few tenths of a millimetre or even better (Kärrholm 1989). New techniques are currently developed to omit the use of tantalum markers on the implant, but use contour detection techniques instead (Valstar et al. 2001).

Measurements of induced displacements require a precision that is an order of magnitude better than the measurement of migration. This is not too difficult to obtain in vitro, but it is almost impossible in vivo. Most studies of implant relative movement are therefore performed in vitro, using linear variable differential transformers (LVDT) or extensometers (Monti et al. 1999). Further improvements of the RSA technique could make possible to measure induced displacements in vivo in a clinical setting.

At K.U.Leuven an RSA set-up and data processing software were developed to use the technique in an animal model (Bellemans 1999). Later on, a clinical study was done in which digital X-rays were used with the DIRSA-software developed in Leiden (Labey et al. 2000, Vrooman et al. 1998). RSA was also used to investigate the accuracy of scoliosis corrections (Liu et al. 1997) and to compare the correspondence between intramedullary pin placement in knee surgery and the mechanical axis of the tibia (Denis, 2001).

Experimental set-ups were designed to measure the complete three-dimensional rigid body movement of tibial trays and femoral stems in cadaver bones. These set-ups were used for the evaluation of both initial fixation of prostheses (Vander Sloten et al. 1994) and fixation after in vivo cycling (Bellemans 1999; Labey et al. 1996).

Depending on osseointegration and bone remodelling processes the stability of orthopaedic implants is also related to the quality of surrounding bone which can be assessed by measuring the bone mineral density (BMD) by dual X-ray absorptiometry (DXA) (Kiratli et al. 1996) or other methods (Njeh et al. 1999).

Other X-ray based methods for evaluating the stability and detecting the loosening of orthopaedic implants are substraction arthrography, scintigraphy and nuclear arthrography. (Oyen et al. 1996, Temmerman et al. 2007)

Unfortunately, none of the previously presented techniques is appropriate for evaluating the primary fixation of orthopaedic implants during surgery. To overcome measurement difficulties, computer simulations could be used as an alternative (or rather a complementary) tool for pre-clinical testing and design of implants. With models of femora (e.g. based on CT images) and of hip stems it is thus possible to calculate rather than measure

the mechanical behaviour of the implant-bone system and to change parameters like interface friction or stiffness at will to evaluate their importance (Kuiper 1996; Couteau 1998).

Nowadays, objective intra-operative assessment of primary stability of a THR component is a challenge, as surgeons have to rely mainly on their clinical experience, which consists mainly of a sense of mechanical stability when exerting axial force and/or torque on the prosthesis. Moreover, excessive press-fitting of a cementless femoral component can cause intra-operative fractures with an incidence of 5.4% in primary THRs (Lindahl 2007) and up to 30 % in revision cases (Meek et al. 2004).

Therefore, the per-operative characterization of the primary stem-femur contact and the assessment of primary stem stability in the first place may help to improve the survival rate of THR. Moreover, for predicting the success rate of any kind of bone implant, the assessment of initial per-operative stability is needed.

1.3. Vibration analysis on bone implants

Mechanical vibration analysis is a non destructive testing technique, widely used by mechanical engineers to inspect for structural integrity (Doebling et al. 1996). Different methods based on harmonic distortion, resonance frequency shift, or modal analysis (see appendix A4) are used to detect damage or to assess the mechanical properties of a very large variety of structures (simple or composite beams, bearings, gear boxes, terrestrial vehicles, airplanes, bridges, buildings etc.)

The first report of the use of vibration analysis in orthopaedics was in 1932 by Lippmann who used auscultatory percussion for the examination of clavicle fractures (Lippmann 1932). More sophisticated methods have been successfully used to determine bone mechanical properties (Lowet et al. 1993, 1996, Lowet, Van der Perre 1996, Nokes 1999) and clinical applications were monitoring of fracture healing (Lowet et al. 1996, Nakatsuchi et al. 1996, Nikiforidis et al. 1990) and in vivo assessment of bone mechanical properties (Van der Perre, Lowet 1996, Roberts et al. 1996).

Vibration analysis was successfully used to quantify the fixation of dental and craniofacial implants (Heo et al. 1998, Huang et al. 2003, Meredith et al. 1997, Pattijn et al. 2006, Sjöström et al. 2005). A transducer is attached to the implant and the first bending resonance frequency of the resulting system is measured (figure 1.3). The value is affected by the implant stability and a decrease in frequency over time indicates a potential failure. This

method is used in a commercially available system (Osstell™, Integration Diagnostics AB, Göteborg, Sweden).

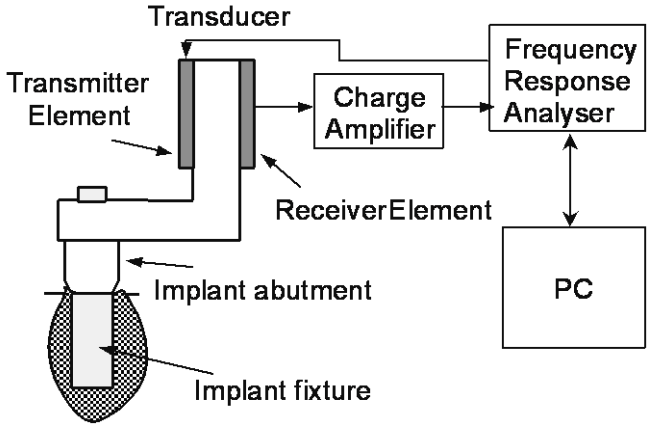

Figure 1.3. Vibration analysis on Brånemark oral implants (after Meredith 1997)

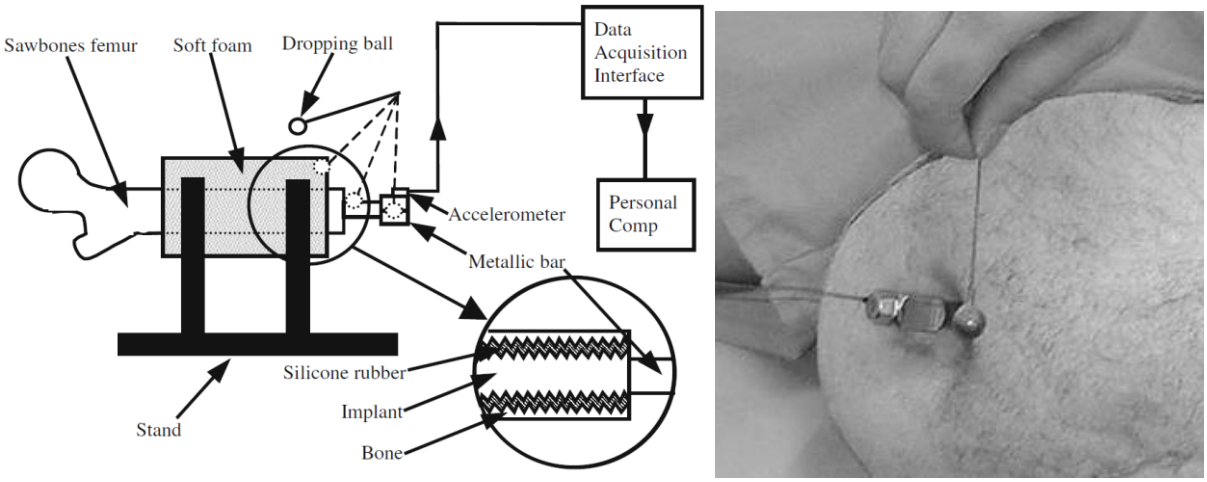

Figure 1.4. Vibration analysis on trans-femoral implants (Shao et al. 2007)[1]
(left) in vitro, (right) in vivo

A similar method was used in vitro and in vivo for the analysis of osseointegration of Brånemark trans-femoral implants (Shao et al. 2007). The implant was excited using a pendulum and the vibrational response was measured using an accelerometer (figure 1.4.) The

[1] With kind permission from Springer Science+Business Media: Shao F., Xu W., Crocombe A., Ewins D. 2007, Natural frequency analysis of osseointegration for trans-femoral implant, Annals of Biomedical Engineering 35 (5), 817–824.

obtained signal was analysed using Fast Fourier Transform (FFT) software to obtain the a resonance frequency of the implant-bone system. The result showed that a high resonance frequency corresponded to a high elastic modulus of the interface material between the implant and bone indicating a good osseointegration.

Vibration analysis seems also to be a promising method to assess the mechanical properties of the hip stem/femur system, but obviously the conditions for THR implants are different from those for dental and orthopaedic Brånemark implants.

A limited number of studies prove the feasibility of detecting several forms of loosening with vibration analysis, in vitro and in vivo (Collier et al. 1993, Georgiou, Cunningham 2001, Li et al. 1995, 1996, Rosenstein et al. 1989, Van der Perre 1984).

In the experimental protocol presented by Georgiou and Cunningham (2001) a harmonic vibration was applied to the femur on the external condyle with frequencies up to 1000-1200 Hz and the response was measured by an accelerometer pressed on the skin against the greater trochanter (figure 1.5).

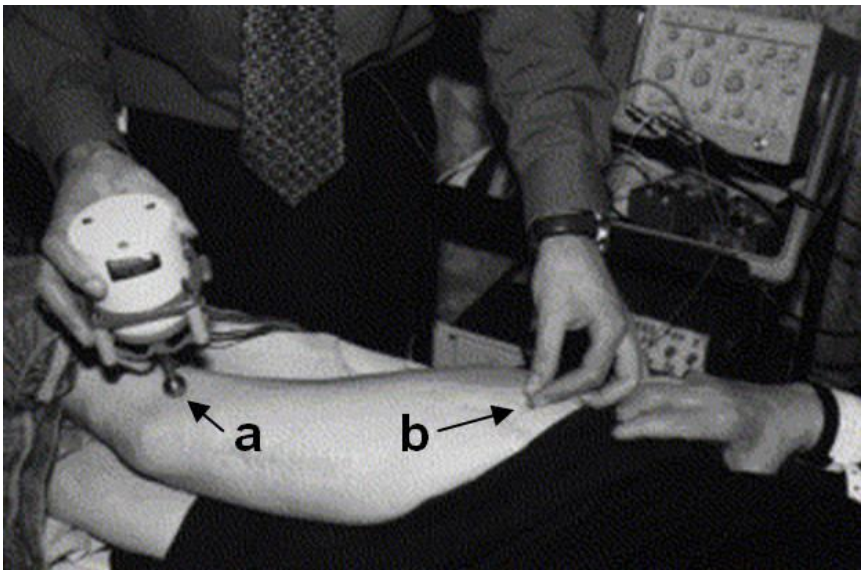

Figure 1.5. Vibration analysis on THR implants (Georgiou, Cunningham 2001)[2]

a. shaker excitation on the external condyle

b. vibrational response measuring on the greater trochanter

[2] Reprinted from Georgiou A.P., Cunningham J.L., 2001. Accurate diagnosis of hip prosthesis loosening using a vibrational technique. Clin. Biomech. (Bristol, Avon) 16, 315-323 with permission from Elsevier

A well-fixed implant/bone structure behaves as a linear dynamic system. If such a structure is harmonically excited, the response will be a harmonic motion described by a sinusoidal graph. When the implant is detached from the surrounding bone, the composite structure behaves as a non-linear system and distortions can be observed in the response signal (see appendix A.4.2.). "Severe loose" hip stems can be well distinguished from securely fixed stems and for this specific purpose, the method can be used clinically in the frequency range below 1000 Hz as reported by Georgiou and Cunningham.

In another research realised in the frame of the European project STIMuLus (Burny et al. 2000), to overcome the attenuation of the output vibration signal as a result of the soft tissues overlying the greater trochanter, an accelerometer embedded in the femoral implant was used (figure 1.6).

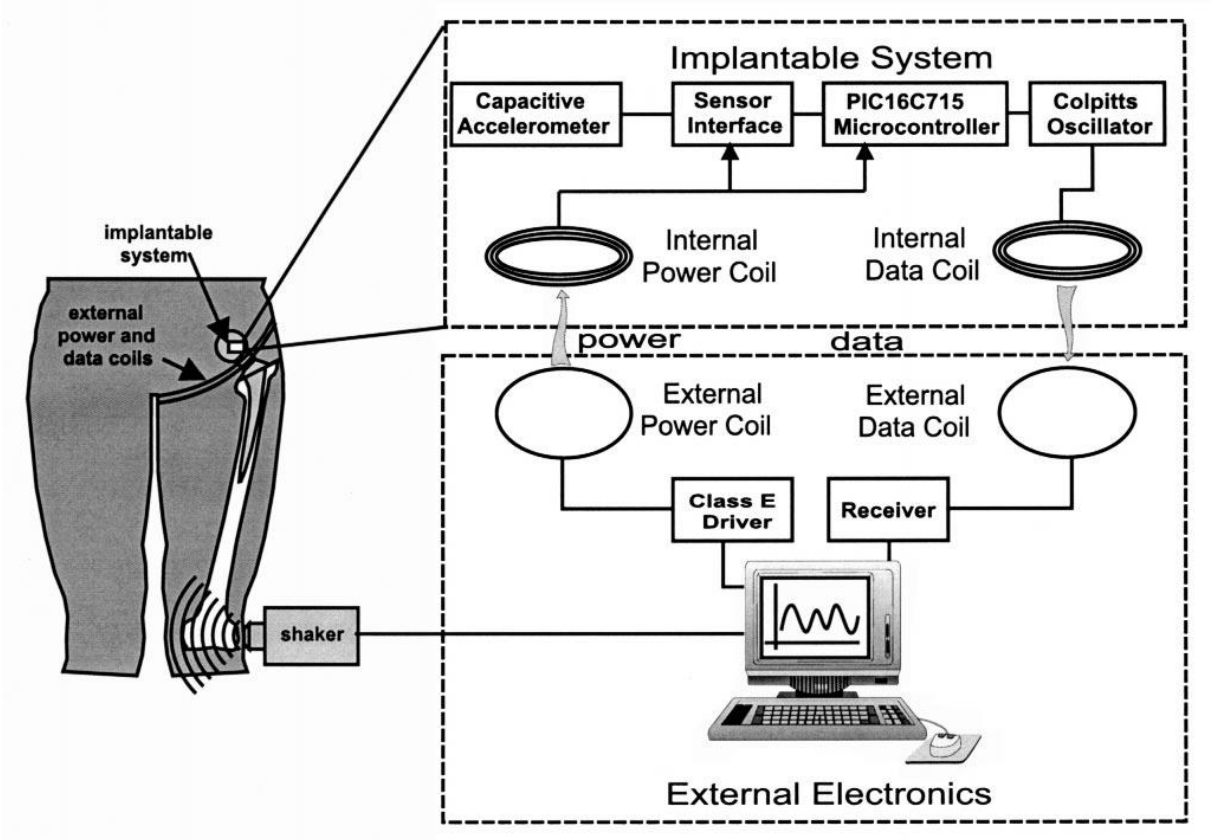

Figure 1.6. Telemetry system for the detection of hip prosthesis loosening (Puers et al. 2000)[3]

The system for powering the implanted electronics and the telemetry system for data transmission and reception are based on inductive links (Puers et al. 2000).

[3] Reprinted from Puers R., Catrysse M., Vandevoorde G., Collier R.J., Louridas E., Burny F., Donkerwolcke M., Moulart F., 2000. A telemetry system for the detection of hip prosthesis loosening by vibration analysis. Sensors and Actuators 85: 42–47 with permission from Elsevier

In a more recent study, the accelerometer was replaced by an ultrasonic probe to measure indirectly the vibrational response of the implant. This technique uses the Doppler shift phenomenon (Rowlands et al. 2008).

Although the vibrational methods based on harmonic distortion are able to detect "severe loosening" their sensitivity seems to be insufficient to detect "early loosening" or to monitor osseointegration in an early stage when the implant-bone structure still behaves in a good approximation of a linear system (Denayer et al. 2000, Georgiou, Cunningham 2001).

In these cases it seems more appropriate to observe changes in the resonance frequencies. From finite element (FE) studies it appears that the most sensitive band is above 2500 Hz (Qi et al. 2003).

Cristofolini et al. (2006) developed a prototype device to evaluate intra-operatively the stability of cementless femoral implants through resonance frequency analysis. The frequency response function (FRF) of the implant-femur structure is measured before and after applying a torque of 15 Nm. The shift of the main peak of the FRF in the range 1.2-2 kHz could be an indicator of implant stability (Reggiani et al. 2007, Varini et al. 2006, Varini 2007).

1.4. Research hypotheses and objectives

The study described in this paper is mainly oriented towards the assessment of the primary fixation stability of the femoral implants used in THR and it represents only a part of the OT/03/31 "Hip-Hub" research project funded by the K.U.Leuven research council (Asiminei et al. 2007, Claassen et al. 2007a, 2007b, Devos et al. 2007, Pastrav et al. 2007). From the large variety of femoral stems the custom made prosthesis (CMP), also known as intra-operatively manufactured prosthesis (IMP), was chosen. This femoral prosthetic stem is a joint development of the department of orthopaedics and the division of biomechanics and engineering design of K.U.Leuven, Belgium. The advantage of CMP is the extreme adaptability of the geometry design of the implant to match the femoral canal geometry and the position of the centre of the acetabular cup implant (see appendix A2).

The main objective of the research work was the developing of a method based on vibration analysis and the corresponding measuring device for the intra-operatively assessment of CMP stability. Beside its particular application, the derived vibrational method should be general enough to be adapted and extended to other kind of orthopaedic implants.

The research directions were defined by formulating two hypotheses and two questions.

Research hypotheses:

- Excepting the beginning, during the insertion process, the implant-bone structure behaves as a quasi-linear system, therefore the measuring method should be rather based on FRF analysis than on harmonic distortion.
- In the case of lower bending modes, the implant acts more like an added mass and the degree of fixation has no significant influence on the corresponding resonance frequencies. Exciting the more complicated modes, at higher frequencies, would increase the sensitivity of measurements because these modes are more influenced by the stress and contact conditions at the bone-implant interface.

Research questions:

- Can vibration analysis provide an objective measure for the increase in stability during the insertion in the case of cementless THR stems and by cement curing in the case of cemented THR stems?
- Can vibration analysis provide an objective criterion to detect the insertion endpoint of a cementless THR stem?

The research work started with a preliminary in vitro experimental study on cemented ABG II stems and cementless CMP stems inserted in artificial and human bones. FRF of stem-femur structure was measured in different conditions and its evolution was analysed. A per-operative protocol and a measuring device were developed and tested in a human cadaver (chapter 2).

The frequency domain was extended up to 10 kHz to verify the hypothesis that the higher frequency modes are more influenced by changes in stem stability.

Unlike in other studies, the vibration analysis was not focused on the shift of specific resonance frequencies, but on the evolution of the whole FRF graph. To objectively quantify the difference between two FRF spectra, the Pearson's correlation coefficient and the cross correlation function were used (see appendix A6).

Later, finite element models (FEMs) were created and the influence of contact distribution at the bone-implant interface on resonance frequencies and vibrational mode shapes were analysed in static and dynamic situations (chapter 3).

For evaluating in vivo the initial stability of cemented and cementless CMP stems the per-operative protocol was used in the case of 83 patients (chapter 4).

Since the results obtained were very promising for the stem-like implants, the vibrational method based on FRF analysis was adapted and tested on spherical implants. In a series of preliminary in vitro experiments, presented in chapter 5, the primary fixations of a reverse shoulder implant (metal on metal contact), of a femoral hip resurfacing implant (contact on the concave surface of the implant), and of an acetabular implant (contact on the convex surface of the implant) were analysed. The frequency domain was extended up to 20 kHz. To obtain a quantitative correlation between the resonance frequencies and the resistance against extraction, several pulling tests were performed on a femoral hip resurfacing implant.

2. *In vitro* study

The *in vitro* study analyses the FRFs corresponding to stem-femur structures at different degree of fixation.

Section 2.2 presents a series of experiments performed on ABG cemented hip stems to test the efficiency of a vibrational technique based on FRF analysis in assessing the implant fixation.

Section 2.3 is dedicated to the experiments performed on cementles CMP during the insertion process. The evolution of the FRF graph measured at successive insertion stages gives information related to the implant fixation and stability change.

A torsion test intended to discriminate between well fixed and quasi fixed femoral implants is described in section 2.4.

The content of this chapter was partially published in the Journal of Applied Biomaterials & Biomechanics (Pastrav et al. 2008).

2.1. Introduction

The *in vitro* experimental research described in this chapter studies the evolution of frequency response function (FRF) of hip stem/femur structure in different fixation situations to derive a method based on vibration analysis that could be used to obtain reliable information concerning the implant stability, to identify the optimal insertion end point during surgery, and for post-operative monitoring.

During the insertion of the prosthesis in the bone, a hip stem/femur system changes from a “severe loose” stage at the beginning, to a well fixed stage at the end point.

A well-fixed implant/bone structure behaves as a linear dynamic system. When severe loosening has occurred, the composite structure behaves as a non-linear system and distortions can be observed in the response signal when a harmonic excitation is applied. However, during the early stage of implant loosening, the implant/bone structure still behaves in a good approximation of a linear system and a vibration analysis based on harmonic distortion will have a low sensitivity. In these cases it seems more appropriate to observe changes in the FRF.

Vibration theory states that the increase of a mechanical structure stiffness results in the increase of the resonance frequencies of that structure (Heylen et al. 1997). Somewhat simplifying the phenomenon that occurs, in the case of a prosthesis/femur structure, it can be deduced that if the resonance frequenciy spectrum shifts to the right then the stiffness of the

implant/bone connection increases and, consequently, the fixation of the implant increases as well. If the FRF does not change between two successive insertion stages, then the mechanical properties of the prosthesis-femur structure did not change, thus the stem-bone connection is stable and the insertion end point is reached.

The FRF evolution during the implant insertion was studied on human and artificial femurs.

The frequency domain was extended above 2000 Hz to verify the hypothesis that the higher frequency modes are more influenced by changes in stem stability (Jaecques et al. 2004, Qi et al. 2003, Varini et al. 2006).

To objectively quantify the difference between two FRF spectra, the Pearson's correlation coefficient and the cross correlation function are used (see appendix A6).

2.2. Cemented ABG prosthesis

By cementation it is relatively simple to obtain different contact distributions on the surface of the femoral stem and, as a consequence, to simulate different fixation stages. The goal of the study presented in this section was to test the efficiency of a vibrational technique based on FRF analysis in assessing the stability of a femoral implant.

2.2.1. Experimental setup

For convenience and elimination of inter-individual variations, this work was performed on artificial human femora (Sawbone® nr. 3306, Left Large Composite Femur, **www.sawbones.com**, further referred to as "Sawbone"). This type of artificial femur can be considered mechanically equivalent to an average human cadaver femur, both for the static and the dynamic mechanical properties (Heiner, Brown 2001).

An ABG II prosthetic stem (Anatomical Benoist-Girard, subsidiary of Stryker-Howmedica-Osteonics, France) was chosen to be implanted. This stem was fixed with orthopaedic bone cement. The Sawbones were suspended horizontally in approximately free-free conditions by means of compliant elastic straps.

The influence of the connection between the prosthesis and the femur was studied by measuring the FRF of a Sawbone/ABG system in three conditions: well cemented, only cemented in the distal region of the stem and "clinically mobile", where a displacement of approximately 1 mm could be sensed by hand in the frontal and sagittal planes (figure 2.2 left).

The experimental setup is represented in figure 2.1. The excitation was realized on the Sawbone (figure 2.1a) by a shaker (figure 2.1g) through white noise signal input and the input force was measured by a force cell (figure 2.1h). An accelerometer (figure 2.1c) attached to the prosthesis neck (figure 2.1b) by orthopaedic wax measured the response acceleration.

The accelerometer and the force cell signals were amplified by a PCB Piezotronics amplifier – model 441A42 (figure 2.1d) and processed by a Hewlett Packard spectrum analyser – model 3582A (figure 2.1e). A second amplifier (figure 2.1f) was used to amplify the excitation signal that was generated by the spectrum analyser and sent to the shaker.

The FRF was measured in the range between 0 and 5000 Hz (16 averages).

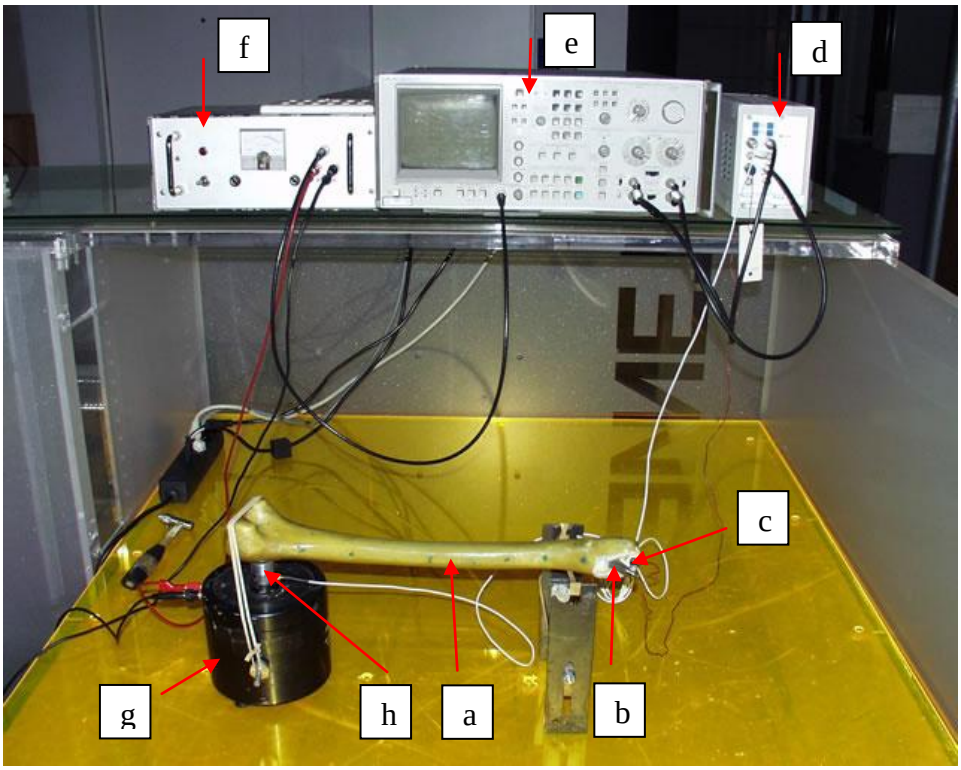

Figure 2.1: Setup for measuring the frequency response function of a femur/prosthesis system.

a. Sawbone
b. Prosthesis neck
c. Accelerometer
d. Amplifier 1
e. Spectrum analyser
f. Amplifier 2
g. Shaker
h. *Force cell*

2.2.2. Results and discussion

Figure 2.2 (right) compares the FRF of a Sawbone/ABG system among the "well cemented", "only distally fixed" and "clinically mobile" states.

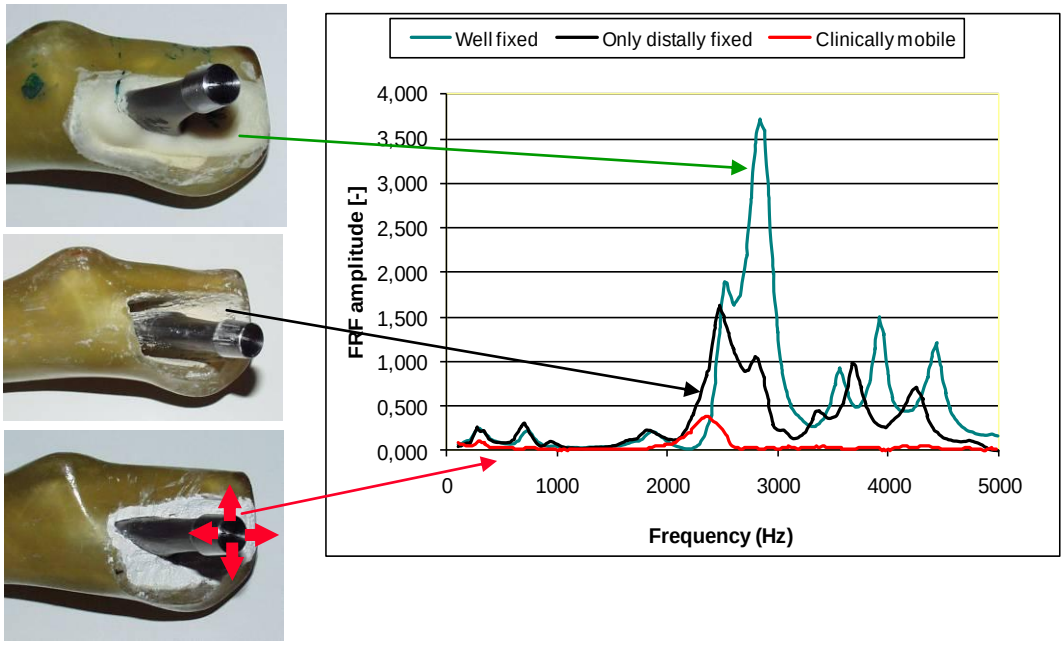

Figure 2.2: Comparison among the FRFs of a Sawbone/ABG cemented system in the "well fixed", "only distally fixed" and the "clinically mobile" state.

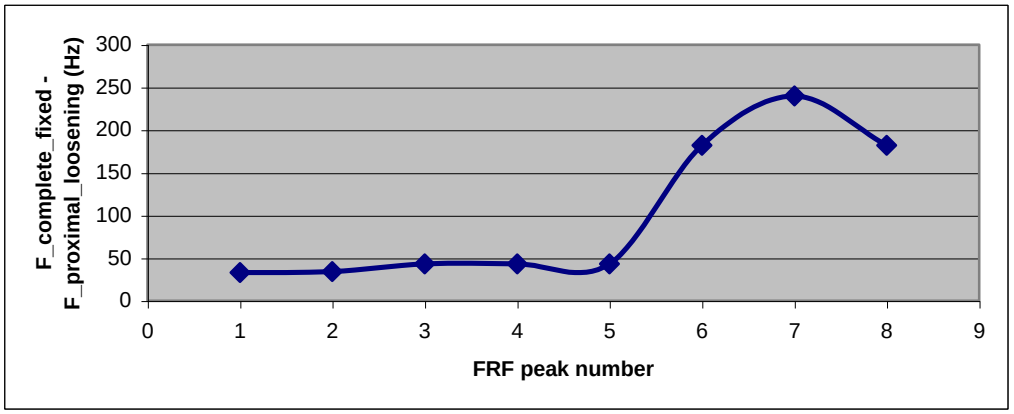

Figure 2.3: Shifts of the resonance frequencies of a Sawbone/ABG system between the well cemented and the "only distally fixed" states, plotted for increasing complexity of the mode shapes. The fitted line is only illustrative and does not represent a general model for the phenomenon.

In figure 2.3, the shifts of the resonance frequencies of a Sawbone/ABG system between the well cemented and the "only distally fixed" states, are plotted for increasing complexity of the mode shapes.

In this experiment the distally only cemented stem simulates a loosening in the proximal part and the clinically mobile stem simulates a severe loosening. The change in fixation is reflected by the FRF evolution i.e. the graph corresponding to the only distally fixed stem shifted to the left with respect to the graph corresponding to the well fixed stem.

The differences in amplitude might be the result of changes in vibrational mode shapes, in energy distribution between modes or in damping.

In the case of the clinically mobile stem the connection between the prosthesis and the bone is too weak to allow the prosthesis to participate in the deformation of the femur and a rattling phenomenon occurs. The system then behaves in a strongly non-linear way and the interpretation of the shifts in FRF peaks is no longer valid.

In this case, similar to severe loosening of the implant, a more appropriate detection method that could be applied in post-operative follow-up seems to be the vibrational analysis based on harmonic distortions (Georgiou, Cunningham 2001, Rosenstein 1989).

The experiment on the Sawbone with ABG stem in three different stages of fixation confirms also that the shifts of the resonance frequencies of the system increase with increasing complexity of the mode shape.

2.3. Cementless custom made prosthesis in human and artificial femur

2.3.1. Experimental setup

In a preliminary stage, the feasibility and the sensitivity of the method were tested on a single anatomical specimen, available at the orthopaedic surgery department of the University Hospital. In this stage an anatomical femur was preferred to a composite artificial femur as it allowed the use of the standard surgical reaming protocol. This dry human femur was prepared by an orthopaedic surgeon for insertion of a cementless custom made prosthesis (CMP) manufactured by Advanced Custom Made Implants, Leuven, Belgium. The stem was inserted loosely in the cavity (step 0) and subsequently the stem was hammered in with light hammer blows (steps 1…n), taking care to administer approximately the same impact with each blow. After each blow, the FRF of the system was measured (8 averages) by impulse excitation on the prosthesis' neck, with an accelerometer attached opposite to the impact site (figure 2.4 right). The insertion process was stopped when no further changes to the peak positions of the FRF were observed.

During the measurements, the CMP/femur system was suspended with elastic wires in order to reproduce free-free conditions. The accelerometer and the force cell signals were

amplified by a PCB Piezotronics amplifier – model 441A42 and processed by a Hewlett Packard spectrum analyser – model 3582A (figure 2.4 left). In this experiment impulse excitation with an instrumented hammer was used (figure 2.4 right).

The degree of FRF similarity between two successive insertion steps was quantified by the Pearson's correlation coefficient between FRFs and by normalised cross correlation function (NCCF), calculated over the 100-5000 Hz interval (see appendix A6).

Due to the fact that there is no linear dependence of one graph with respect to the other, the two graphs are identical if the correlation coefficient is 1.

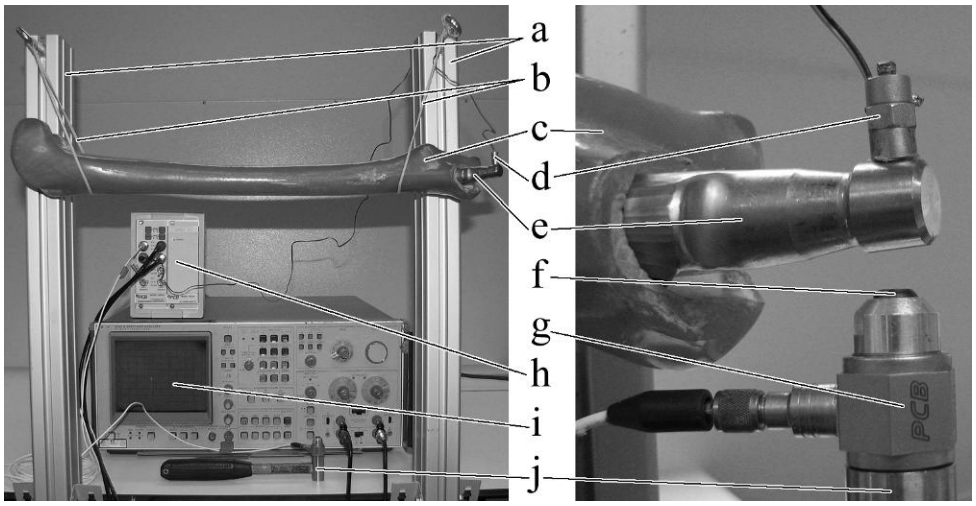

Figure 2.4: Experimental setup used for human and artificial femurs

(left: general view, right: detail of impulse excitation)

a. Support
b. Elastic bands
c. Femur specimen
d. Accelerometer
e. Hip stem
f. Hammer tip
g. Force cell
h. Input signal amplifier
i. Spectrum analyser
j. Excitation hammer

The normalised cross correlation function (NCCF) between the current FRF graph and the previous FRF graph was used to assess the direction and the magnitude of the FRF graph shift. The frequency corresponding to the maximum value of NCCF indicates the frequency shift of the FRF. A positive value means that the current FRF graph shifted to the right with respect to the previous FRF graph. The maximum value of the cross correlation function

indicates the similarity of the two FRF graphs. When two graphs are identical, the cross correlation function becomes the autocorrelation function and its normalised maximum is equal to one and it is located at frequency zero.

After the above described feasibility test on a single anatomical specimen, that produced a 'proof of principle', the reproducibility of the technique was tested by repeating the experiment on five artificial human femora (Sawbone) The five Sawbones were identically prepared by an orthopaedic surgeon for insertion of a CMP and a CMP was manufactured in order to fit the Sawbone identical cavities.

2.3.2. Results

The CMP insertion in a dry human femur was stopped after seven steps (step0...step6). The frequency response functions measured after each step are graphically represented in figure 2.5 (a…f). In order to see the evolution of the resonance frequencies, two successive FRFs are represented in each figure.

Only six hammering steps (step0...step5) have been necessary to completely insert the CMP in Sawbones and the measured FRFs for a typical case are similarly represented in figure 2.6 (a…e).

Analysing figure 2.5, it can be observed that new FRF peaks appear during the first insertion steps and, as the prosthesis is being introduced deeper into the medullar cavity of the dry human femur, the FRF graph shifts to the right, meaning that the resonance frequencies increase. However, between two consecutive insertion steps, the peak shifts are greater for the frequencies above 1500-2000 Hz than for lower frequencies.

The changes that appeared in the FRF between steps 2 and 3 are represented in figure 2.5c. Figure 2.7b presents the differences for the first three important peaks.

As hitting the prosthesis to insert it deeper continues, the resistance it opposes also increases and the FRF graph shifts less. Practically, there are no important differences between the FRF graphs corresponding to steps 5 and 6.

A similar behaviour was observed during the CMP insertion in artificial femurs. The results that have been obtained for a typical case are represented in figure 2.6a-e and figure 2.7a.

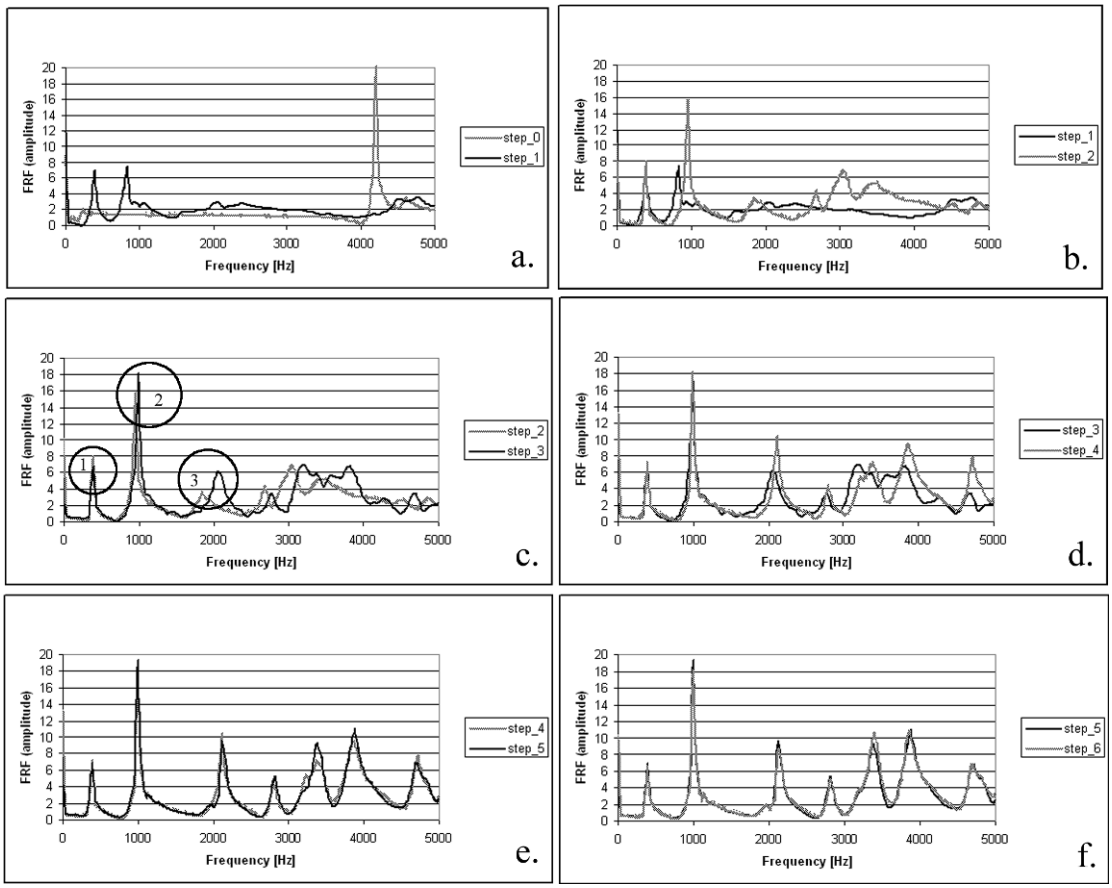

Figure 2.5 Change in FRF of a CMP/dry human femur system between two successive insertion steps

a. Step0 & step1
b. Step1 & step2
c. Step2 & step3
d. Step3 & step4
e. Step4 & step5
f. Step5 & step6

In order to objectively evaluate the FRF graph change, the Pearson's correlation coefficient and the normalised cross correlation function were calculated for pairs of successive FRF graphs.

The evolution of the correlation coefficient between two consecutive FRF graphs is represented in figure 2.8a and 2.8b. At the beginning of the insertion process the differences between successive FRF graphs are important and, consequently, the Pearson's correlation coefficient has lower values. During the last insertion stages the FRF graphs are nearly identical, thus the correlation coefficient becomes 0.99, approximating 1.0.

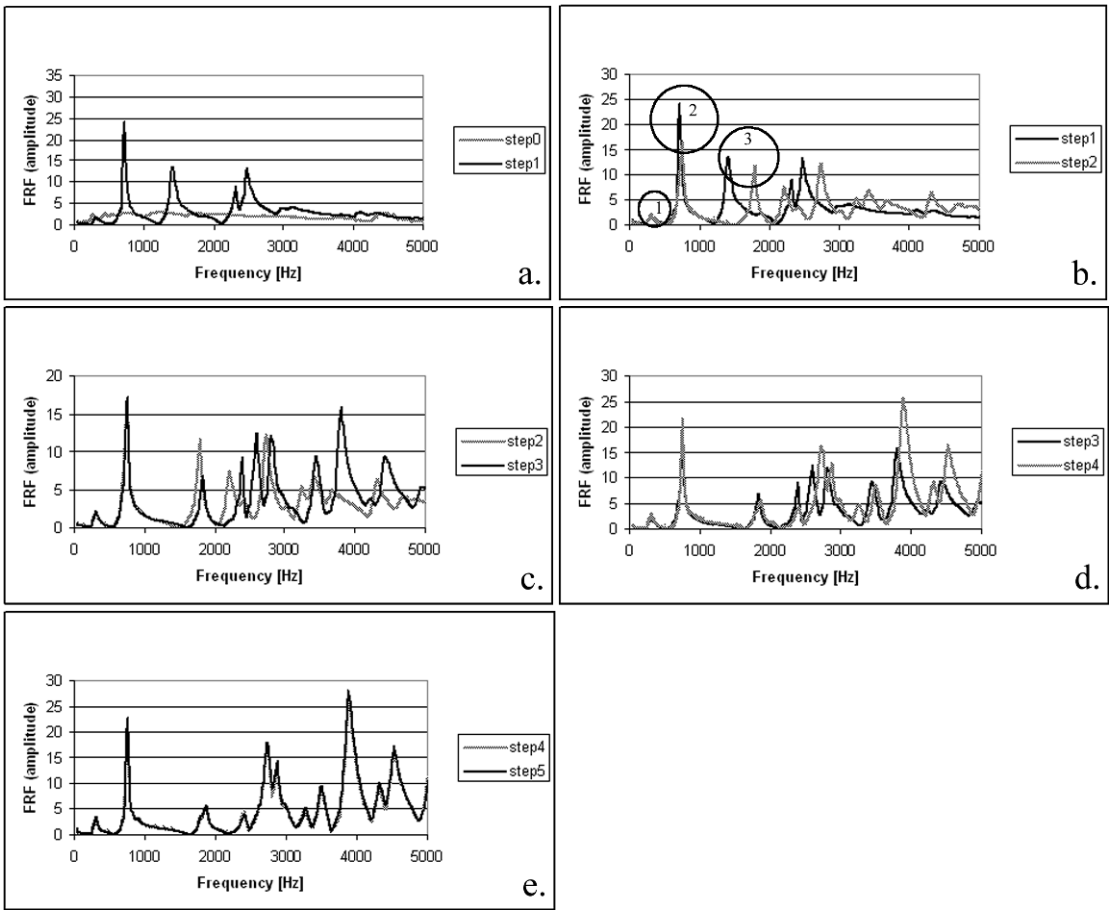

Figure 2.6 Change in FRF of a CMP/artificial femur system between two successive insertion steps

a. Step0 & step1
b. Step1 & step2
c. Step2 & step3
d. Step3 & step4
e. Step4 & step5

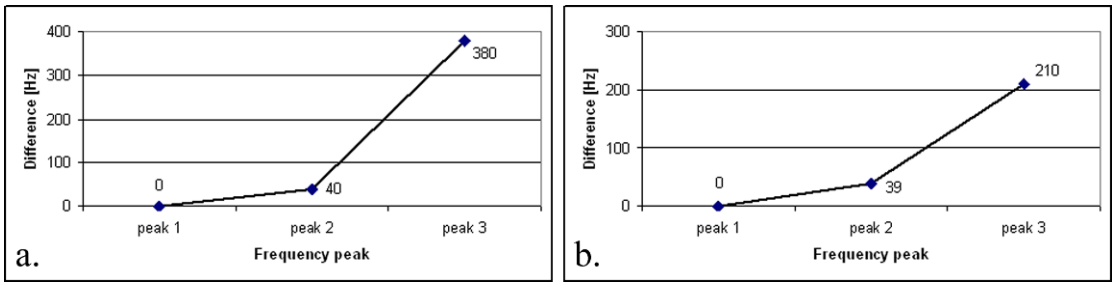

Figure 2.7 Shifts of the resonance frequencies of a CMP/femur system between two successive steps in the hammering process, plotted for the first three vibration modes.

a. CMP/artificial femur, step1 & step2
b. CMP/dry human femur, step2 & step3

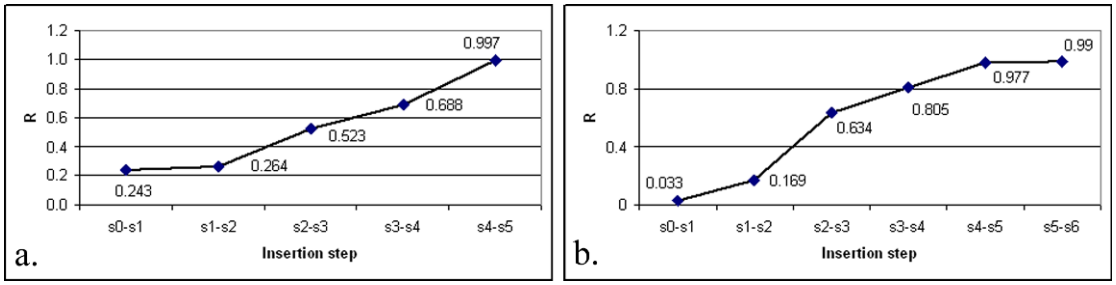

Figure 2.8 Pearson's correlation coefficient between two successive FRFs, calculated over the 100-5000 Hz interval

a. CMP/artificial femur

b. CMP/dry human femur

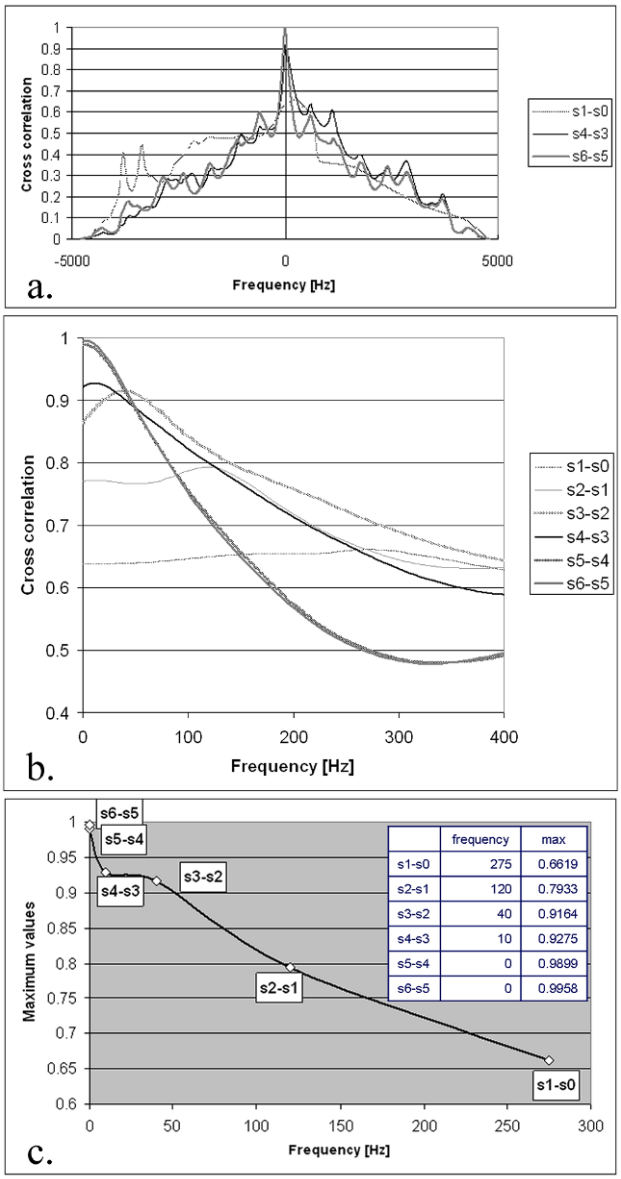

Figure 2.9 Normalised cross correlation functions(NCCF) calculated for the FRF pairs represented in fig. 2 (dry human femur)

a. Entire domain (-5000 Hz …5000 Hz)

b. Detail (0 … 400 Hz)

c. Maximum values of the NCCFs represented in fig. 6b

The evolution of the NCCF corresponding to the human femur can be observed in figure 2.9.

For visibility reasons only three NCCFs calculated for three FRF pairs were represented in figure 2.9a. Since the most interesting part is situated around the maximum values, in figure 2.9b all the six NCCFs corresponding to the six FRF pairs were represented on the 0…400 Hz interval.

Figure 2.9c shows only the maximum values of the six NCCFs. The abscissa of each maximum value is situated in the positive domain, thus the FRF shifted to the right after each insertion stage indicating an increasing stiffness of the bone/implant system. The maximum value of the NCCF calculated for the last two insertion stages has the coordinates 0 and 0.9958 indicating the last two FRFs are quasi identical.

The NCCFs corresponding to the artificial femora had a similar pattern.

2.3.3. Discussion

Since the geometry and mechanical properties of the femur and the stem geometry are variable from one patient to another, it is difficult to obtain absolute objective information concerning the stem stability in femur using a single FRF graph. In order to assess the stability evolution during the stem insertion, the comparison between the FRF graphs corresponding to successive insertion stages was used.

The results represented in figure 2.5c, 2.6b, 2.7a, 2.7b confirm the hypothesis that the changes in stem stability determine more important change of the FRF in the range of higher frequencies, thus the more complicated modes are more influenced by the evolution of the connection between the stem and the femur.

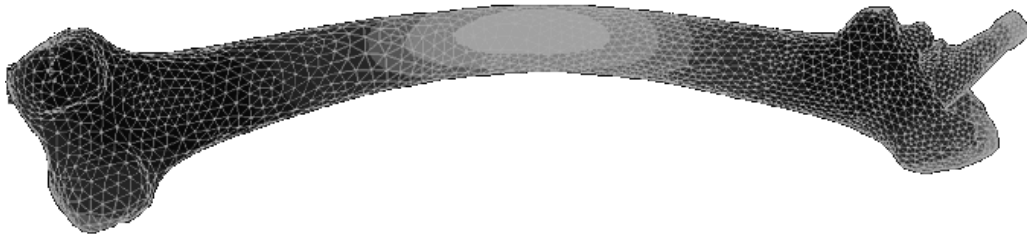

Figure 2.10. The first bending mode of a femur with a fully inserted implant. A finite element model.

The first bending mode of the femur (figure 2.10) is hardly affected by the presence of the prosthesis. The effect of the prosthesis on this mode shape is mainly to increase the mass of the system, but the stiffness is hardly affected since the deformation of the proximal part of the femur is very small in the single bending mode. Only severe loosening will be detectable when the first bending mode of the femur is excited: in this case the connection between the prosthesis and the bone is too weak to allow the prosthesis to participate in the deformation of the femur and a rattling phenomenon will occur. The system then behaves in a strongly non-linear way and the interpretation of the shifts in FRF peaks is no longer valid.

The experiments confirm that the changes in FRF occur mainly in the higher modes (above 1000 Hz). After the first insertion step, the shift of the resonance frequencies below 500 Hz is below the detection limit of the used technique. In contrast, the peaks above 1500 Hz undergo a slight shift until the final stage of the hammering process, when the prosthesis is deemed fully seated upon visual inspection and manual testing of the mobility.

This observation is in accordance with the work of Qi (Qi et al. 2003) who stated that the most sensitive frequency band for observing defects in the femur/prosthesis connection is above 2500 Hz.

The absence of any noticeable changes between two consecutive FRFs leads to the conclusion that the mechanical parameters of the prosthesis/femur structure are not changing anymore.

Considering the obtained results as a starting point, a per-operative protocol based on FRF analysis can be designed to assess the stability of cementless hip prosthesis, and to detect the insertion end point.

During the insertion procedure the surgeon should corroborate the information obtained through the visual and tactile control of the prosthesis/femur structure with the information referring to the FRF evolution, Pearson's correlation coefficient and normalised cross correlation function.

A shift to the right of the resonance frequencies means an increase of the implant stability and a Pearson's correlation coefficient above 0.99 should signal the reach of the insertion end point. An extra hit will not lead to the increase of the prosthesis stability but will increase the risk of femur fracture. The appearence of femur fractures during the insertion would lead to the decrease of the stiffness of the connection between the implant and the bone and could be signalled by a FRF shift to the left.

Because the FRF changes are greater for frequencies above 1500-2000 Hz, the upper limit of the measuring domain should be at least 5000 Hz.

Obviously, such a protocol must be tested and validated under more realistic situations, i.e. on cadaveric specimens and then under per-operative conditions.

2.4. Torsion test

Inspired by a series of studies realised at Università degli Studi di Bologna (Cristofolini et al. 2006, Reggiani et al. 2007, Varini et al. 2006, Varini 2007), an experiment to discriminate between well fixed and quasi fixed femoral implants was designed.

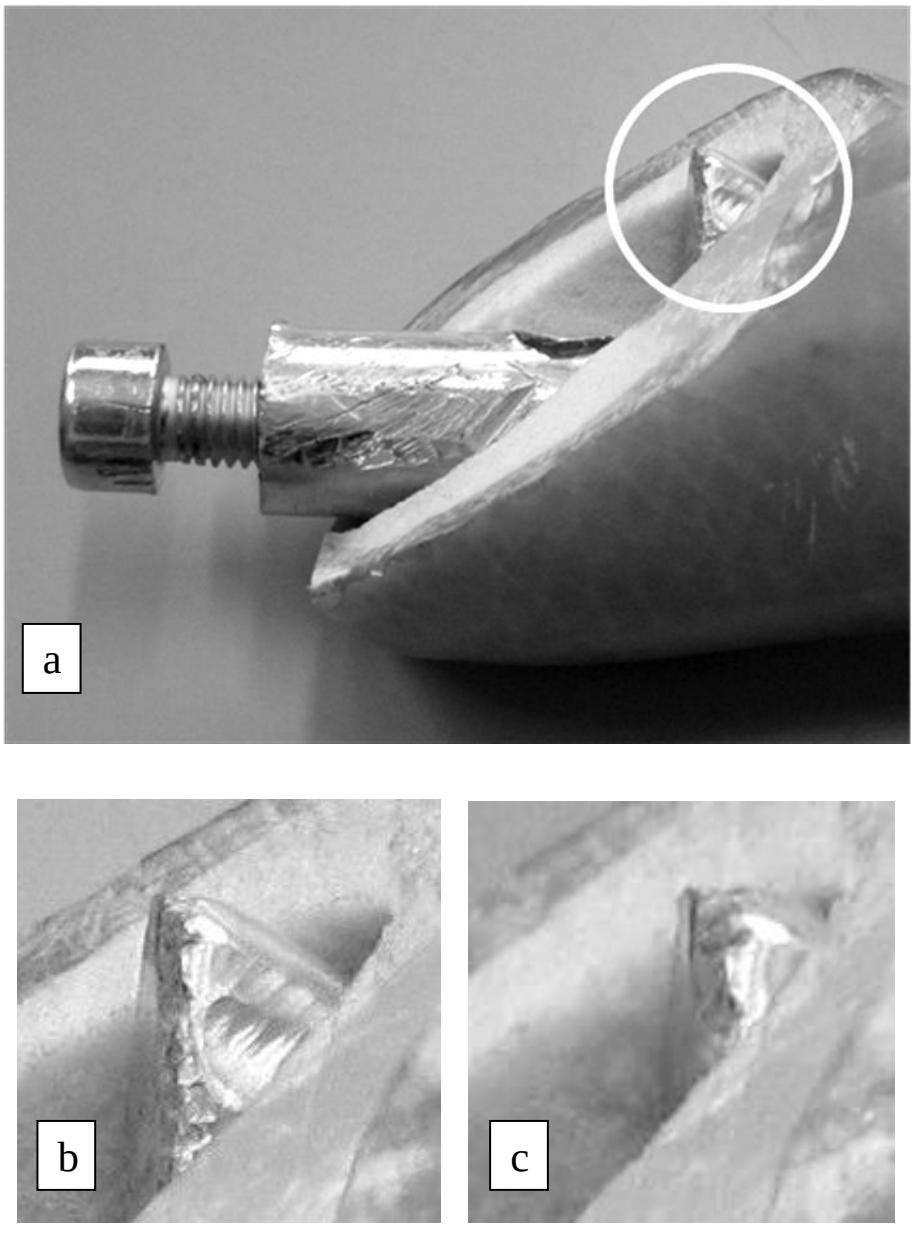

Figure 2.11 Modified CMP stem inserted in artificial femur for torsion testing

a. General view
b. Detail of quasi fully inserted stem
c. Detail of fully inserted stem

The method presented in this section is based on the comparison of the FRF graphs obtained before and after applying a torque on the implanted femoral stem. Its originality consists in analyzing the whole FRF between 0 and 7000 Hz, not only the main peak below 2000 Hz as the Italian group did.

2.4.1. Experimental setup

The experimental setup is similar to that presented in section 2.3.1. (figure 2.4). The head of the cementless CMP used in this experiment was modified in order to allow the use of a torque wrench to apply a controlled torque on the inserted stem (figure 2.11a). For machinability and economical reasons, the stem was made of aluminium. The Young's moduli of titanium (105-120 GPa) and aluminium (70 GPa) are comparable.

Two fixation situations were compared. The quasi fixed and well fixed situations corresponded to quasi fully inserted stem (figure 2.11.b) and respectively fully inserted stem (figure 2.11c). In the longitudinal direction, the difference between the two situations was 1.5 mm which is hardly observable during the real surgical procedure. Clinically, no difference in fixation could be detected.

In both situations a torque of 15 Nm was applied on the head of the stem, the direction of the moment vector coinciding to the longitudinal axis of the stem.

Before and after applying the torque, the FRF of the structure composed by the modified CMP and the artificial femur was measured by impulse excitation on the prosthesis' neck, with an accelerometer attached opposite to the impact site.

2.4.2. Results and discussion

The typical graphs corresponding to the FRFs measured during the experiment are presented in figures 2.12 and 2.13.

In the case of the quasi fixed stem, a relatively important difference between the FRF graphs obtained before and after applying the torque was visible. Some peaks simply shifted to the left indicating a lowering stiffness while other peaks suffered more complex changes indicating important modifications of vibrational modes probable due to relatively important contact change at the interface between the implant and the artificial bone.

The corresponding Pearson's correlation coefficient was 0.89.

In the case of the well fixed stem, the FRF graphs obtained before and after applying the torque were nearly identical and the corresponding Pearson's correlation coefficient was 0.99. This indicates the mechanical properties of the tested structure almost did not change between the two measurements.

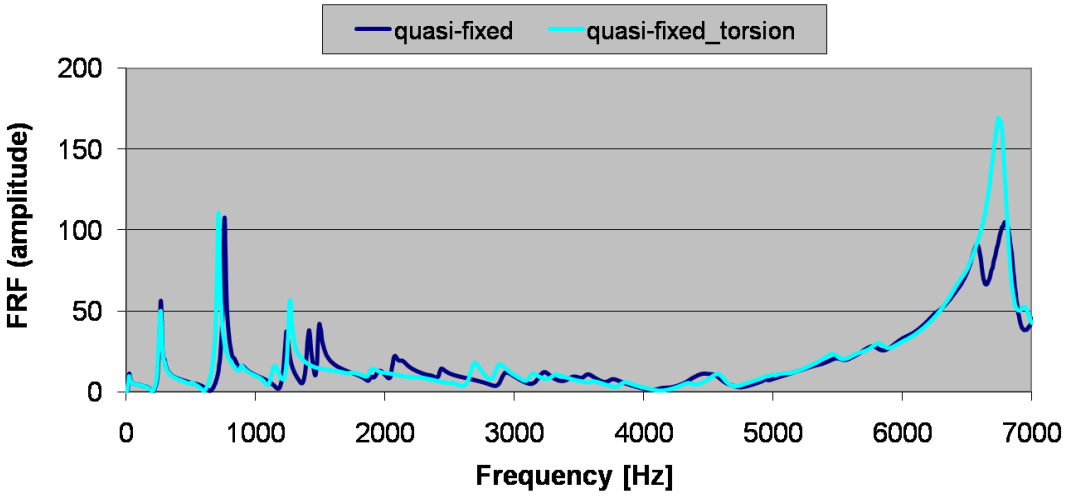

Figure 2.12 Change in FRF of a quasi fixed CMP/artificial femur system before (dark blue graph) and after (light blue graph) applying a torque.

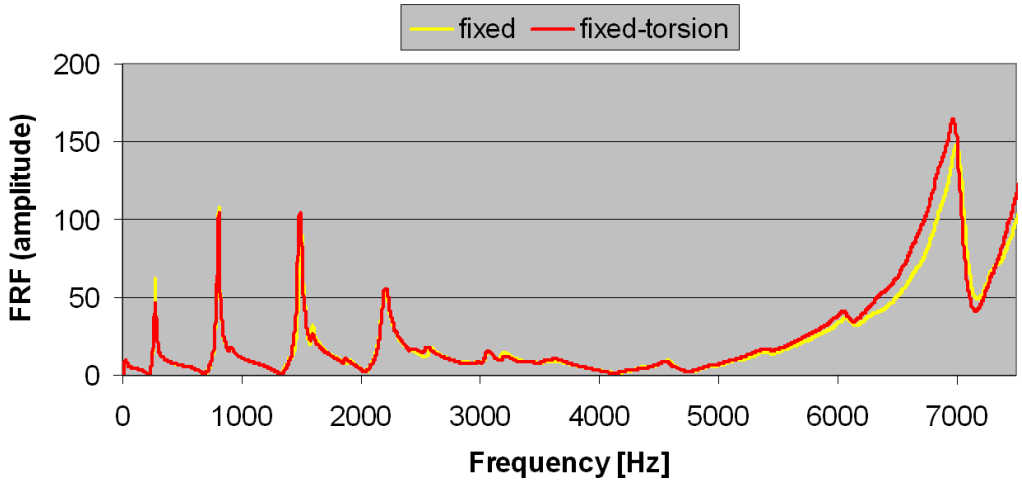

Figure 2.13 Change in FRF of a well fixed CMP/artificial femur system before (yellow graph) and after (red graph) applying a torque.

However, applying a torque on the implant may result in plastic enlargement of the femoral cavity and, as a consequence, in reducing the stability of the stem. This hypothesis is confirmed by a slight shift to the left of the peaks situated above 5000 Hz.

Although the method presented in this section was proven to be sensitive enough to discriminate between quasi fixed and well fixed implants, it was considered not suitable for testing the primary stability of the femoral implants during surgery. The main reason for this decision was the possible rotation of the implant under the testing torque which would result in the deformation of the femoral cavity in an unwanted way, decreasing the stability. Such a

scenario is very probable due to the relative weakness of the unhealed bone that supports the load transmitted by the implant.

2.5. Conclusions

The results obtained during the *in vitro* experiments presented in this chapter have shown that vibrational techniques based on FRF analysis are sensitive enough and might be used for assessing the initial stability of femoral implants. An experimental setup and a protocol were designed to monitor the stability of CMP and detect the end point of the insertion during the surgical procedure.

After testing on a cadaver, the vibrational technique was optimised and applied on 83 volunteer patients who received hybrid cemented or uncemented CMPs.

The methods and materials, the results, and the conclusions derived after the *in vivo* experiments are presented in Chapter 4.

3. Finite element study

To better understand the influence of changing contact conditions on the resonance frequencies of the stem-femur structure a finite element study was set up.

In the first approach, presented in section 3.2, the hip stem was considered fully inserted in the femur. Modal analyses on the hip stem-femur system were performed in various contact situations.

In the second approach, presented in section 3.3 the hip stem insertion was simulated and, after each insertion step, modal analyses on the hip stem-femur system were performed.

Section 3.4 describes the effect of an inserted prosthesis (added mass effect versus added stiffness effect).

The results are in agreement with previous experiments and finite element studies: contact increase causes positive resonance frequency shifts and, in general, the higher modes are more sensitive to the contact change.

The contents of sections 3.2 and 3.3 were published in the Journal of Medical Engineering & Physics (Pastrav et al. 2009a) and, respectively, in the Proceedings of ISMA2008 International Conference on Noise and Vibration Engineering (Pastrav et al. 2008).

3.1. Introduction

In the previous chapter an end criterion for prosthesis insertion based on vibration analysis of IMP-femur system during the operation was derived.

Specifically, the endpoint criterion to stop the hammering was derived from the correlation coefficient R between the frequency response function (FRF) of two successive insertion stages. During the insertion the implant stability increases as a result of the increase in contact area between bone and implant and the development of contact pressure. As a consequence, the resonance frequencies increase and the FRF graph shifts to the right. Based upon the in vitro experiments it was proposed that when a correlation of 0.99 is reached, which means that two successive FRFs are practically identical, the contact conditions are stable and further hammering would not increase the stability of the implant but would only increase the risk of fracture (Jaecques et al. 2006, Pastrav et al. 2006, 2008).

However the influence of changing contact conditions on the resonance frequencies was not yet quantitatively understood and therefore a finite element analysis (FEA) was set up (Bathe 1996).

In section 3.2 the pure effect of the change in contact area on the resonance frequencies is investigated, without accounting for changes in relative position of the prosthetic stem with respect to the femur and without accounting for contact pressure. By analysing the effect of one isolated parameter, namely the influence of the contact conditions, on the resonance frequencies the presented study does not simulate the insertion process in all its aspects but rather the loosening or osseointegration stages after operation.

In a first stage the femur and the prosthesis were separately analysed to verify the accuracy of the simulated resonance frequencies against experimentally obtained data.

In a second stage, modal analyses on the IMP-femur system were performed in various stages of contact. By modelling the contact changes by means of the contact tolerance options in the FE software, contact could be varied while keeping other system parameters constant.

In a third stage of the analysis, the contact was successively changed in the proximal, central and distal zones to analyse the sensitivity to the location of contact changes.

Section 3.3 presents a full simulation of the hip stem insertion process (including change in prosthesis position, contact, and pressure) and the change of the resonance frequencies over several insertion stages is analysed.

Section 3.4 presents some aspects related to the modal shapes obtained for finite element models of femur-CMP structure.

3.2. The influence of boundary conditions change on the resonance frequencies

3.2.1. Methods

A finite element model of a femur with an implanted IMP was created to provide insight into the dependence of the dynamic behaviour of the system on system parameter variations.

The geometry of the parts was created, based on CT scans of an artificial human femur (Sawbone® nr. 3306, Left Large Composite Femur, www.sawbones.com) and Standard Tessellation Language (STL) files of a corresponding IMP (courtesy of Advanced Custom Made Implants, Leuven, Belgium), by using the software Magics® and Mimics® (Magics X SP2 V10.1.1.17, Mimics 9.11 V9.7.1.1, Materialise, Haasrode, Belgium). The femoral cavity was obtained by applying a boolean operation that extracted the prosthesis volume from the

femur, thus the femoral cavity and the prosthesis stem have the same shape and size (figure 3.1).

Next, the created shapes were meshed using Patran® (Patran 2005r2 v13.1.116, MSC.Software, Gouda, The Netherlands). To generate the solid mesh a 3D 4-node linear, isoparametric, tetrahedral element was chosen. This kind of element is appropriate for the intended analysis (Cook et al. 1989) and was already used in similar studies (Saxena et al. 1999)

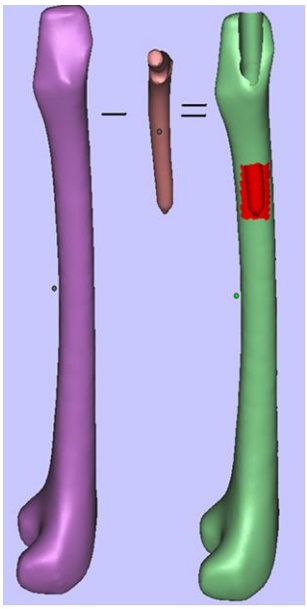

Figure 3.1: The boolean operation applied with Magics ®

Table 3.1: Material properties assigned to the various materials in the FE models (Wirtz et al. 2000)

Variable	Unit	Cortical bone	Trabecular Bone	Prosthesis TiAl6V4	Orthogonal system
Young's modulus E11	GPa	6	0.375	110	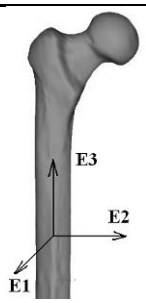
Young's modulus E22	GPa	6	0.375	110	
Young's modulus E33	GPa	13	0.6	110	
Poisson ratio ν12= ν23= ν31		0.3	0.12	0.3	
Density ρ	kg/m^3	1800	500	4520	

Orthotropic, linear elastic behaviour was selected for the bone mechanical properties (Wirtz et al. 2000). The prosthesis material (Ti6Al4V alloy) was considered isotropic and linear elastic. The mechanical properties of the materials and the reference orthogonal system are represented in Table 3.1.

To take into account the division between cortical and trabecular bone in the femur, cortical bone and trabecular bone properties were assigned to the two outer layers of elements and the remaining inner elements respectively.

To evaluate the accuracy of the mesh and to select the optimal size of the elements, a convergence criterion was used. Since the chosen element type assures a monotonic convergence to the exact solution, plotting the results as a function of the number of elements, indicates the mesh size that gives an acceptable result. However, when choosing the mesh density, the available computer power and time limitations have to be taken into account as well.

Since the modal behaviour, characterised by the resonance frequencies, is the most important system property in this study, the convergence criterion was applied to the resonance frequencies of the system.

As predicted by the theory of numerical modelling, the resonance frequencies shift to lower values as more elements are used. Splitting the geometry up into more elements reduces the apparent stiffness of the system (Saxena et al. 1999).

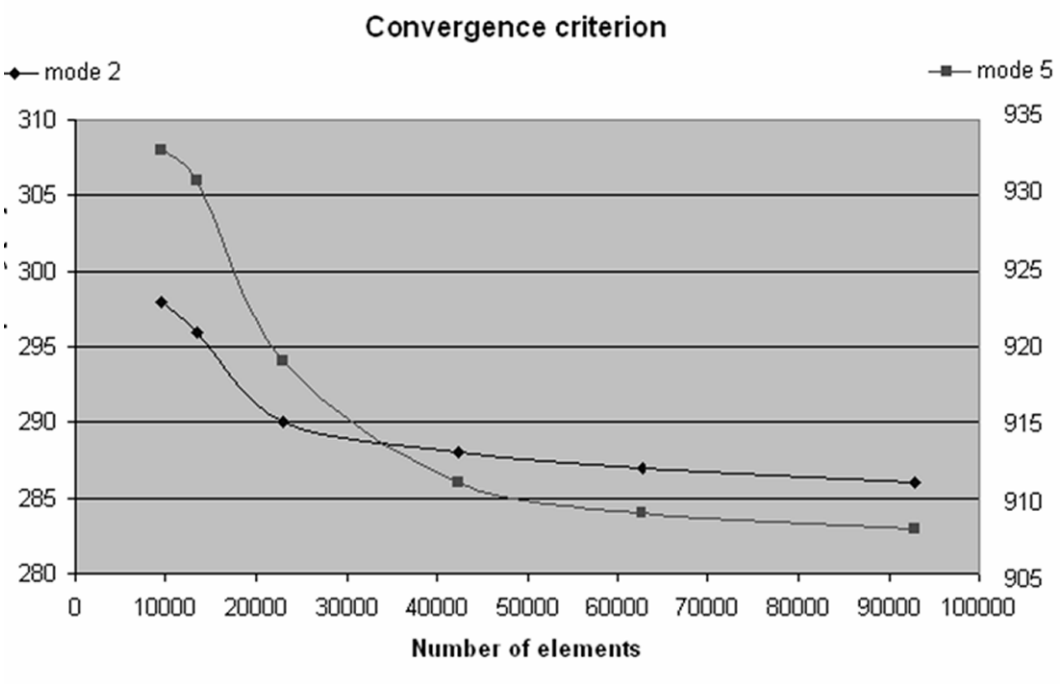

Figure 3.2: Evolution of the RF in function of the number of elements for two modes.

Figure 3.2 shows the second and the fifth resonance frequencies of the human femur model in function of the number of elements in the mesh. It indicates that convergence starts from a total number of 40.000 elements. It was considered that approximately a number of

60.000 elements, or an average edge length of 2.5mm, gives the optimal results taken into account the time needed to perform the analyses.

To justify the proposed end criterion for the insertion (Jaecques et al. 2006, Pastrav et al. 2006), the observed changes in the FRF have to be linked to contact increase. Previous work (Jaecques et al. 2004, 2006, Pastrav et al. 2005, 2006) already showed that contact increase causes changes in the dynamic behaviour and that the importance of these changes depends on the considered contact zone. Three zones are considered: proximal, central and distal, corresponding to respective Gruen zones 1 and 7, 2 and 6 and 3 to 5 (Gruen et al. 1979, see appendix A3).

The set up of the model implies a perfect fit between the prosthesis and the femur, which represents a 100% contact between the two parts. Situations of partial contact were simulated by varying the contact tolerance option in Marc FE software (MSC.Software, Munich, Germany, version 2005r3, 32 bit). This option allows the user to set the distance below which the software considers a node and a surface in contact. Because of the meshing procedure, this distance varies over the geometry of the prosthesis, as illustrated in figure 3.3.

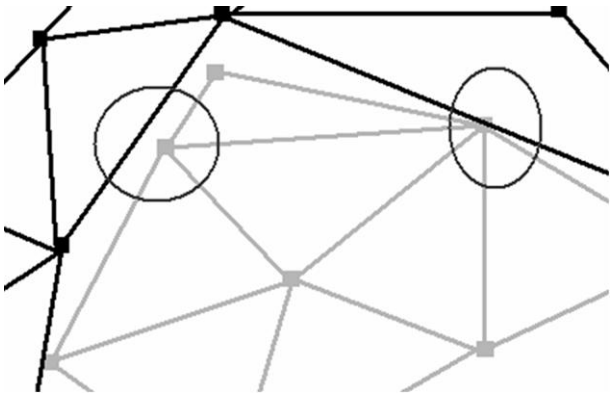

Figure 3.3: The distance between a node on the prosthesis surface and the femur surface varies over the geometry of the prosthesis (prosthesis mesh in gray)

The contact tolerances used were 0.01, 0.03, 0.05, 0.08 and 0.14 mm. These values were chosen to obtain a node-contact-increase of 20% of the total surface area between two successive configurations when applied to the complete prosthesis surface.

Table 3.2 illustrates the correlation between the contact tolerance and the percentage of nodes in contact.

Table 3.2: Correlation between contact tolerance and nodal contact

Contact tolerance [mm]	Nodal contact [%]
0.01	15%
0.03	38%
0.05	56%
0.08	76%
0.14	98%

This method based on contact tolerance, allowed a simulation of the successive contact stages by gradually increasing the area of contact between the prosthesis and the femur. The contact configuration could be changed without altering other system parameters such as the dimensions or the geometric position of the prosthesis in relation to the femur. The highlighted zones on figure 3.4 represent for various situations, the elements of the femur in contact with the prosthesis.

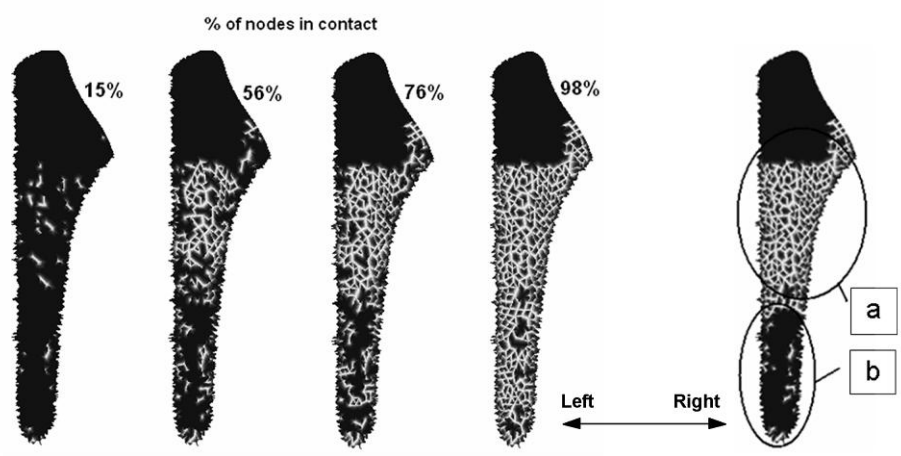

Figure 3.4: Change of contact distribution
(left) Progressive increase of general contact (four cases)
(right) Different contact areas in different zones
(a) proximal and central zones
(b) distal zone

By dividing the prosthesis into several contact bodies, different contact tolerances could be established at will in different parts of the prosthesis. This method was used to create unevenly distributed contact configurations, in which one part of the prosthesis is less fixed to the femur than the others (figure 3.4 right). This allows investigating the sensitivity to the location of the zones of contact changes and thus simulating various situations of loosening.

Because of the large disparity in mechanical properties between the bone and the stem, the latter being an order of magnitude stiffer than the bone, no sensitivity analysis to the bone properties was undertaken.

The influence of the boundary conditions was studied in two situations:

1) The stem-femur system was considered in free-free suspension which corresponds in a good approximation to the per-operative conditions (Van der Perre, Lowet 1996).
2) The central part of the femoral cavity was considered fixed.

All analyses have been performed using the Marc FE software and the Mentat post processor (version 2005r3, 32 bit; MSC.Software, Gouda, The Netherlands).

3.2.2. Results and discussion

Modal analysis has been used to calculate the resonance frequencies and to obtain the vibrational mode shapes. The frequency range used for the finite element analysis fitted within the range used for the experimental studies (Jaecques et al. 2006, Pastrav et al. 2006), notably 0 to 10.000 Hz.

In a first stage the femur and the prosthesis were analysed separately.

In total, the range between 0 and 10 kHz contains 70 resonance frequencies of the femur. The first 5 resonance frequencies were compared with experimental results found in the literature and the finite element analysis results fit within the range of the experimentally obtained values (table 3.3).

Table 3.3: Numerically calculated values of resonance frequencies of the femur compared to experimentally obtained values
** in the plane of minimal EI, practically coinciding with the coronal plane*
*** in the plane of maximal EI, practically coinciding with the sagittal plane*

	1st bending mode * [Hz]	**1st bending mode ** [Hz]**	**1st torsion mode [Hz]**	**2nd bending mode * [Hz]**	**2nd bending mode ** [Hz]**	**Mass [kg]**	**Length [m]**
Numerical (current study)	264	277	646	782	820	0,42	0,471
Havermans, Daenen, 2002	254	266	453	694	719	0,57	0,485
Couteau et al. 1998	301	353	612	886	931		
Khalil et al. 1981	250	315	563	825	879		

Mainly three types of modes occurred:

- Bending modes
- Torsion modes
- Ring modes in which the cross section deforms.

The latter modes often occur in systems with a stiffer outside layer and a compliant inside material, such as tubes (Wang, Mechefske 2007).

The corresponding resonance frequency of the first ring mode (~3000 Hz) is remarkably higher than the first resonance frequencies of the bending (~250 Hz) and torsion (~600 Hz) modes.

For higher frequencies, the modes become very complicated, a mixture of torsion, bending and ring modes, which makes the identification difficult. figure 3.5 illustrates the difference between a relatively simple bending mode (1772 Hz, mode nr. 8) and a complicated mode (8644 Hz, mode nr. 54).

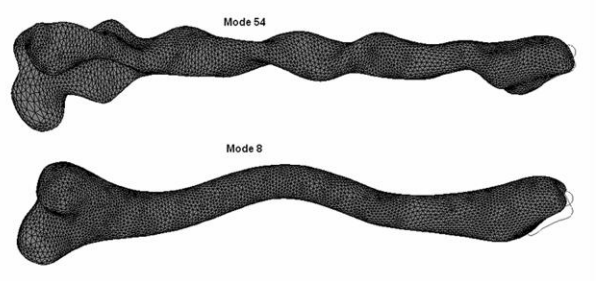

Figure 3.5: A simple (down) and a complicated (up) mode shape of the femur

The numerically calculated resonance frequencies of an IMP (for free-free boundary conditions) were compared to the experimental values, measured using a CADA-X system (LMS International, Leuven, Belgium, www.lms.be). Only four resonance frequencies can be distinguished appearing in two groups of two: around 3700 Hz and around 8500 Hz.

Table 3.4: Numerical and experimental resonance frequencies of an intra-operatively manufactured prosthesis

	1st mode **[Hz]**	2nd mode **[Hz]**	3d mode **[Hz]**	4th mode **[Hz]**
Experimental	3559	3950	7900	8400
Numerical	3523	4042	8418	8541

The corresponding mode shapes of the IMP model are presented in figure 3.6a and the experimentally obtained FRF is presented in figure 3.6b.

In a second stage, modal analyses on the IMP-femur system were performed. The prosthesis was fully inserted and the overall contact area changed in 5 steps from 15% to 98%.

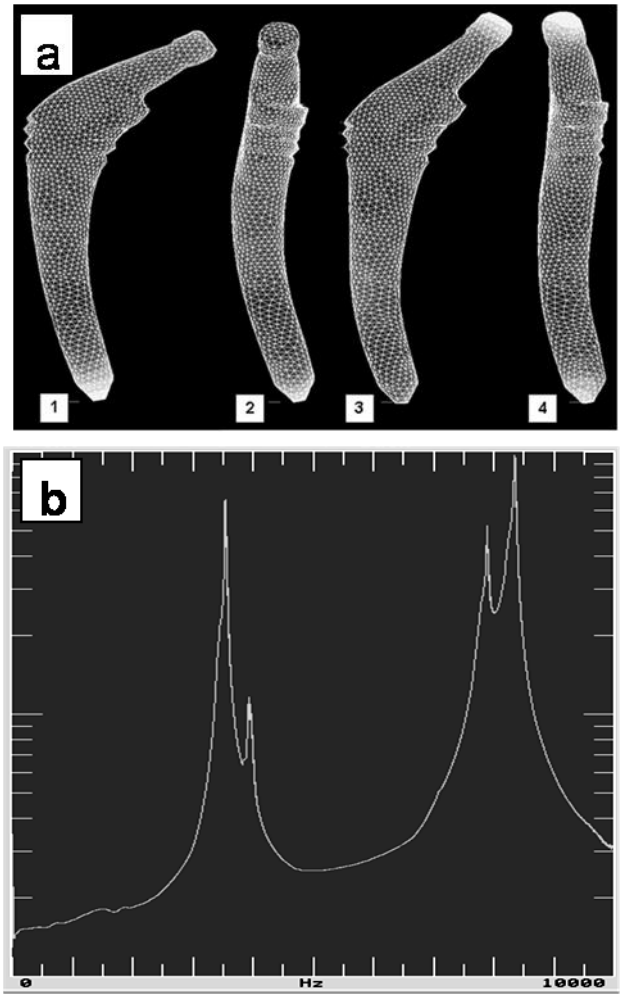

Figure 3.6: Resonance frequencies of the prosthesis
a. First four vibration mode shapes of an IMP model
b. Experimental FRF – first four resonance frequencies

In the range between 0 and 10 kHz the femur-IMP system presented 65 vibrational modes. For a contact area equal to 98% from the total surface of the stem, the first resonance frequency is 233 Hz and the last resonance frequency is 9874 Hz.

The resonance frequency shift between various contact situations is represented as a function of mode number in figure 3.7a and as a function of frequency in figure 3.7b.

The higher resonance frequency shifts between two subsequent steps were obtained for a contact area increase from 15% to 38% (brown graph). The resonance frequency differences are always positive but less important for a contact area increase from 38% to 56% (green graph) and from 56% to 76% (blue graph).

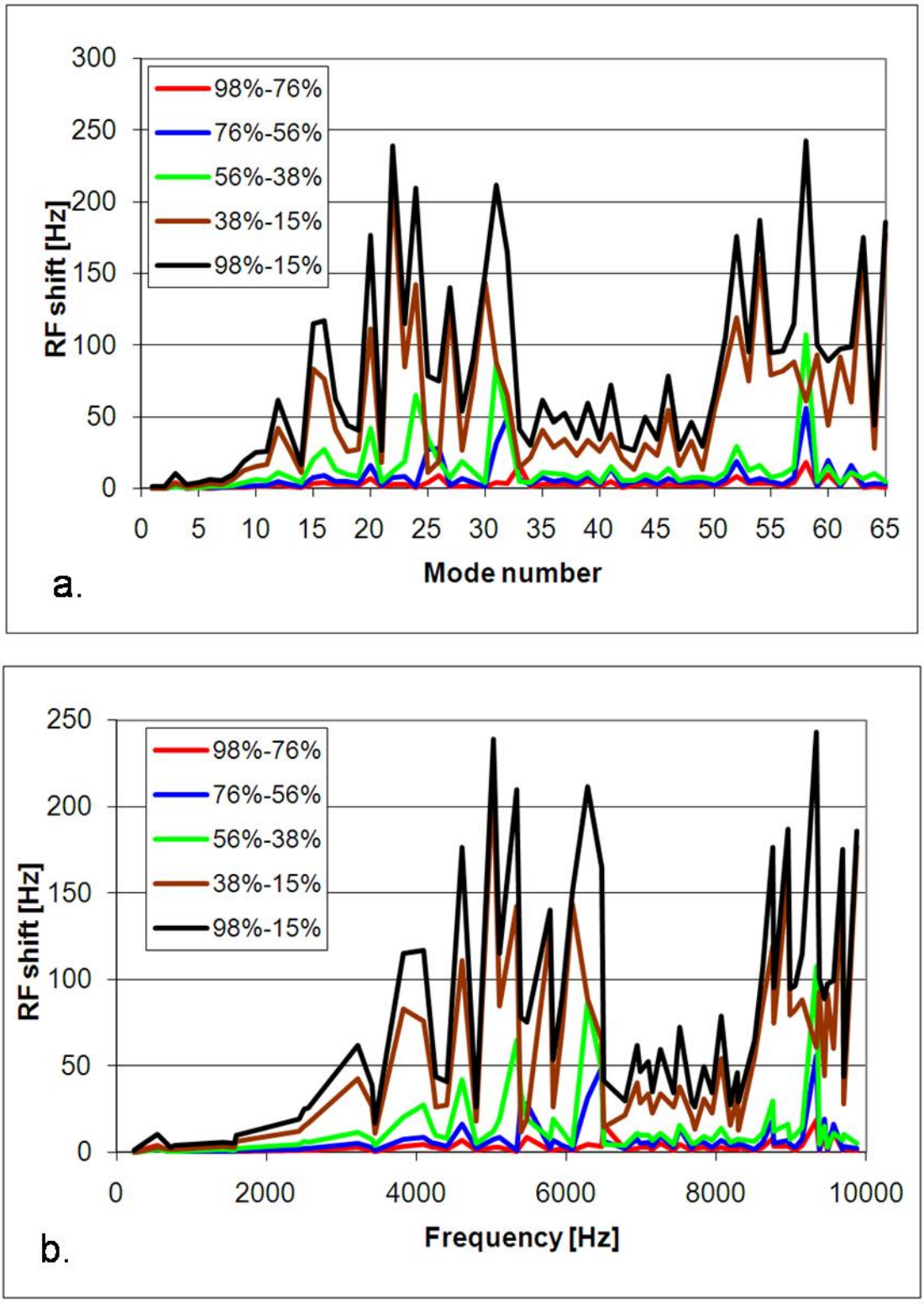

Figure 3.7: Resonance frequency shift

a. Represented as a function of mode number

b. Represented as a function of the frequency associated to 98% contact

In the case of the contact area change from 76% to 98% the resonance frequency increase is almost negligible (red graph). The black graph represents the resonance frequency shift between the so called “initial step” (15% contact area) and the “final step” (98% contact area).

As predicted earlier by our group (Jaecques et al. 2006, Pastrav et al. 2006), by other groups (Varini et al. 2006, Qi et al. 2003) and in agreement with the modal analysis theory (Heylen et al. 1997, Thomson 1998), an increase of the contact area between the prosthesis and the femur leads to an increase of the resonance frequencies. The most sensitive band is situated above the mode number 10 (higher than 2500 Hz). In addition to the fact that constant contact area increase was simulated (approximately 20% extra nodal contact per insertion stage), those shifts were less important for later insertion stages. The explanation could be that in the latest stages the contact area change diminishes with respect to the previous stage, i.e. from 15% to 38% the contact increase is 153%, but from 76% to 98% the contact increase is only 29%.

Although the finite element analysis did not establish a monotonous relationship between the mode number and the magnitude of the resonance frequency shift, in general the higher modes are more sensitive to the change in contact area. This observation is in accordance with previous work (Qi et al. 2003).

The explanation is that, in the case of simple bending modes of the femur, the stem acts just as an added mass (not involving a deformation of the prosthesis) and its influence depends more on the position (which was not varied in our analysis) than on the fixation conditions. In the case of more complicated mode shapes, associated with the higher modes, the interaction between the stem and the femur becomes more complicated and the interface conditions affect more the corresponding resonance frequencies.

In a third stage of the analysis, the contact was successively changed in the proximal, central and distal zones of the stem.

The zonal sensitivity to contact change found in previous studies (Qi et al. 2003) was confirmed. The same percentage of contact decrease (from 98% to 38%) provokes different resonance frequency shifts for the different contact zones (figure 3.8) While the contact area percentage was changing from 98% to 38% in one zone, the contact area was kept at 98% in the other two zones.

The dynamic behaviour of the IMP-femur system in free-free suspension is the most influenced by proximal contact decrease, whereas it is hardly affected by central contact decrease (the black dotted graph and respectively the red graph in figure 3.8).

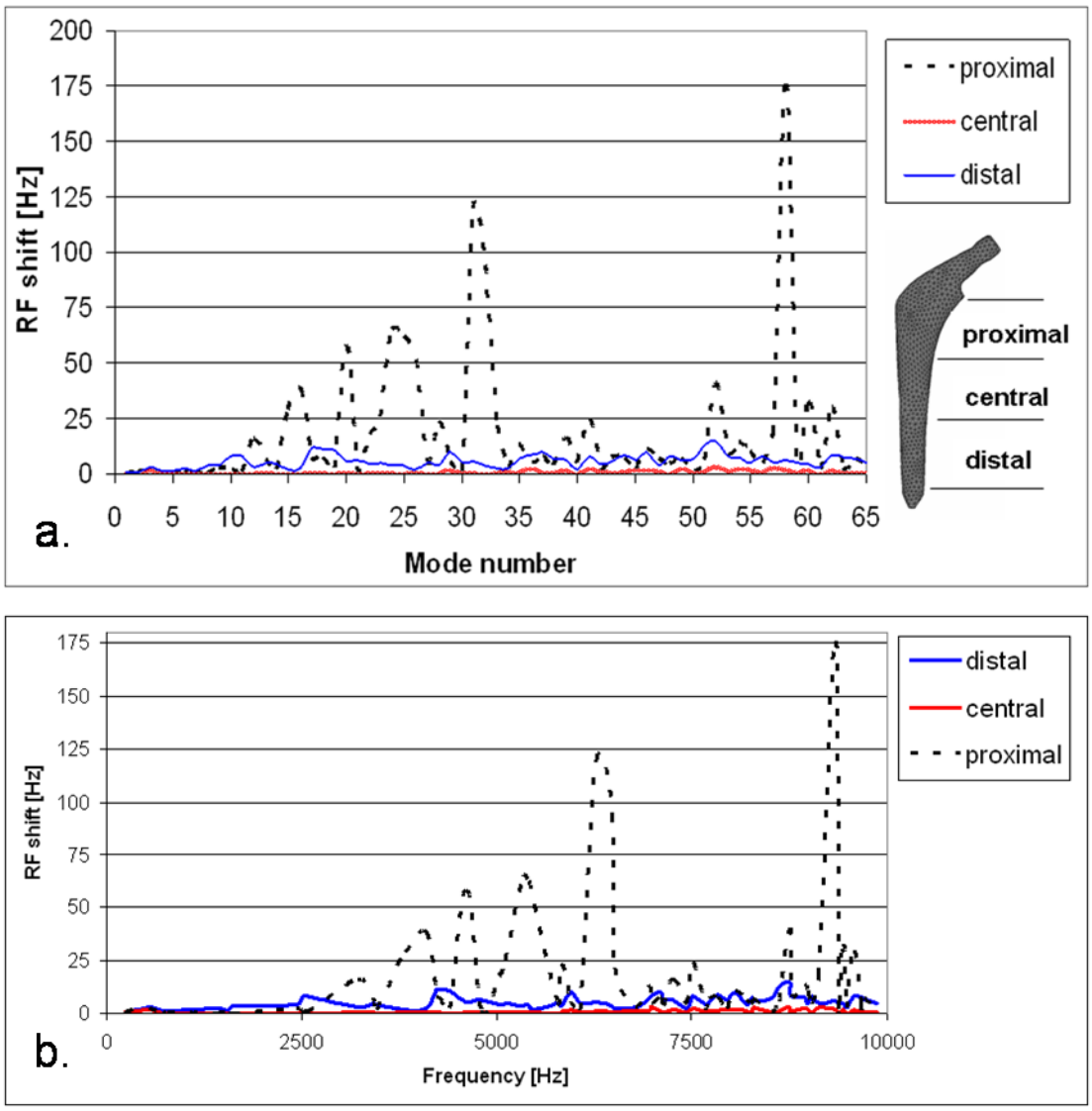

Figure 3.8: Resonance frequency shift plotted for proximal, central and distal part contact decrease (98 -38%), free-free suspension of the IMP-femur system

a. Represented as a function of mode number

b. Represented as a function of the frequency associated to 98% contact

Moreover, it was found that the boundary conditions significantly affect the impact that a zone has on the dynamic behaviour. By applying a fixed boundary condition to the central part of the cavity for example, the central contact zone became more important than the distal zone (the red and respectively the blue graphs in figure 3.9). When performing measurements in a per-operative clinical setting, there is no need for extensive measures to ensure an approximately 'free-free' suspension of the femur if the patient's leg is handled gently by the conventional procedures (Lowet et al. 1993, Van der Perre, Lowet 1996). It is only when the femur bone would be tightly clamped at the diaphysis with an instrument of

high stiffness, that there would be a possibility of significant change in the boundary condition.

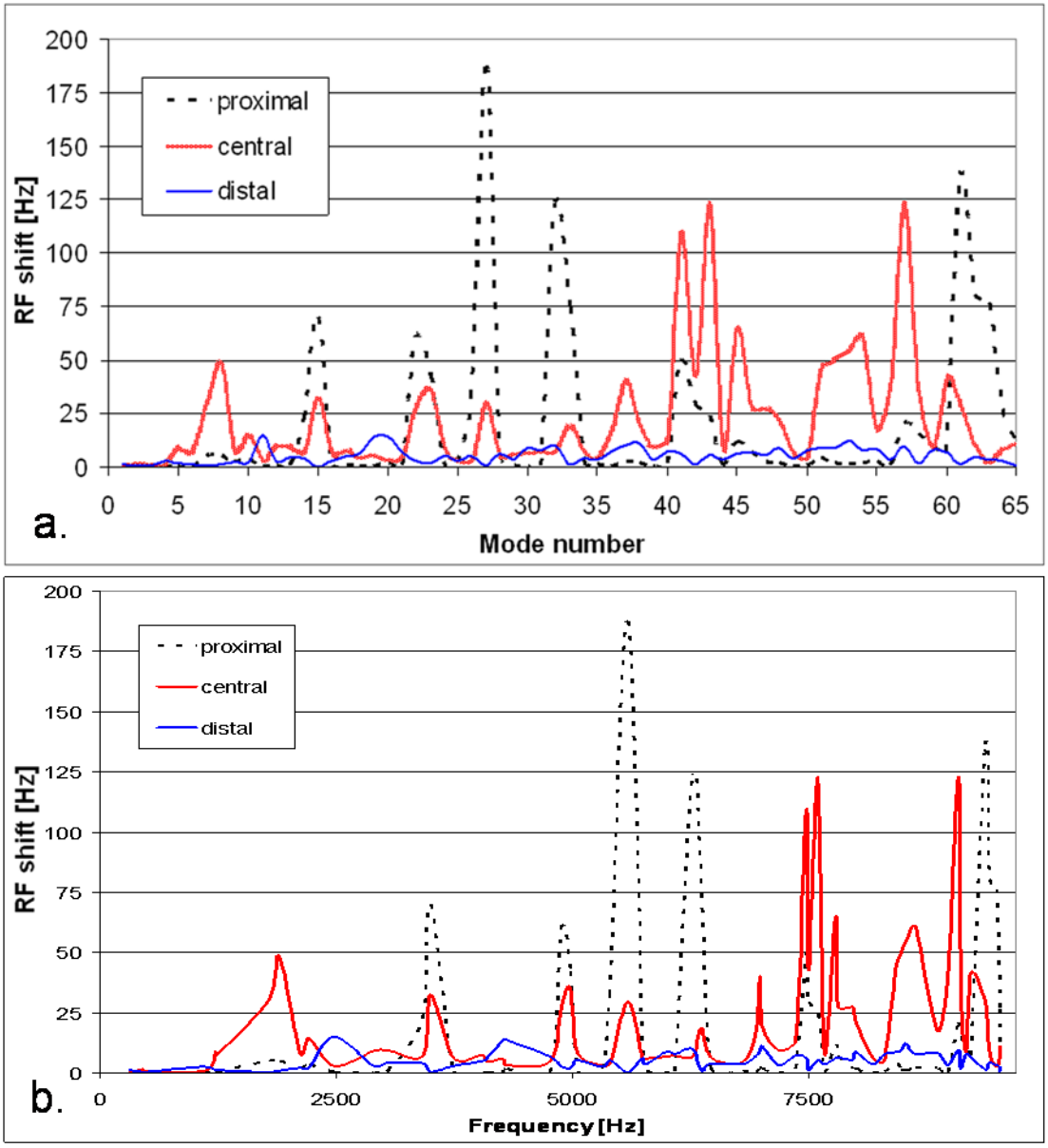

Figure 3.9: Resonance frequency shift plotted for proximal, central and distal part contact increase (38 -98%), femur fixed in the central part of the cavity

a. Represented as a function of mode number

b. Represented *as a function of the frequency associated to 98% contact*

3.3. Insertion simulation. Resonance frequencies change.

3.3.1. Methods

Although a similar finite element model of a femur with an implanted IMP was created to simulate the stem insertion, there are some differences (Asiminei et al. 2007).

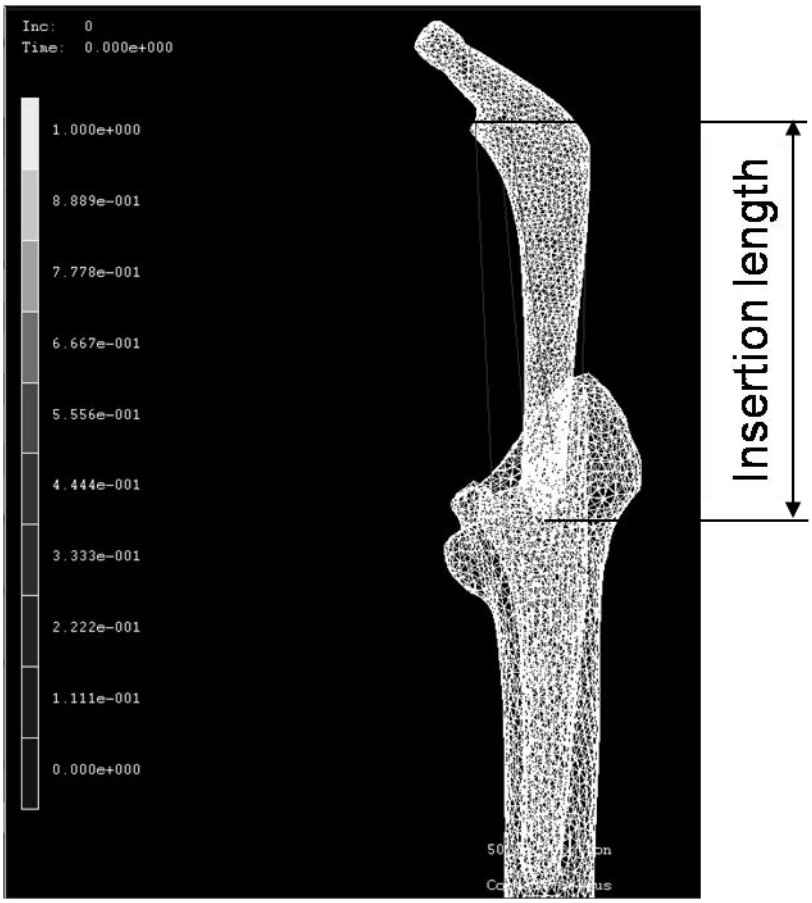

Figure 3.10: Initial stage of the insertion

The femur model was designed starting from the CT scan of a human femur. Based on the geometry and the size of the femur, the stem was selected to obtain a realistic bone-implant combination. The femoral cavity was created by a Boolean subtraction of the mould volume from the femur instead of a subtraction of the stem volume. In this way a more realistic model was obtained because in reality the mould reproduces the geometry of the femoral cavity while the stem has an optimised geometry that eliminates the possible interlocking problems. The marrow channel was created by extruding the distal part of the mould and then applying a Boolean subtraction of the obtained volume from the femur.

All the model components were meshed in MSC.Patran® using 4-node linear isoparametric three-dimensional tetrahedron elements with 2 mm edge size.

Linear elastic and isotropic material properties were assigned (El'Sheikh et al. 2003) for the cortical bone (Young's modulus E=16.2 GPa, Poisson ratio ν=0.36, mass density ρ=1990 kg/m3) and for the trabecular bone (E=389 MPa, ν=0.3, and ρ=500 kg/m3).

To simulate the insertion, the implant was placed at the entrance in the femoral cavity (figure 3.10) and forced to have a displacement equal to the "active" part of the stem (120 mm) along the longitudinal axis of the femur, by applying an increasing force. The femur was fixed at the condyles.

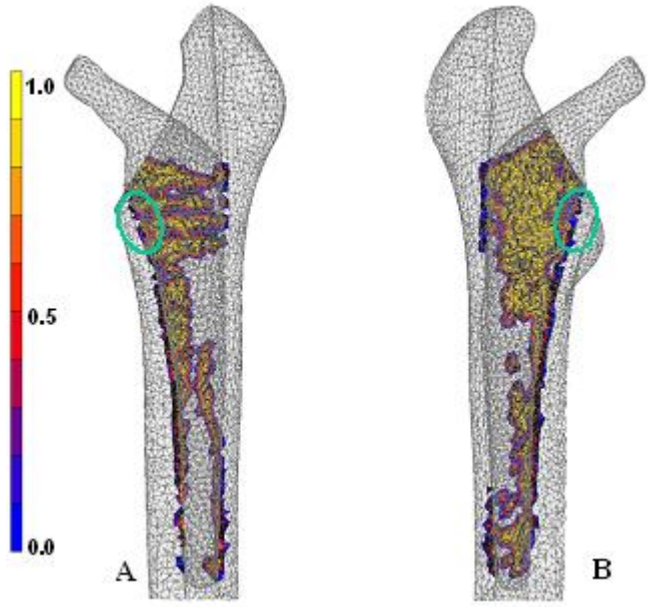

Figure 3.11: The contact zones after the last step of insertion – end of insertion (coloured zones)
(A) dorsal view
(B) frontal view

During the insertion the prosthesis does not perform only a translation along the femoral axis but it tilts and rotates as result of contact reaction forces finding the minimum resistance way to the end point. Due to the irregular stem shape the total contact surface and the contact area distribution showed irregular evolution during the insertion. The prosthesis was considered fully inserted when maximal contact was reached in the proximal third of the stem, especially in the calcar zone (figure 3.11).

3.3.2. Results and discussion

The evolution of the contact during the insertion is shown in figure 3.12. In the first four steps the stem displacement is 102 mm and the number of nodes in contact increases from 0 to 6.5%.

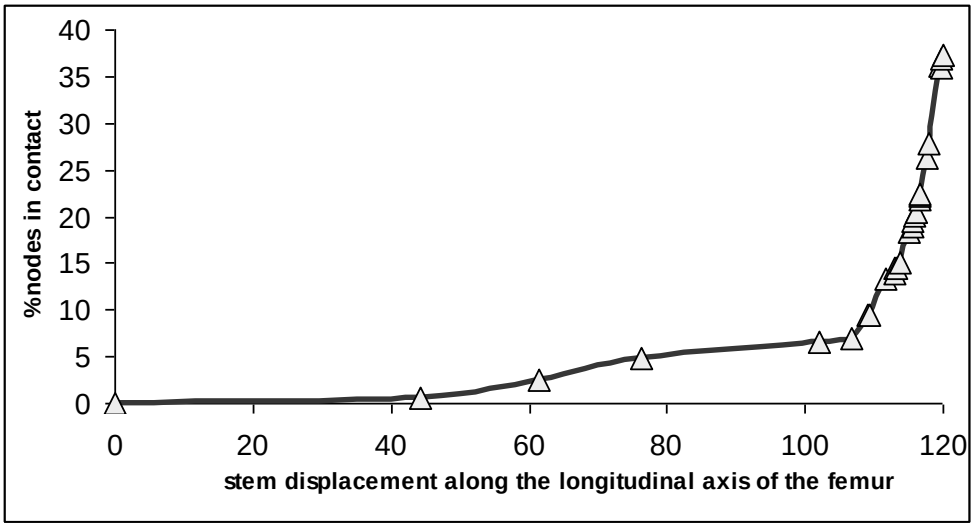

Figure 3.12: Contact evolution during the stem insertion

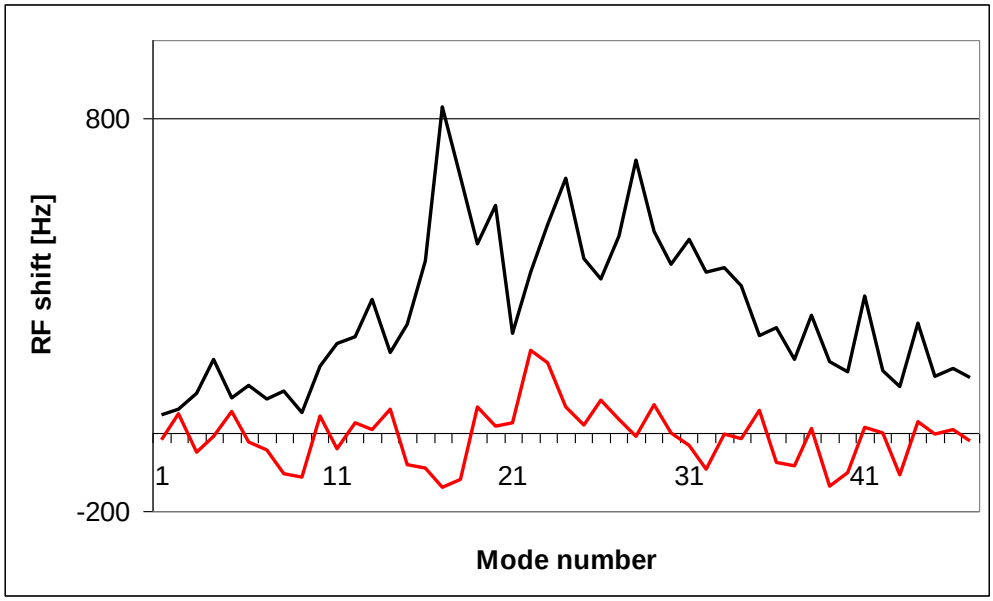

Figure 3.13: Resonance frequency shift between different insertion steps
(black) contact change from 27.8% to 36.1%
(red) contact change from 36.1% to 36% (sic)

During the next insertion steps the contact increase is more important and, as a consequence, the resistance against the displacement increases as well. At the end of the

insertion the number of nodes in contact represents 37.3% of the total number of nodes of the femoral cavity.

The resonance frequency shift between different insertion steps is represented in figure 3.13 as a function of vibration mode number.

The black graph represents the resonance frequency shift when an important contact increase (from 27.8% to 36.1%) was observed between two successive insertion steps. In this case the resonance frequencies increased for all vibration modes.

The red graph corresponds to the situation when the displacement and the contact configuration hardly changed. For a stem displacement of 0.2 mm, the contact changed from 36.1% to 36%. This contact area decrease might be the result of the remeshing that is performed after each insertion step. The resonance frequency change is less important and different modes are differently influenced. Some resonance frequencies increased while others decreased. [4]

3.4. Effect of an inserted prosthesis: added mass effect versus added stiffness effect

In this section the modal shapes obtained for finite element models of the femur prepared for stem insertion and of the femur-stem structure at different sizes of contact surface are discussed in correlation to the resonance frequency changes.

The resonance frequencies of the first 20 modes corresponding to the femur without prosthesis, femur with prosthesis at 15% contact, and femur with prosthesis at 98% contact are presented in table 3.5, columns c2, c3, and c4 respectively.

The frequency changes between these situations are presented in the columns c5, c6, and c7. The frequency shifts calculated in column c5 are represented graphically in the figure 3.14.

The resonance frequency shifts between the femur-implant structure at different sizes of contact surface and the femur prepared for stem implantation are presented in figure 3.15 for the first 65 vibrational modes.

[4] The study of the contact evolution during the insertion and the influence on the vibrational behaviour is a part of a larger study realised in collaboration with the PhD student Aida Asiminei (Pastrav et al. 2008). The detailed analysis of the contact, stress and strain evolution is the object of her thesis.

Table 3.5: Resonance frequencies corresponding to the first 20 vibrational modes

Mode number	Resonance frequency			Frequency difference		
	Femur without prosthesis	Femur with prosthesis totally inserted				
		Contact 15%	Contact 98%	c4-c3	c4-c2	c3-c2
c1	c2	c3	c4	c5	c6	c7
	Hz	Hz	Hz	Hz	Hz	Hz
1	263.6	231.2	232.6	1.4	-31	-32.4
2	276.6	251.9	253.4	1.5	-23.2	-24.7
3	646.2	529.7	540.1	10.4	-106.1	-116.5
4	781.6	715.3	718.2	2.9	-63.4	-66.3
5	819.9	773.1	777.1	4	-42.8	-46.8
6	1517	1417	1423	6	-94	-100
7	1562	1563	1568	5	***6***	***1***
8	1772	1593	1603	10	-169	-179
9	2330	2421	2440	19	***110***	***91***
10	2405	2481	2506	25	***101***	***76***
11	2454	2534	2560	26	***106***	***80***
12	3117	3153	3215	62	***98***	***36***
13	3293	3375	3414	39	***121***	***82***
14	3401	3438	3455	17	***54***	***37***
15	3797	3712	3827	115	***30***	-85
16	3922	3978	4095	117	***173***	***56***
17	3963	4157	4219	62	***256***	***194***
18	4144	4212	4256	44	***112***	***68***
19	4253	4361	4402	41	***149***	***108***
20	4302	4429	4605	176	***303***	***127***

In the finite element model presented in section 3.2, the implanted stem influences the resonance frequencies of the femur in two ways mainly:

- the added mass determines a resonance frequency decrease, while
- the added stiffness implies a resonance frequency increase.

The proportion between these two influences is strongly dependent on the mode shapes of the femur and stem and on the amount of contact existing between the bone and the implant. Eight examples are presented in figures 3.16–3.23. Nevertheless, the mode shapes of the independent femur and stem interfere and the resulting mode shapes of the femur-stem structure are influenced by the size of contact surface.

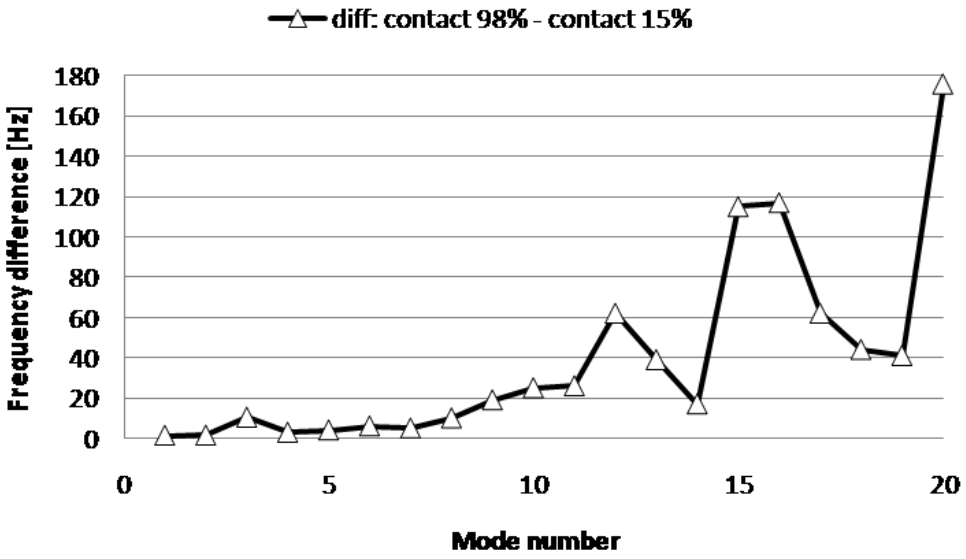

Figure 3.14: Resonance frequency shift after increasing the contact area between the prosthesis and the femur from15% to 98%

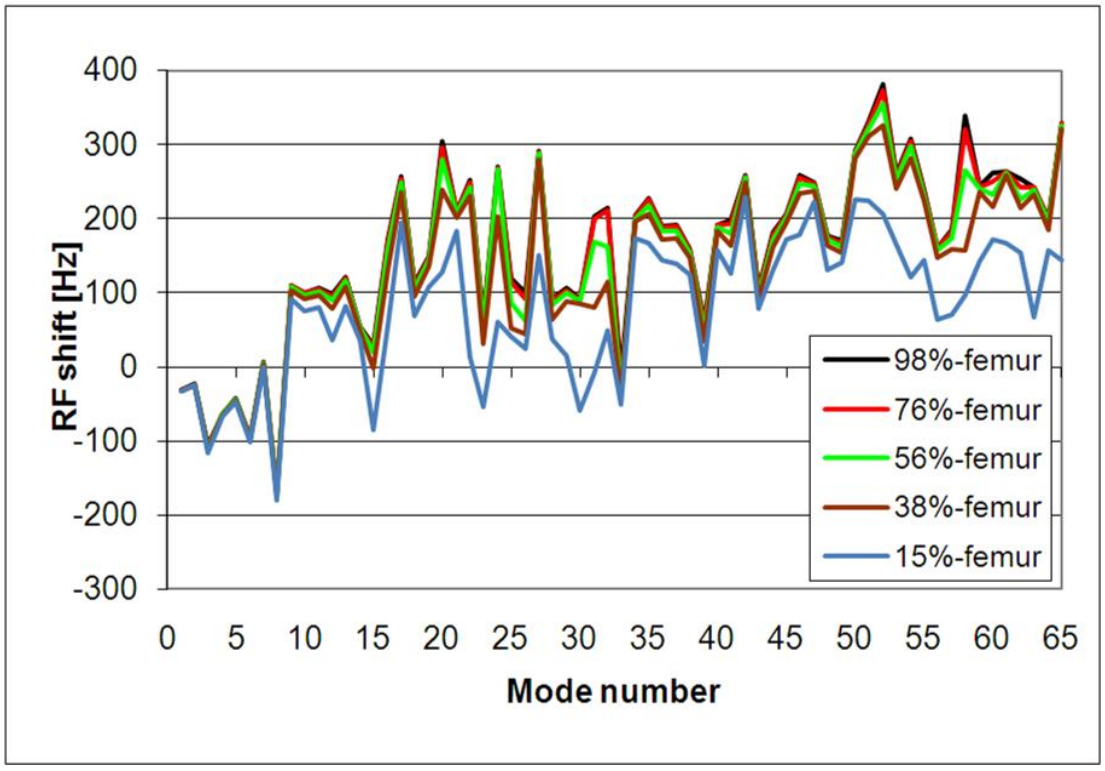

Figure 3.15: Resonance frequency change between the femur with the prosthesis fully inserted and the femur without prosthesis.

Blue graph: 15% contact between the implant and the bone after insertion
Brown graph: 38% contact between the implant and the bone after insertion
Green graph: 56% contact between the implant and the bone after insertion
Red graph: 76% contact between the implant and the bone after insertion
Black graph: 98% contact between the implant and the bone after insertion

Analysing the graphs presented in figure 3.15, it can be observed that the resonance frequencies corresponding to the first six modes of the system femur-implant are lower than the respective first six resonance frequencies of the femur, indicating that the influence of the added mass is more important than the influence of the added stiffness. Moreover, for these modes, the contact area increase results in relative small resonance frequencies increase.

In the first mode the prosthesis is not deformed and acts as an added mass only. In figure 3.16a the first bending mode of the femur without prosthesis is presented. Comparing figures 3.16a, 3.16b, and 3.16c it can be observed that the deformation of the femur is hardly affected by the presence of the prosthesis. A contact area increase from 15% to 98% of the stem surface results in a resonance frequency increase of 1.4 Hz only.

The influence of the contact area change is more important in the case of the third resonance frequency (figure 3.14) which corresponds to a torsional mode (figure 3.17). A contact area increase from 15% to 98% of the stem surface results in a resonance frequency increase of 10.4 Hz. The influence of the prosthesis on the deformation of the femur is still difficult to observe.

The mode #7 is the first mode where the influence of the added stiffness overcomes the influence of the added mass and a deformation of the prosthesis similar to one of its bending modes is visible (figure 3.18). The presence of the stem determines a phase change.

Starting with mode #9 the resonance frequencies of the femur-implant structure at 98% contact are always higher than the corresponding resonance frequencies of the femur, indicating a strong influence of the added stiffness. For few modes (#15, #23, #30, #33) the influence of the added mass is still superior to the influence of the added stiffness, but only for lower values of contact area, i.e. 15 - 38% (figure 3.15).

The mode #15 is represented in figure 3.19. The prosthesis is deformed and, due to the contact increase, a phase change and other modifications can be observed between the modal shapes represented in figures 3.15b and 3.15c.

Although the influence of the added stiffness is relatively important for the higher and complicated modes, the sensitivity to the size of contact surface is variable. For example, the modes #20 (figure 3.20) and #32 (figure 3.21) are very sensitive to the contact change. The frequency shift between 15% and 98% contact is 174 Hz for mode #20 and 164 Hz for mode #32. The presence of the prosthesis and the contact change clearly influence these two mode shapes of the femur. Such modes are very important for the assessment of the stability of the implant.

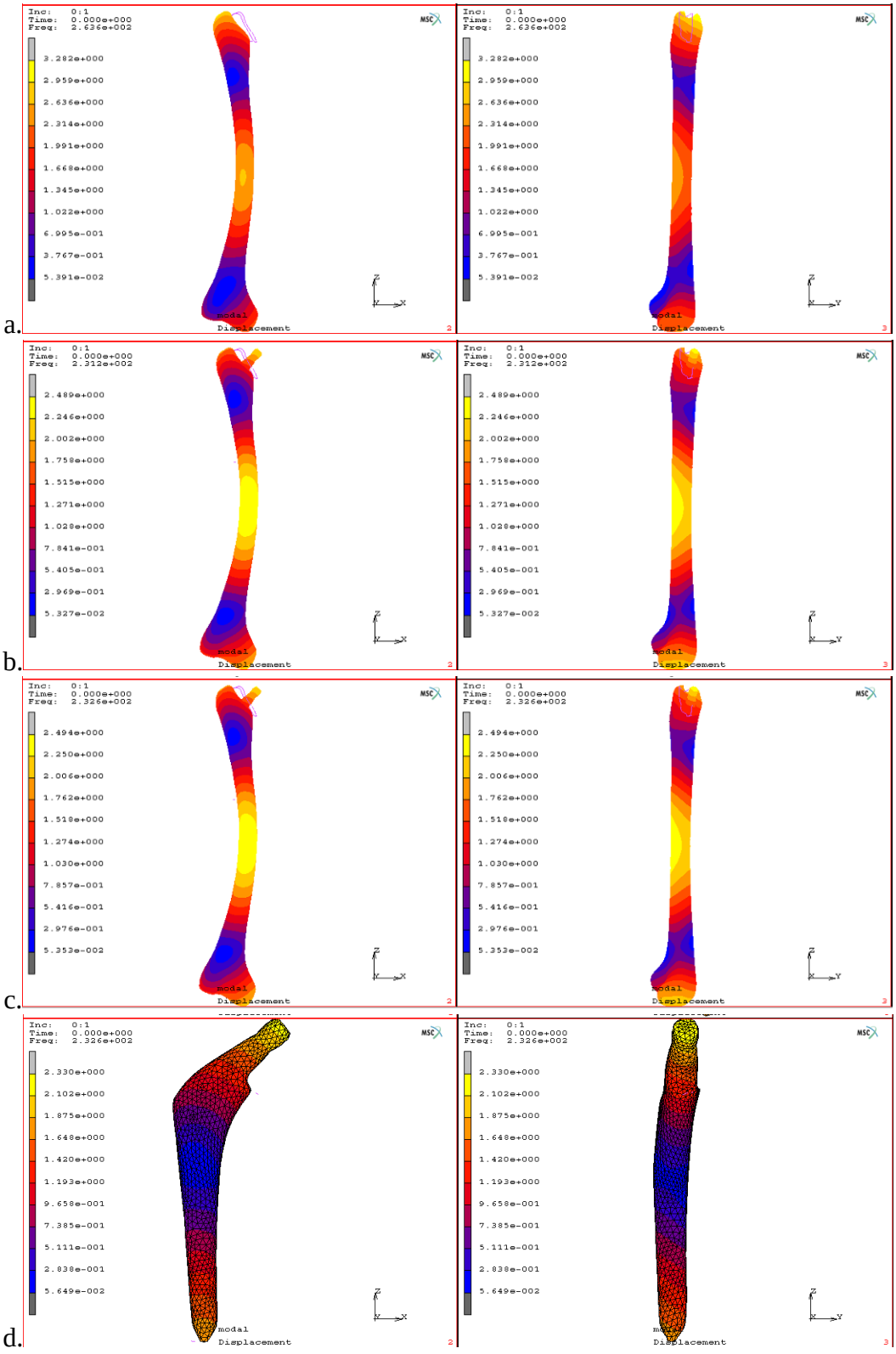

Figure 3.16: Mode #1. Left: antero-posterior view, Right: medio-lateral view

a. Femur (263.6 Hz). b. Femur & stem (231.2 Hz, 15% contact)

c. Femur & stem (232.6 Hz, 98% contact). d. Same as c, only the stem is visible.

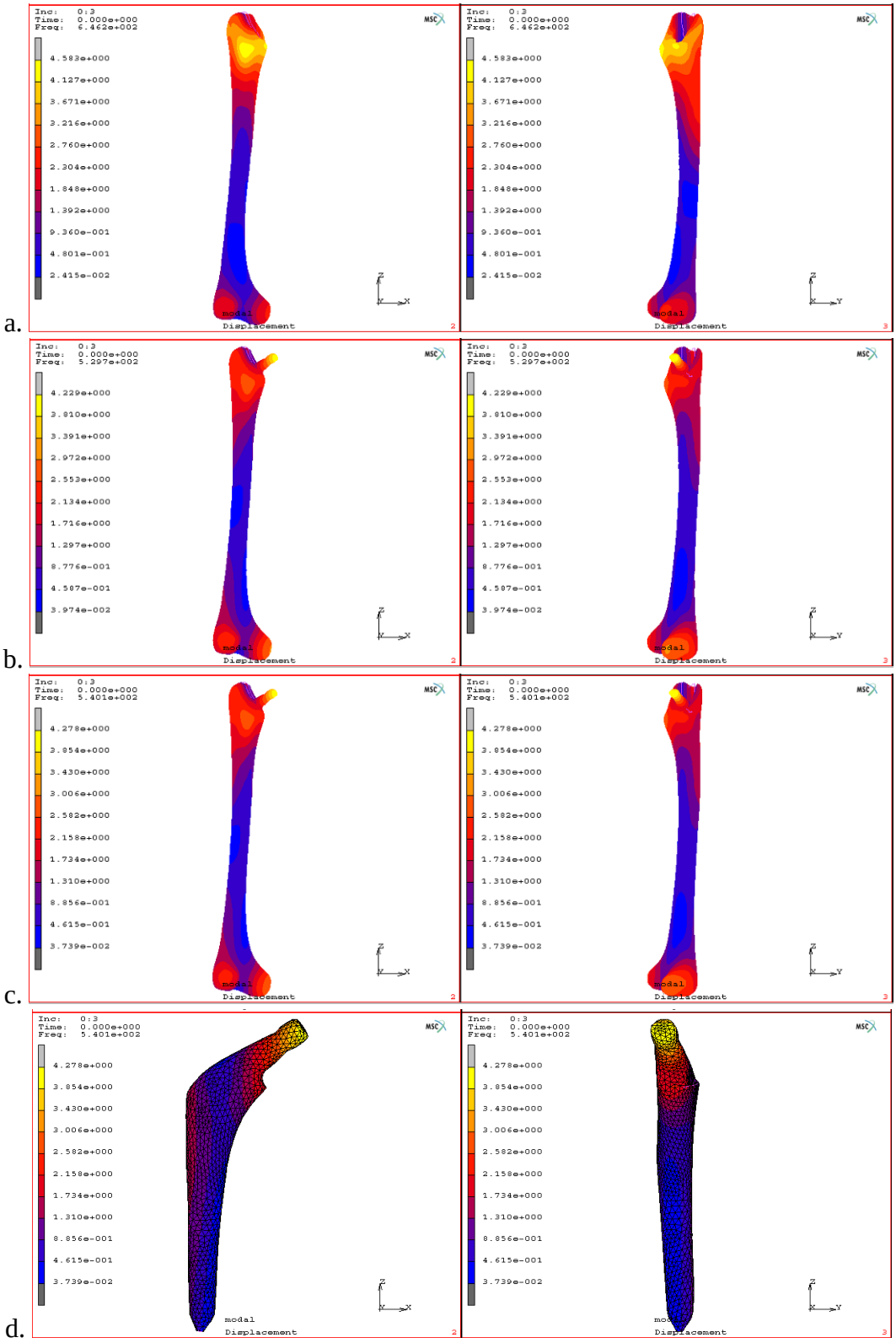

Figure 3.17: Mode #3. Left: antero-posterior view, Right: medio-lateral view

a. Femur (646.2 Hz). b. Femur & stem (529.7 Hz, 15% contact)

c. Femur & stem (540.1 Hz, 98% contact). d. Same as c, only the stem is visible.

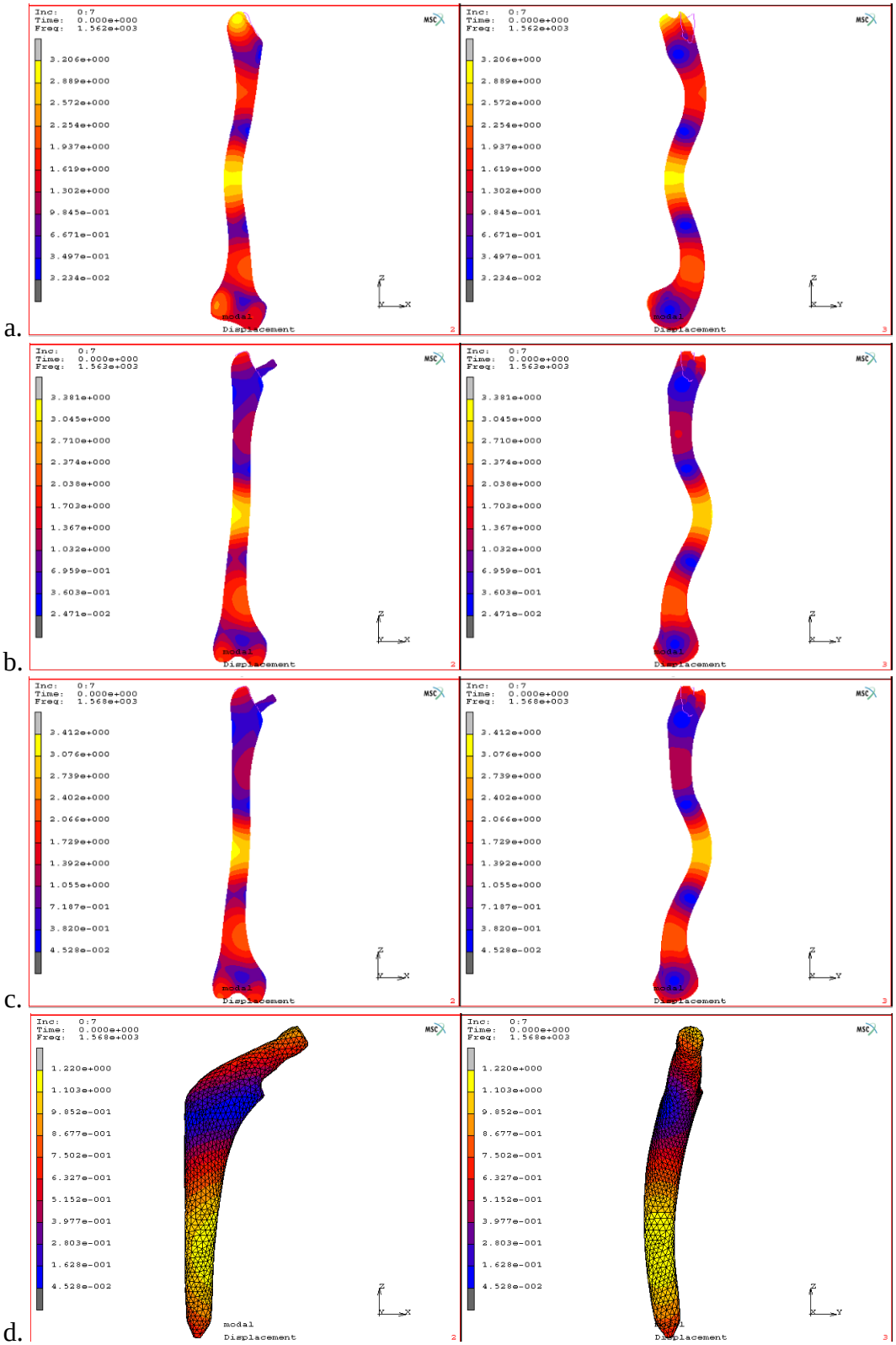

Figure 3.18: Mode #7. Left: antero-posterior view, Right: medio-lateral view

a. Femur (1562 Hz). b. Femur & stem (1563 Hz, 15% contact)

c. Femur & stem (1568 Hz, 98% contact). d. Same as c, only the stem is visible.

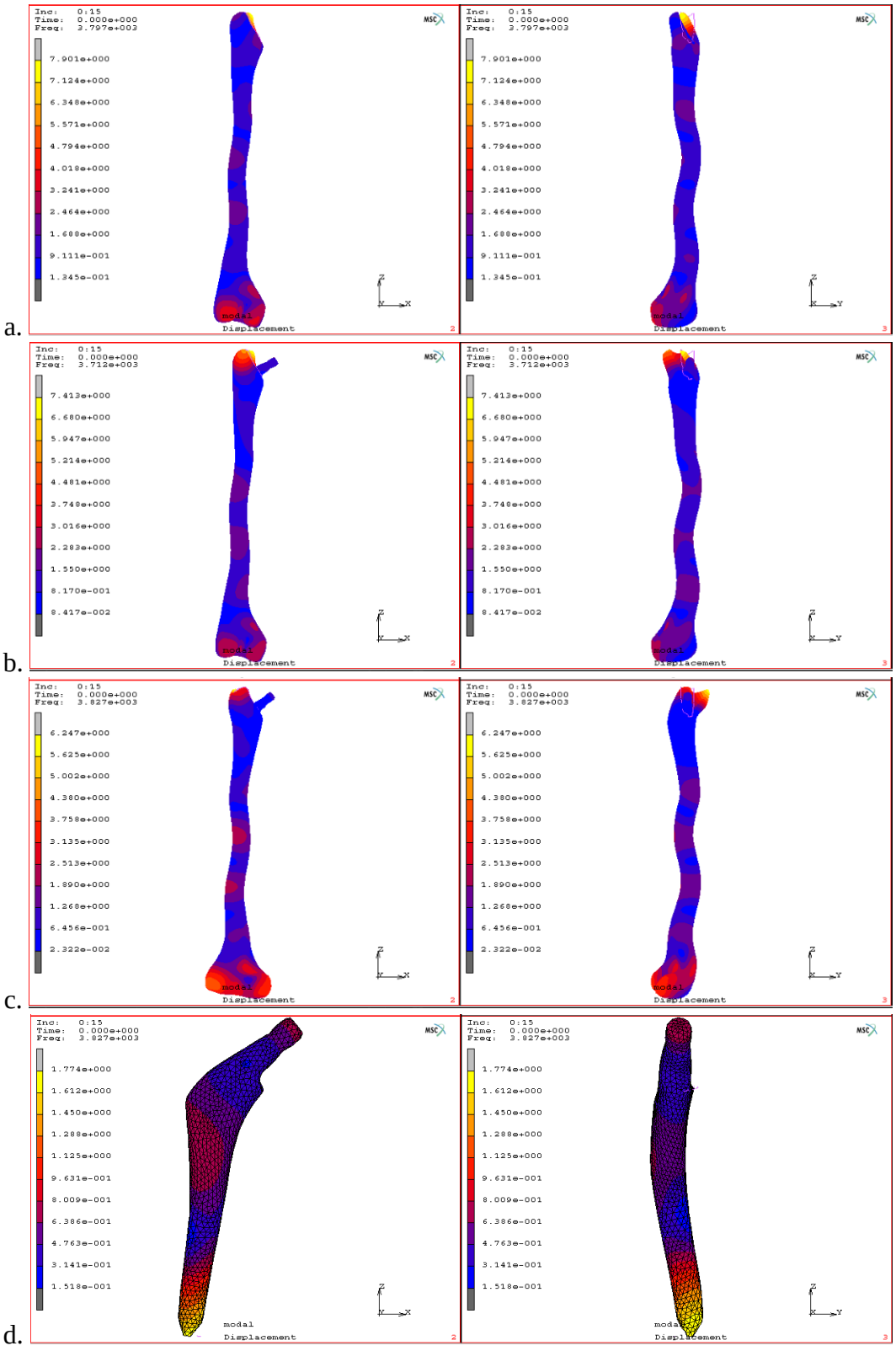

Figure 3.19: Mode #15. Left: antero-posterior view, Right: medio-lateral view

a. Femur (3797 Hz). b. Femur & stem (3712 Hz, 15% contact)

c. Femur & stem (3827 Hz, 98% contact). d. Same as c, only the stem is visible.

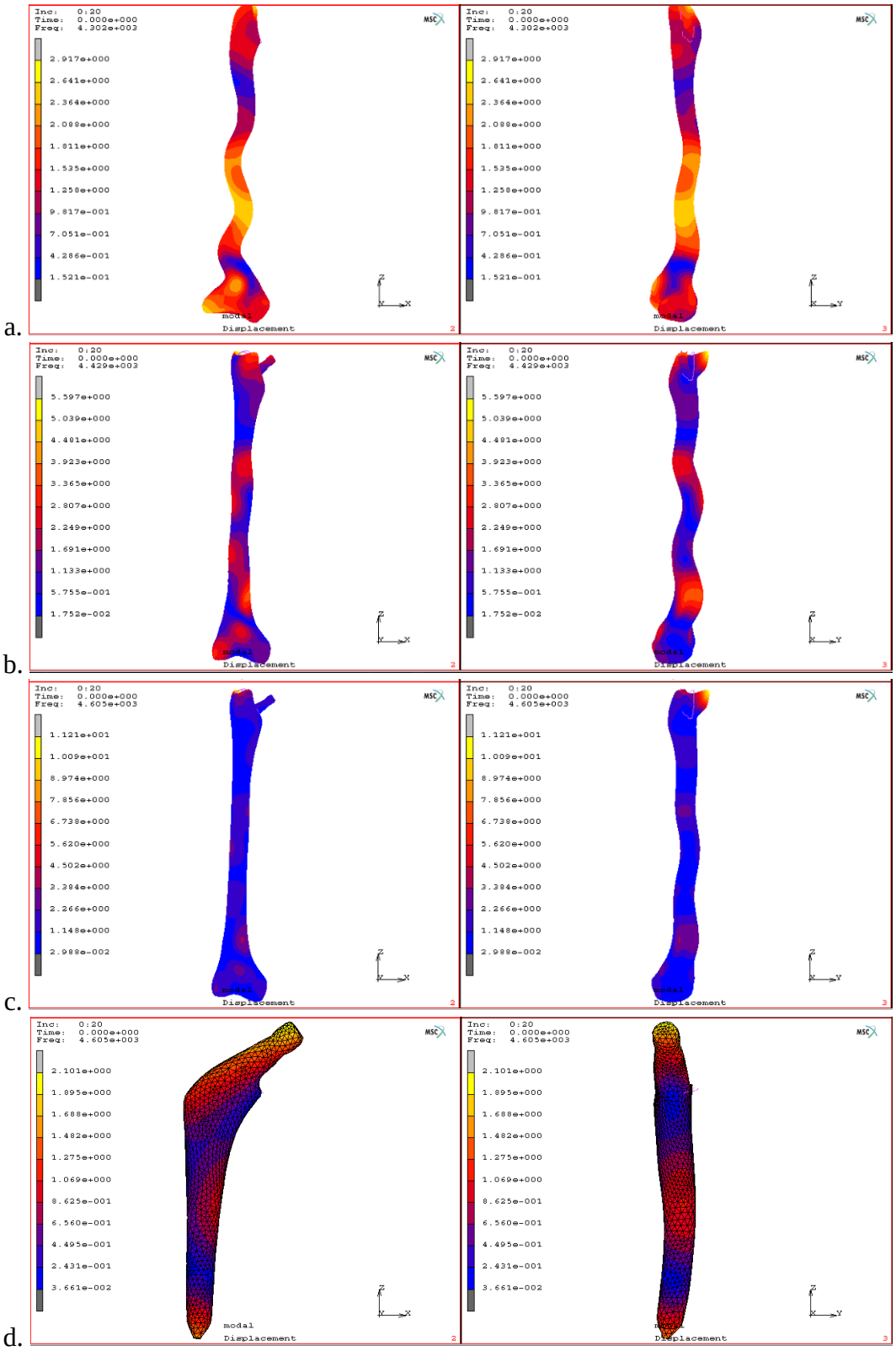

Figure 3.20: Mode #20. Left: antero-posterior view, Right: medio-lateral view

a. Femur (4302 Hz). b. Femur & stem (4429 Hz, 15% contact)

c. Femur & stem (4605 Hz, 98% contact). d. Same as c, only the stem is visible.

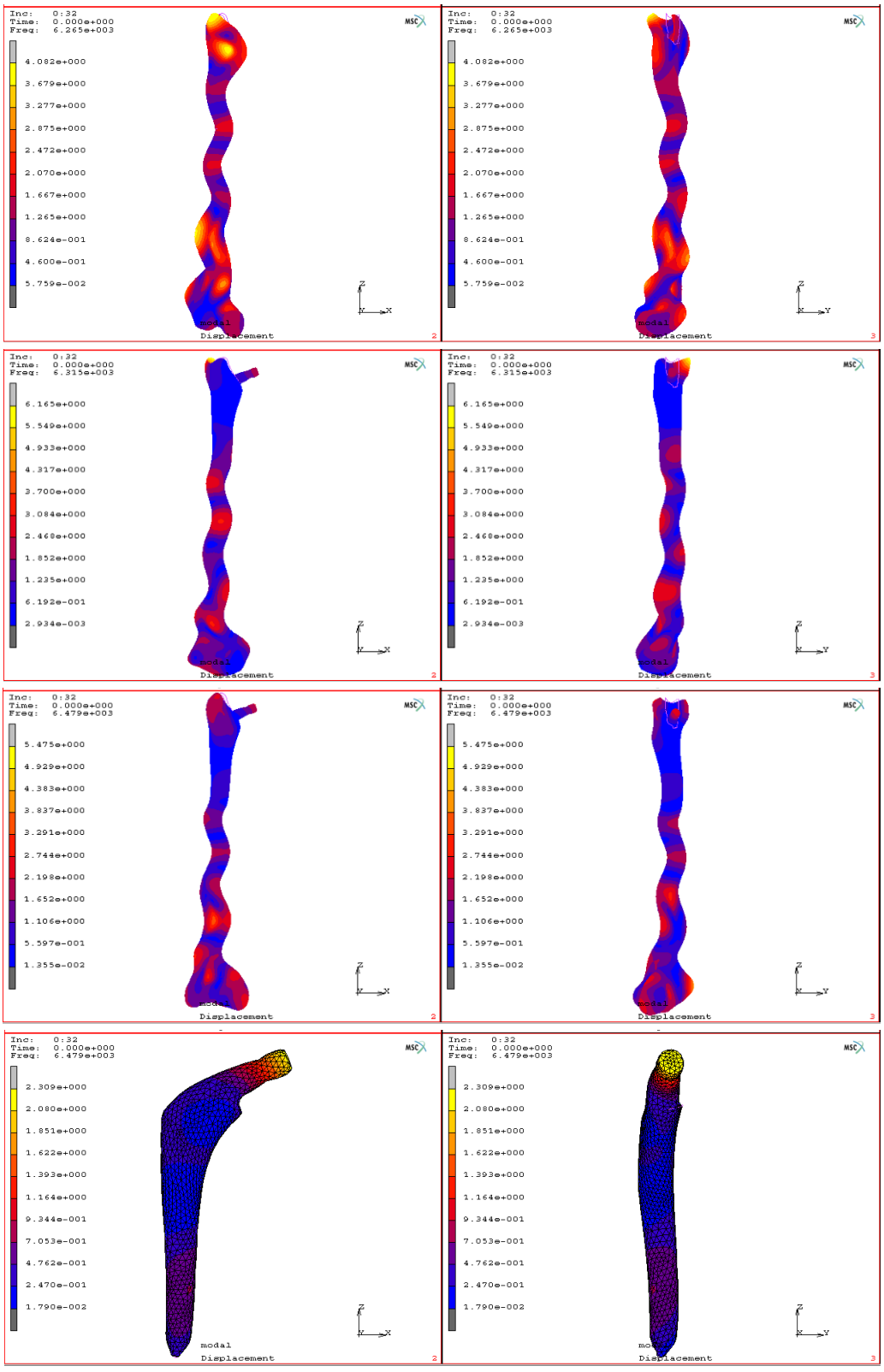

Figure 3.21: Mode #32. Left: antero-posterior view, Right: medio-lateral view

a. Femur (6265 Hz). b. Femur & stem (6315 Hz, 15% contact)

c. Femur & stem (6479 Hz, 98% contact). d. Same as c, only the stem is visible.

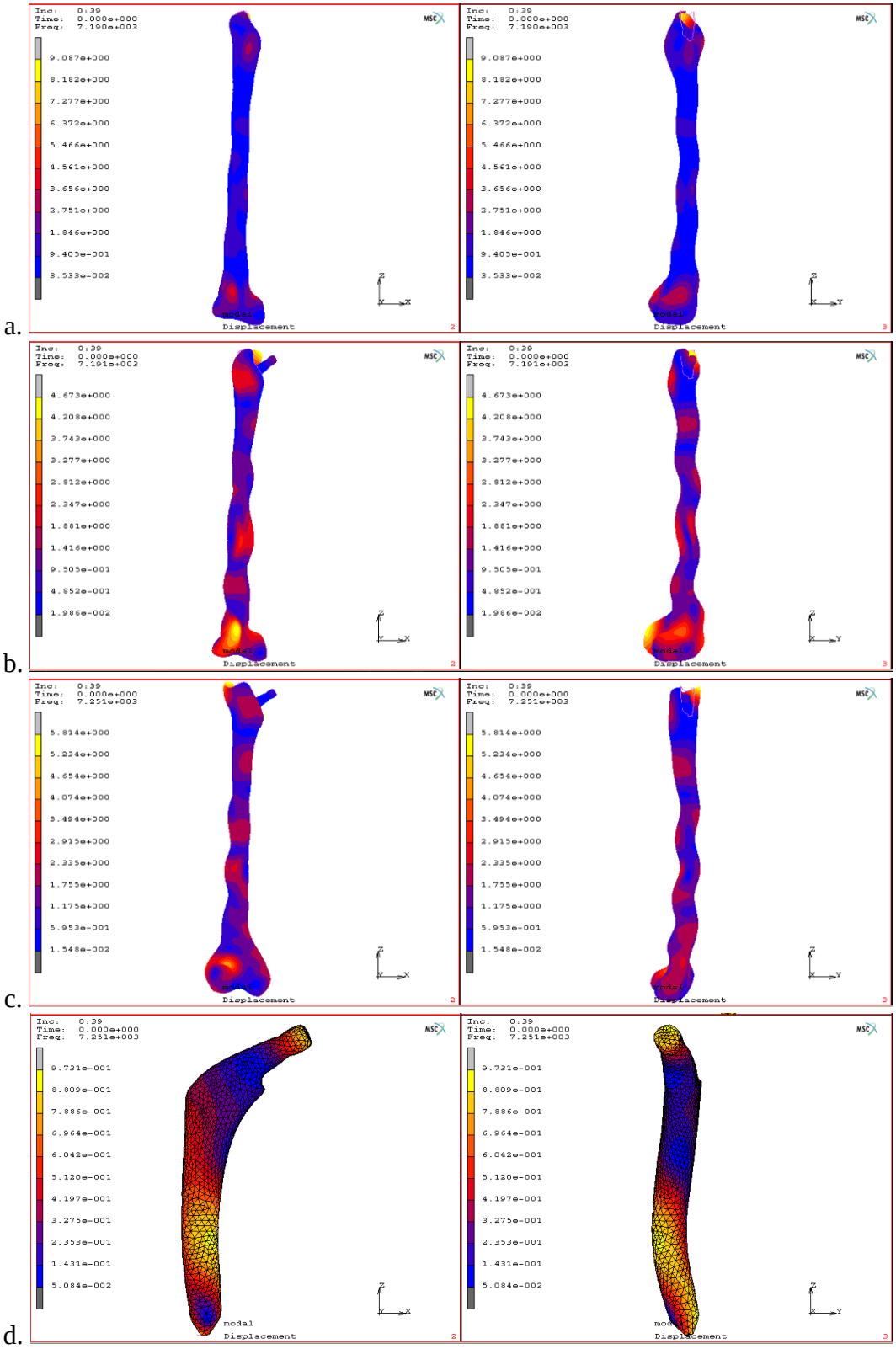

Figure 3.22: Mode #39. Left: antero-posterior view, Right: medio-lateral view

a. Femur (7190 Hz). b. Femur & stem (7191 Hz, 15% contact)

c. Femur & stem (7251 Hz, 98% contact). d. Same as c, only the stem is visible.

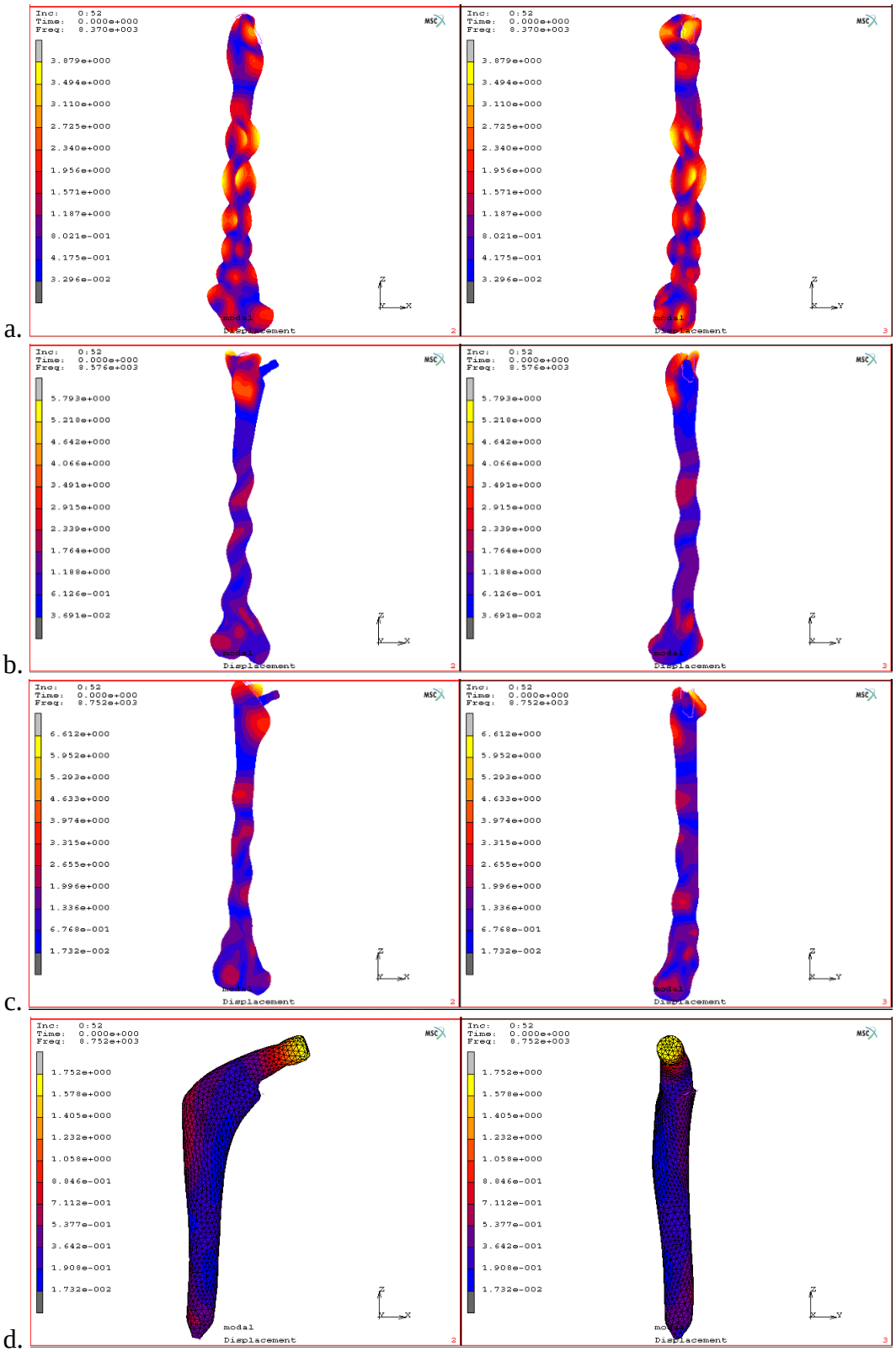

Figure 3.23: Mode #52. Left: antero-posterior view, Right: medio-lateral view

a. Femur (8370 Hz). b. Femur & stem (8576 Hz, 15% contact)

c. Femur & stem (8752 Hz, 98% contact). d. Same as c, only the stem is visible.

The mode #39 (figure 3.22) is less sensitive, the corresponding frequency shift being 60 Hz only. Although the prosthesis is deformed, the contact change influence on this resonance frequency of the femur is not so important, probably because the stem vibrates in phase with the bone (figures 3.22c and 3.22d).

The mode #52, presented in figure 3.23, is an example of mode with a very complicated shape that suffers important transformations due to the presence of the prosthesis and due to the contact change. The frequency shift is important as well.

3.5. Conclusions

The results of the reported finite element analysis are in agreement with observations from previous experimental work: contact increase causes positive resonance frequency shifts and the dynamic behaviour is most influenced by proximal contact changes.

In addition, it was found that the same percentage of contact increase causes different resonance frequency shifts for different insertion stages. Depending on the amount of contact that is already established, shifts are larger or smaller.

Although the finite element analysis did not establish a monotonous relationship between the mode number and the magnitude of the resonance frequency shift, in general the torsional and higher bending and complicated modes are more sensitive to the change in contact area which is in agreement with other finite element studies (Qi et al. 2003).

This phenomenon can be understood from the fact that in the lower bending modes the prosthesis moves as a rigid body and only exerts an added mass effect (figure 3.16) whereas in the higher modes the interaction between the stem and the femur becomes more complicated (figures 3.19-3.23) and the interface conditions affect the resonance frequencies.

The influence of the boundary conditions on the sensitivity of the contact zones implies the possibility to decide about distal, central and proximal contact by altering the boundary conditions. Vibration analysis of a free-free suspended bone-prosthesis system gives information about proximal and distal contact whereas a centrally fixed femur gives information about central contact variation.

4. Per operative study

From the previous studies presented in chapters 2 and 3, a per-operative protocol using a vibration analysis technique for the characterisation of the primary bone-prosthesis stability was derived and tested in 83 patients.

The frequency response function change provides reliable information regarding the evolution of stability of the stem-femur system during the insertion. The protocol described in this paper can be used to accurately detect the insertion end point and to reduce the risk for intraoperative fracture.

The results of the per-operative study were published in Ortopedia Traumatologia Rehabilitacja, (Mulier et al. 2008) and in the Journal of Orthopaedic Surgery and Research (Pastrav et al. 2009b).

4.1. Introduction

Beside the design, material composition and surface characteristics of the implant, the initial per-operative fixation of the stem in the femoral bone has a critical influence on its long term fixation stability. This is especially the case for non cemented, press-fit fixed stems.

Nowadays objective intra-operative assessment of primary stem stability is a challenge, surgeons having to rely on their clinical experience, which consists mainly of a sense of mechanical stability when exerting axial and/or torque forces on the prosthesis. Moreover, excessive press-fitting of a THR femoral component can cause intra-operative fractures with an incidence of up to 30 % in revision cases (Meek et al. 2004). Therefore there is a need for an objective and quantitative technique for the per-operative assessment of primary stem stability.

This thesis presents the development and the first clinical application of a per-operative vibration analysis technique for the mechanical characterization of the primary bone-prosthesis stability.

In chapter 2 the feasibility and validity of a vibration analysis technique for the assessment of the femur-stem fixation in vitro was demonstrated (Jaecques et al. 2004, 2005, Pastrav et al. 2005, 2008). The stem insertion process was performed on a dry cadaver femur and synthetic composite femurs and the FRF change was analysed.

In chapter 3 finite element analyses were presented that were made to gain insight into the dependence of the FRF on system parameter variations.

In this chapter the vibration analysis technique is applied for the per-operative assessment of fixation stability in 83 THR patients who obtained an intra-operatively manufactured prosthesis (IMP) provided by Advanced Custom Made Implants, Leuven, Belgium. The IMP approach aims at optimal stem stability through a maximum fit and fill of the femoral cavity (Mulier et al. 1989, see appendix).

The objective of this clinical study was to apply and evaluate an endpoint criterion (as developed in chaper 2) for the insertion of the stem by successive surgeon-controlled hammer blows. The endpoint-of-insertion criterion is based upon the Pearson's correlation coefficient R between the FRFs of two successive insertion stages. The FRF evolution is also analysed using the normalised cross correlation function (NCCF) as described in sections 2.3.1 and 2.3.2.

4.2. Materials and methods

From the previous in vitro studies a protocol was derived to be applied in per-operative conditions.

The prosthesis neck was attached to a shaker (Bruel & Kjaer, Naerum, Denmark, model 4810) using a stinger provided with a clamping system. The stinger is approximately perpendicular to the plane defined by the longitudinal axes corresponding to the stem and to the neck. The excitation was realized through white noise in the range 0-12.5 kHz. The input force and the response acceleration were measured in the same point with an impedance head (PCB Piezotronics, Depew, NY, USA, model nr 288D01) mounted between the shaker and the stinger.

The excitation system used low amplitude vibrations and introduced approximately 0.5W of power into the femur-prosthesis system. This is considered as safe and no adverse effects have been reported by other authors using a similar excitation system (Nakatsuchi et al. 1996, Nikiforidis et al. 1990). The experimental setup is shown in figure 4.1.

The FRF was measured (64 averages) and recorded by a Pimento vibration analyser (LMS International, Haasrode, Belgium) connected to a portable computer provided with the appropriate software (Pimento 5.2, LMS International, Haasrode, Belgium). The vibration analyser generates the excitation signal which is amplified and sent to the shaker. The vibration analyser, the portable computer and the amplifier were installed in the surgical theatre but outside the so-called laminar flow area (figure 4.2).

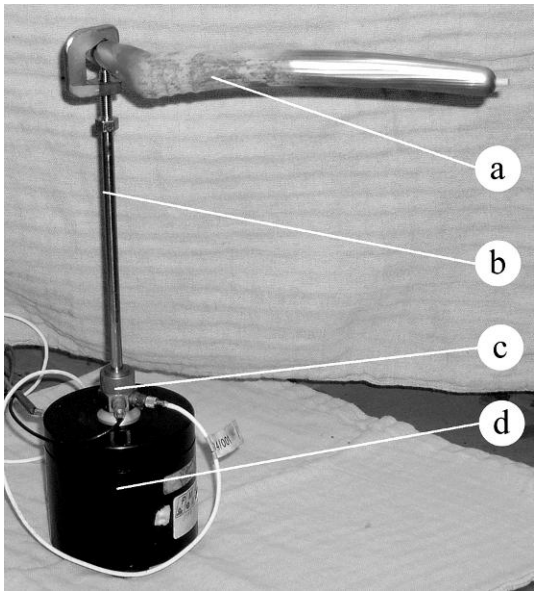

Figure 4.1: Experimental setup

a. hip stem

b. stinger and clamping system

c. impedance head

d. shaker

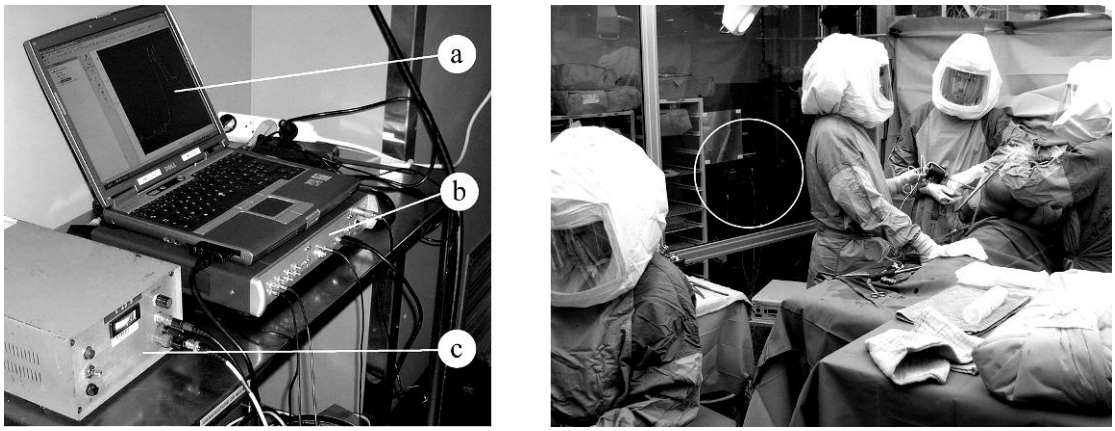

Figure 4.2: Measuring hardware (left) and surgical theatre (right – the circle indicates the place of the measuring hardware, behind the transparent wall)

a. portable computer

b. vibration analyser Pimento

c. power amplifier

Patients, eligible for THR, received full information relative to the surgical intervention and the study objectives, including the scheme for follow-up visits. The study protocol was approved by the institutional review board. Patients were included after giving

written informed consent. Thirty patients received non cemented IMP stems and fifty three patients received distally cemented IMP stems. The decision between the two procedures was made by the surgeon on clinical criteria. All stems were proximally coated with hydroxyapatite.

Before starting the measurements on patients the full protocol was tested in a cadaver study.

4.2.1. Non cemented prostheses

The surgeon inserted the implant in the femoral canal through successive controlled hammer blows. After each blow, the FRF of the implant-bone structure was measured directly on the prosthesis neck in the range 0-10 kHz. The FRF changes were used as indicators of the evolution of the stiffness of the implant-bone structure and, as a consequence, the evolution of the implant stability. When the FRF graph did not change noticeably anymore the hammering was stopped. Extra blows would not improve the stability of the prosthesis but would increase the fracture risk.

The similarity of two successive FRF graphs was evaluated using the Pearson's correlation coefficient. A correlation between the FRFs of successive stages of R=(0.99 +/- 0.01) over the range 0-10000 Hz is proposed as an endpoint criterion.

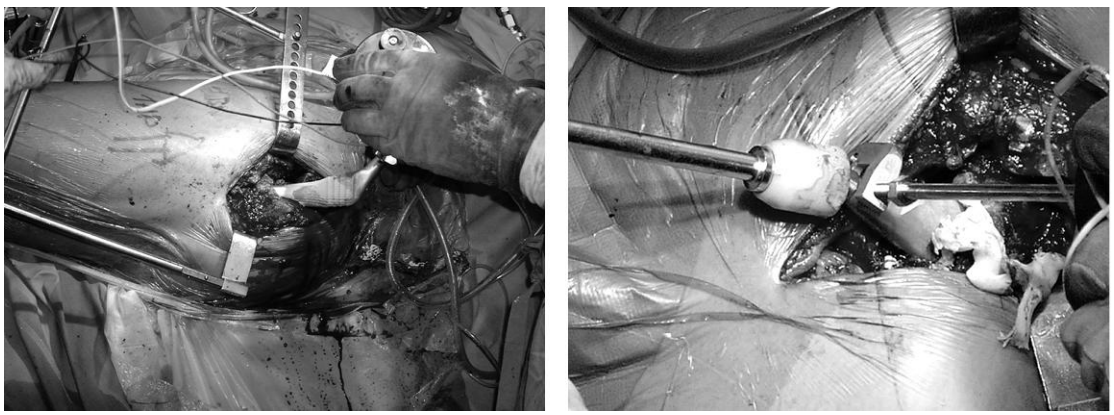

Figure 4.3: Hip stem insertion
non cemented (left), hybrid cemented (right)

The NCCF calculated between two successive FRF graphs was used to assess the direction and the magnitude of the FRF graph shift. (see sections 2.3.1, 2.3.2, and appendix A6)

4.2.2. Hybrid cemented prostheses

The per-operative protocol presented above was adapted to assess the stability of hybrid IMPs that were cemented only distally using Palacos® (Zimmer Inc. Warsaw, IN, USA) bone cement (Mulier et al.1989).

In a first stage, the surgeon inserted the stem completely in the femur without cement, for a trial reduction of the artificial joint. In a later stage, the stem was removed, cement was introduced in the distal part of the femoral canal, the stem was re-introduced and after the cement has fully cured, the implant was supposed to be completely fixed. The FRF was measured in both stages using the same method as in the non cemented stems case. (figure 4.3). In some randomly chosen cases, the FRF was measured also at various stages of cement curing i.e. 6, 10, 12, and 14 minutes after cement preparation.

4.3. Results

4.3.1. Non cemented prostheses

Thirty cases of non cemented stems were studied in vivo and a typical evolution of the FRF graph is shown in Figures 4.4a-d.

Stage 0 corresponds to the FRF calculated after the stem was introduced in the femur by hand; stage 1 corresponds to the FRF calculated after the first hammer blow series, stage 2 after the second hammer blow series and so on. The surgeon needed five stages (0…4) to completely insert the stem in this case

The Pearson's correlation coefficient (R), calculated for consecutive pairs of FRFs, is presented in figure 4e. The NCCF was also calculated for the same successive FRF pairs and presented in figure 4.4f. The evolution of maximum values of NCCF can be observed in figure 4.4g.

The maximum of the NCCF corresponding to insertion stages 2 and 1 has the coordinates +201 Hz and 0.962. This means that the FRF graph corresponding to the stage 1 has to shift 201 Hz to the right in order to obtain the maximum correlation (0.962) with the FRF graph corresponding to the stage 2. In other words, after the hammer blows, the FRF graph corresponding to the stage 2 shifted to the right with respect to the FRF graph corresponding to the stage 1.

The maximum of the NCCF corresponding to insertion stages 3 and 2 has the coordinates +85 Hz and 0.985. The FRF graph shifted less indicating an increasing resistance against the insertion and the two FRF graphs corresponding to stages 3 an 2 are more similar.

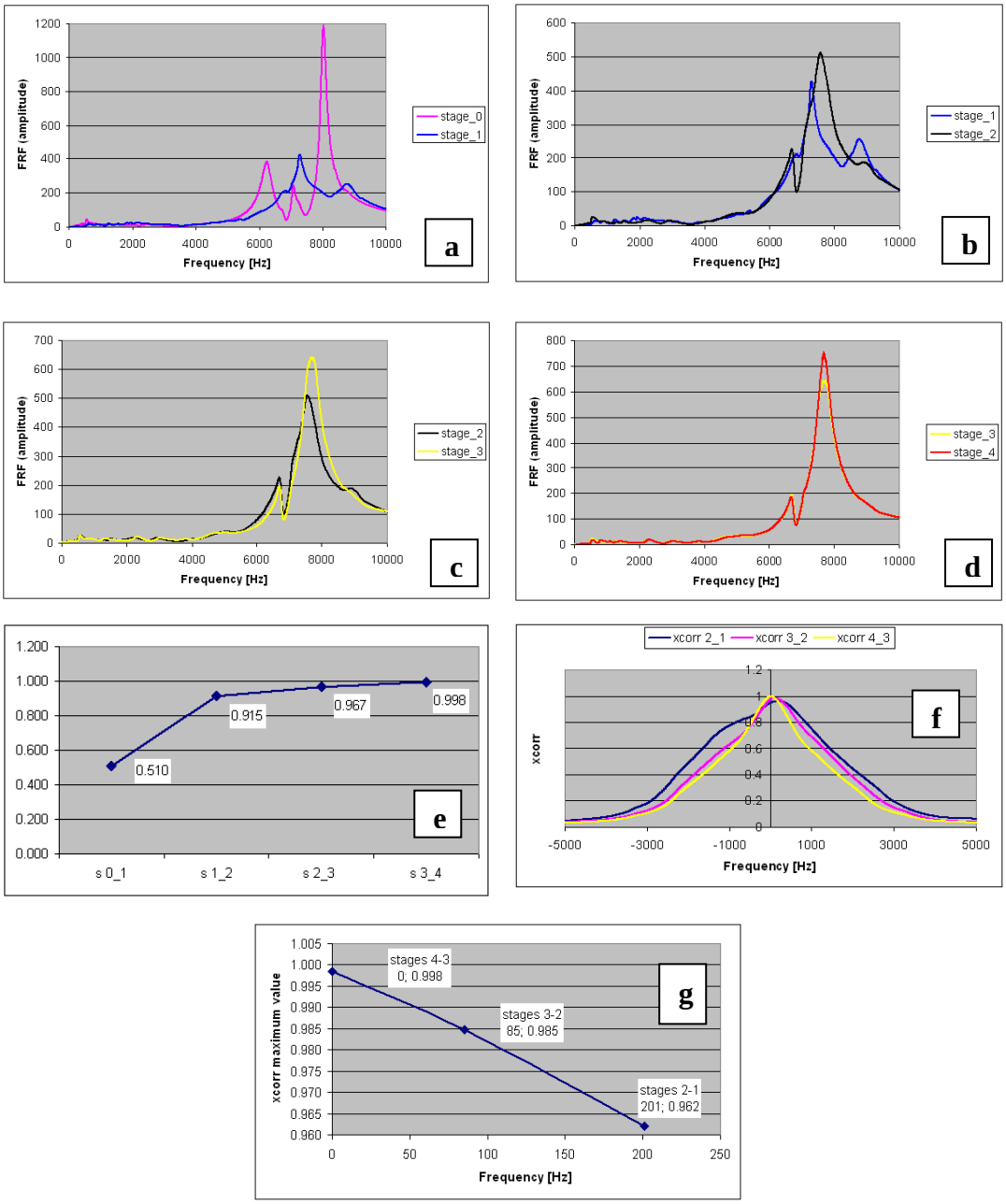

Figure 4.4: Cementless stem

a-d: FRF graphs for successive insertion steps;

e: Pearson's correlation coefficients calculated for the FRF pairs represented in figure 4.4 a-d

f: Normalised cross correlation functions calculated for the FRF pairs represented in figure 4.4 b-d

g: Maximum values of the cross correlation functions represented in figure 4.4 f

Finally, the maximum of the NCCF corresponding to insertion stages 4 and 3 has the coordinates 0 Hz and 0.998 indicating that the insertion end point has been attained. The FRF graph did not shift after the hammer blows and the two final FRF graphs are quasi similar.

In twenty six out of thirty cases (86.7%), the correlation coefficient between the last two FRFs was above 0.99 when the surgeon stopped the insertion. In the other four cases, when the surgeon decided to stop the insertion because of suspected bone fragility, the final correlation coefficient reached lower values but still exceeding 0.95.

4.3.2. Non cemented prostheses – non-typical cases

Case 1. While testing the per-operative protocol on a human cadaver, the stem was deliberately inserted until the femur was fractured. The last three FRF graphs are presented in Figures 4.5a and 4.5b.

The FRF graph slightly shifted to the left at the fifth insertion stage indicating a decrease of the stability before the sixth stage when the bone was fractured. The final FRF graph is totally different with respect to the previous graph indicating an important change in the stem-femur structure.

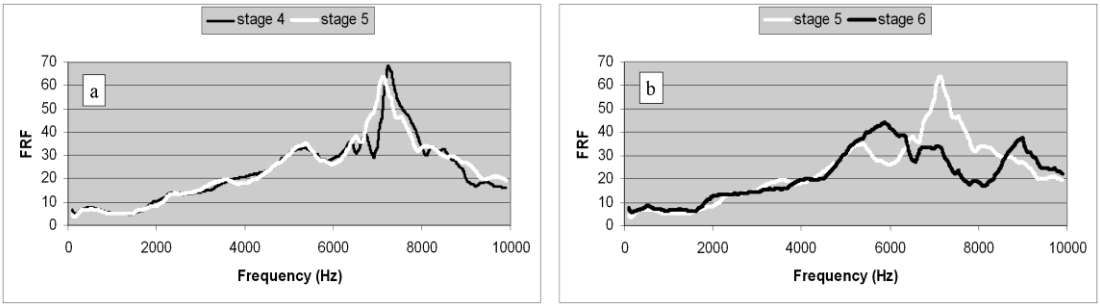

Figure 4.5: Non cemented stem in human cadaver

a. FRF corresponding to the insertion stages 4 and 5

b. FRF corresponding to the insertion stages 5 and 6 (fracture)

Case 2. During a per-operative experiment, when the stem was quasi fully inserted, the highest peak of the FRF graph slightly shifted to the left (stage B in figure 4.6a).

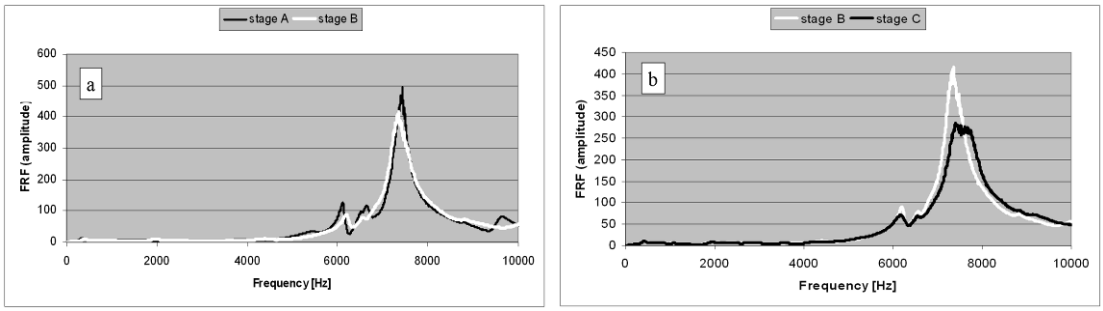

Figure 4.6: Per-operative fracture

a. FRF corresponding to the insertion stages A and B (left shift)

b. FRF corresponding to the insertion stages B and C (small fracture)

After a supplementary hammer blow series, the corresponding FRF graph presented an abnormal shape (stage C in figure 4.6b). Inspecting the bone, a small fracture was observed and the hammering was stopped.

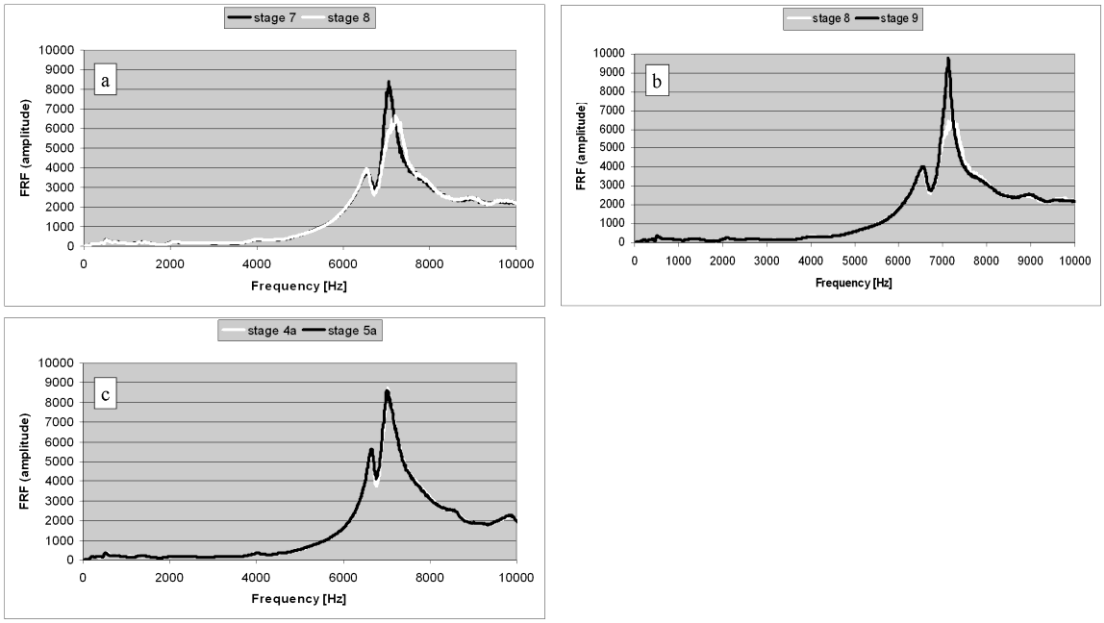

Figure 4.7: Correction of the femoral canal

a. FRF corresponding to the insertion stages 7 and 8 (normal right shift)

b. FRF corresponding to the insertion stages 8 and 9 (abnormal left shift)

c. FRF corresponding to the final insertion stages 4a and 5a (reinsertion after the correction of the femoral canal)

Case 3. An oscillating behaviour of the FRF graph was observed during another per-operative hip arthroplasty procedure (stages 7, 8, and 9 in Figures 4.7a and 4.7b).

Since the stem was visibly not fully inserted, the hammering normally had to continue, but the behaviour of the FRF, similar to the FRF evolution presented in case 2, was indicating that the stem was blocked and, as a consequence, there was a risk for fracture.

The problem was solved by pulling out the stem, adjusting the femoral canal and reinserting the prosthesis. The FRF had a normal evolution during the reinsertion and the graphs corresponding to the final two stages are shown in figure 4.7c. The corresponding Pearson's correlation coefficient attained 0.998.

4.3.3. Hybrid cemented prostheses

Fifty three cases of hybrid cemented prostheses were studied in vivo. In forty five cases (84.9%) an important difference was observed between the FRF graph corresponding to the non cemented stage and the FRF graph corresponding to the cemented stage, after complete cement hardening, in frequency and amplitude. A typical example is shown in figure 4.8.

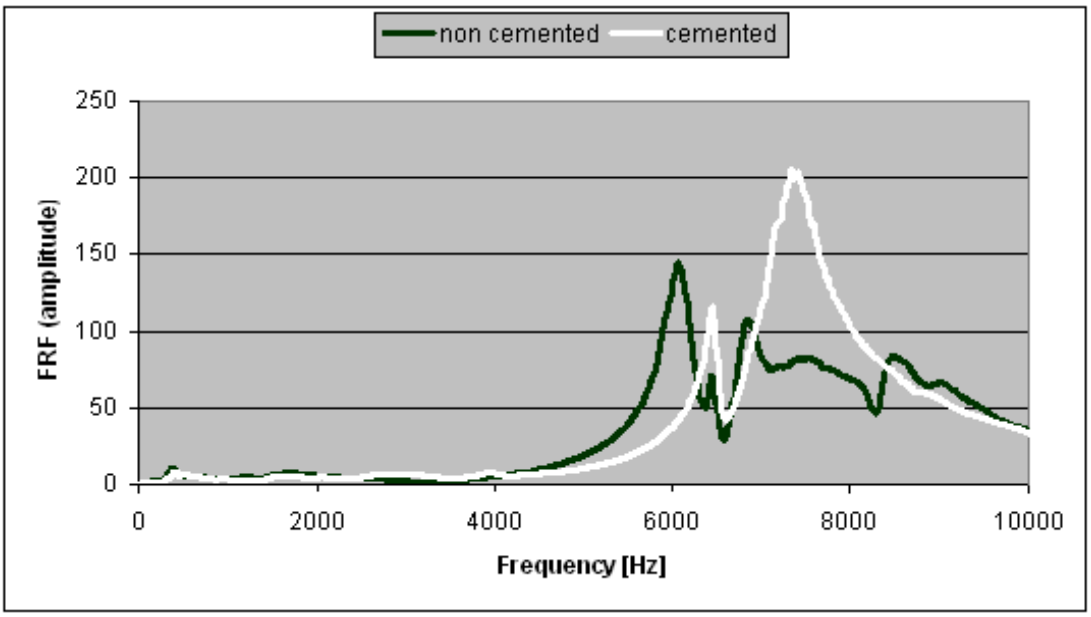

Figure 4.8: Hybrid cemented stem completely inserted in the femur.
FRF graphs for two stages: without cement (black) and cemented (white).
An important change can be observed after cementation.

In the other eight cases, although some alteration could be noticed, the FRF graph did not substantially change after cement curing (figure 9).

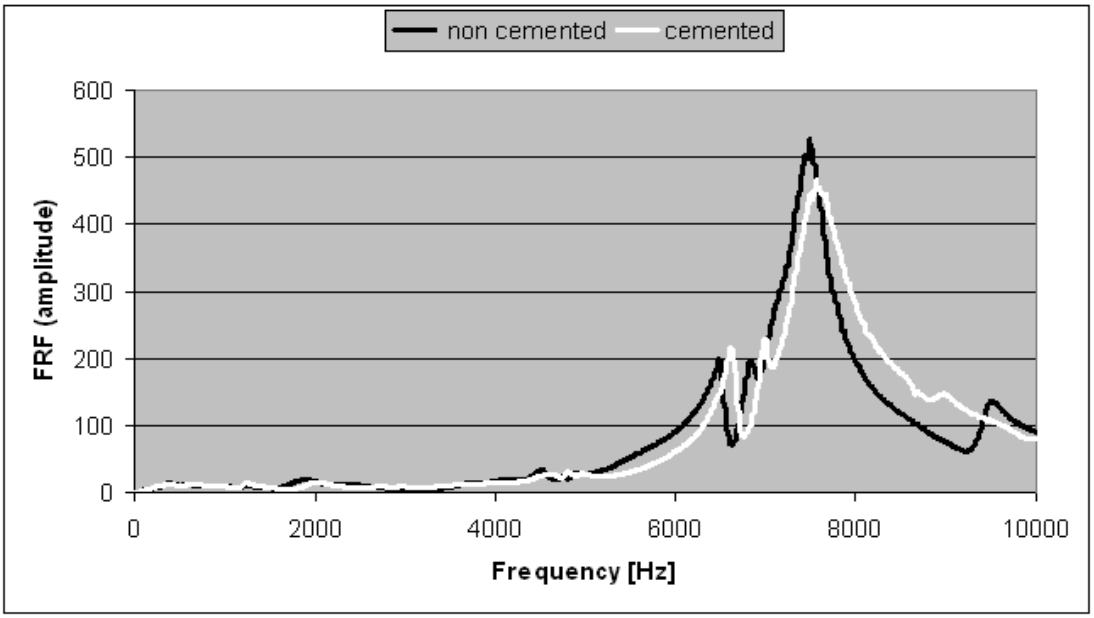

Figure 4.9: Hybrid cemented stem completely inserted in the femur. FRF graphs for two stages: without cement (black) and cemented (white). FRF graph slightly shifted to the right after cementation.

The typical evolution of the FRF graph during the cement curing, at 6, 10, 12, and 14 minutes after cement mixing, is shown in figure 4.10.

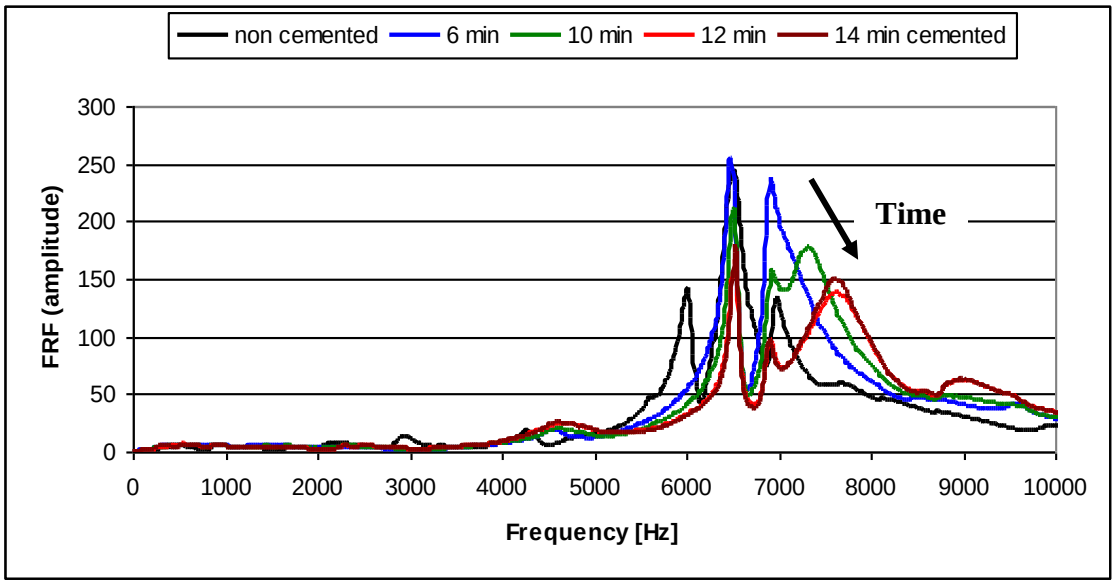

Figure 4.10: FRF graphs of a typical stem-femur system during cement curing at 6-10-12-14 minutes after cement mixing.

When the cement polymerisation sets in, the resonance frequency of the vibration modes associated with the cement increases. For the case presented, the resonance frequency

of the vibration mode mostly influenced by the cement curing increased from 7180 to 7680 Hz. When the polymerisation is complete, no further changes are observed in the FRF. The graphs corresponding to 12 and 14 minutes of cement setting time are nearly identical.

4.4. Discussion

During the insertion of an IMP in a femur, the changes of boundary conditions and implant stability between different stages are reflected by the FRF evolution as observed per-operatively. The higher resonance frequencies are more sensitive to the stability change than the lower frequencies. This observation is in accordance with previous finite element studies (Qi et al. 2003), and can be explained schematically as follows.

During the insertion of the uncemented stem the FRF change is influenced by the stiffness of the implant-femur system and the relative position of the two components. Between successive hammer blows the FRF graph shift to the right is a normal evolution; the fixation stiffness increase being reflected by increasing resonance frequencies. The graph change in shape and position is more important at the beginning of the insertion when the stem displacement is important as well. At the end of the insertion, when the resistance against the stem displacement increases, the shapes of the successive graphs are very similar and the shift is less important. When the FRF graph does not change noticeably between two hammer blows the logical conclusion is that the system mechanical parameters do not change, thus the stem cannot move and the hammering should stop to avoid an intra-operative fracture.

For non cemented stems, the Pearson's correlation coefficient between successive FRFs can be used as a criterion for the detection of the insertion endpoint.

Moreover, the FRF analysis can be used to detect dangerous situations during surgery like stem blockage and fracture risk. An FRF graph shift to the left indicates a decreasing fixation, probably due to plastic deformation of the bone, and should be a serious warning for the surgeon. In two cases hammering after a graph shift to the left resulted in bone fractures (Figures 4.5b and 4.6b).

A possible fracture may have been avoided in the case of an abnormal bone structure and a deformed endomedullary canal as the FRF analysis showed an abnormality and the surgeon was alerted to the situation in time during insertion of the stem (Figures 4.7a-c).

The supplementary information obtained by vibration analysis therefore helps the surgical team to take the optimal decisions.

The curing of bone cement in hybrid cemented hip stem systems can also be monitored by vibration analysis.

In 15% cases the FRF graph did not substantially change after cement curing. A plausible interpretation is that the implant stability did not considerably change after cementation. Probably the stems were already reasonably well fixed in the non cemented stage. However, the small shift to the right of the FRF graph indicates an increased stability after cementation. Comparing the Figures 4.8 and 4.9 it can be observed that the FRF corresponding to the complete curing stages (white graphs) are very similar. Moreover these graphs are very similar to the graphs corresponding to the final stage of the insertion of the cementless stems (Figures 4.4d and 4.7c)

The FRF graphs corresponding to the non cemented and cemented final stages could be used as a reference in postoperative monitoring of fixation and detection of loosening .

The per-operative experimental study is currently completed and validated by an appropriate post-operative follow-up of the patients. In an ongoing clinical study, part of project OT/03/31, migration of the stems is followed up by Roentgen Stereophotogrammetric Analysis (RSA) and bone remodelling is followed up by Dual energy X-Ray absorptiometry (DXA). Conventional follow-up by clinical examination, radiographs and standardised questionnaires is also part of the protocol (Claassen et al. 2007).

4.5. Conclusions

The presented per operative tool was designed to monitor the stability and to detect the insertion end point of non cemented and hybrid cemented hip stems, but it can be adapted for other orthopaedic implants as well.

It does not provide direct quantitative information on the displacements in real life loading conditions, but it is a powerful tool for the quality and safety control of the surgical procedure. It is a sensitive, minimally invasive technique to check whether the insertion process runs normally and results in the best possible fixation for the patient and the prosthesis at hand, and to prevent bone fracture.

5. Extension to other orthopaedic implants

In chapters 2, 3 and 4 it was shown that vibrational analyses based on FRF evolution can be successfully used to assess the stability of hip stem – femur structures either cemented or uncemented. As a consequence, a new question was raised: can the use of this method be extended to other kind of orthopaedic implants?

This chapter presents a few exploratory experimental *in vitro* studies performed on implants used in hip resurfacing arthroplasty and total shoulder replacement. The studies on resurfacing implants focus on metal-on-bone fixation (section 5.1) whereas the study on reverse shoulder prostheses focuses on metal-on-metal fixation (section 5.2). These studies only tested the feasibility and the sensitivity of vibrational methods based on FRF analysis in assessing the fixation of spherical implants.

The results were published in the Proceedings of ISMA2010 International Conference on Noise and Vibration Engineering (Pastrav et al. 2010).

5.1. Hip resurfacing arthroplasty

5.1.1. Introduction

Hip resurfacing represents an alternative to the classical THR which uses a stem inserted in the femoral canal. In hip resurfacing, instead removing the femoral head, a hollow sphere is applied on it. The hip joint is completed by a corresponding cup inserted in acetabulum (figure 5.1).

Although in hip resurfacing the femoral implants are generally cemented (Amstutz et al. 2004, 2006, Heisel et al. 2008, Treacy et al. 2005), a limited number of surgeons use uncemented implants to simplify the surgical procedure and avoid problems specific to cementation procedure (Gross, Liu 2008) .

An initially stable fixation of both the femoral and the acetabular component of a hip resurfacing arthroplasty (HRA) is a condition sine qua non for a good long term performance of the prosthesis. This initial stability is especially important for cementless components, as a good initial stability will limit micromotion, which is an important prerequisite for bone in growth.

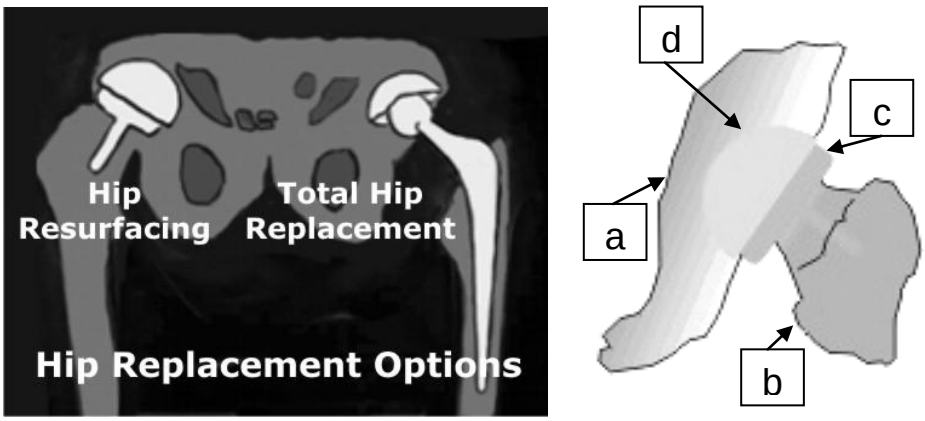

Figure 5.1. Hip replacement

Left: Hip replacement options
Right: Hip resurfacing arthroplasty

a. Acetabulum
b. Femur
c. Femoral implant
d. Acetabular implant

A method that would allow to quantitatively verify whether the implant has reached an optimal stability and detect the endpoint of insertion, would be of great value to the surgeon. This work shows that vibrational techniques are a prime candidate to develop such a method.

5.1.2. Materials and methods

5.1.2.1. Femoral implants

Biomet Orthopedics, Inc. provided two sets of femoral uncemented implants having the nominal diameters of 56, 50, 48, 44, and 38 mm (figure 5.2).

Figure 5.2. Femoral uncemented implants
(diameters from left to right: 56, 50, 48, 44, 38 mm)

Five human femora were prepared by Dr. H. Delport for implants with diameters of 38mm (two pieces), 44mm (one piece), 50mm (one piece), and 56mm (one piece). The experiments were repeated on artificial femora manufactured by Sawbones (www.sawbones.com). Six large left (solid foam, code 1129) femora and six medium left (solid foam, code 1120) femora were prepared by Dr. M. Mulier. The corresponding implants have diameters of 56 and, respectively, 44mm.

The implant-bone structures were excited by using a hammer instrumented with a force cell (PCB Piezotronics). The response of the structure was measured using an accelerometer (PCB Piezotronics) attached to the implant (Figures 5.3 and 5.4). A Pimento vibration analyser (LMS International) and a portable computer were used to analyse the input-output signals and to calculate the FRFs between 0 and 25 kHz (10 averages).

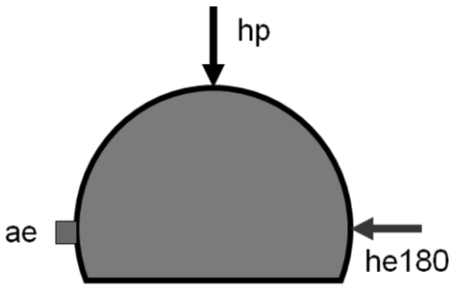

Figure 5.3. Position of excitation hit and accelerometer

- *ae – accelerometer positioned at "equator"*
- *he – hammer blow at "equator"*
- *hp - hammer blow at "pole"*

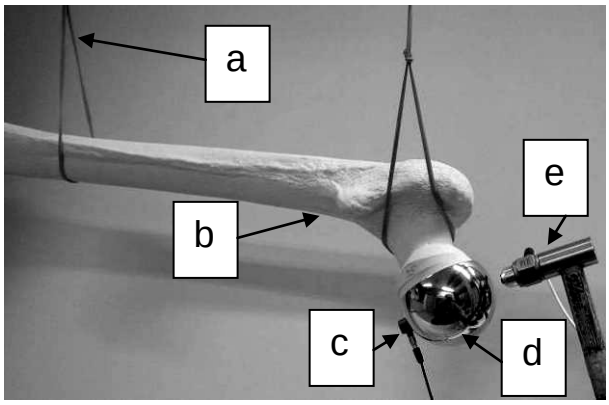

Figure 5.4. Experimental setup (femoral implant)

a. Elastic bands
b. Artificial femur
c. Accelerometer
d. Femoral implant
e. Instrumented hammer

The experimental protocol consisted in four categories of experiments:

The resonance frequencies of the femoral implants were measured in "free-free" conditions. The corresponding FRFs could be used as references.

While the implants were being inserted in human and artificial femora, the FRFs were measured at different insertion stages.

The implants installed on artificial femora were extracted and reinserted. After reinsertion, the FRFs were measured and compared with the corresponding FRFs measured before extraction.

The FRF corresponding to the fully inserted implant was measured in different positions of the accelerometer in order to detect irregularities in contact distribution.

To understand better the relationship between the vibrational behaviour and the contact conditions at the bone-implant interface and the resistance of the implant against the extraction, a femoral resurfacing implant (Ø44) provided by Biomet Orthopedics was inserted on different cylinders made of rigid polyurethane foam that represents a good approximation of the real bone. The fixation is realised on a cylindrical surface which has the nominal dimensions of Ø 37x13 mm (figure 5.5 left). The experimental setup for FRF measurement is presented in figure 5.5 right.

- The FRF was measured (figure 8 right) at different insertion depths (5, 8, and 13 mm) and for different diameters of the cylindrical contact surface (Ø 37, Ø 37.1, and Ø 37.2 mm).
- After the complete insertion, pulling tests were performed and the extraction forces were correlated to the corresponding resonance frequencies.
- After the complete insertion on the cylinder of Ø 37.2 mm, the implant was extracted an fully reinserted. After reinsertion the FRF and the extraction force were measured again to see how much decreased the fixation of the implant.

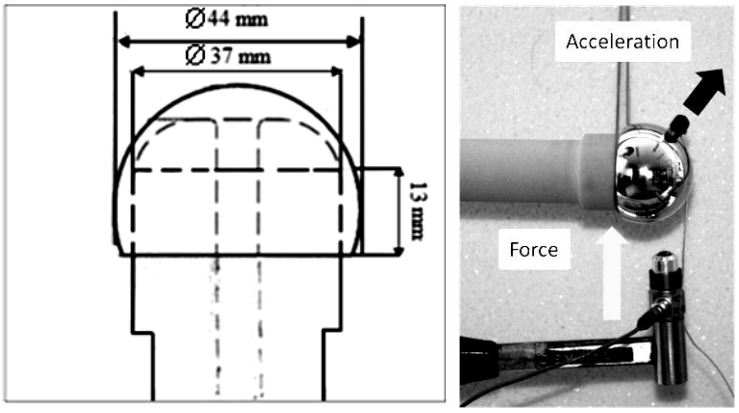

Figure 5.5. Femoral resurfacing implant inserted on polyurethane cylinder
Left: Schematic representation, Right: Experimental setup for measuring FRF

5.1.2.2 Acetabular implants

Although Biomet Orthopedics, Inc. provided several acetabular uncemented implants, due to the limitations imposed by the artificial acetabula (Sawbones) only two dimensions were used.

Five female left (solid foam, code 1304) and five medium left (solid foam, code 1305) acetabula were prepared by Dr. M. Mulier. The corresponding implants have diameters of 50 and, respectively, 54 mm.

All human and artificial bones were prepared by using the instruments and the methodology provided by Biomet Orthopedics (ReCap – Operative Technique, Biomet UK Limited – figure 5.6).

The FRF of the implant-acetabulum structures were measured by using methods and equipment similar to those corresponding to the femoral implants.

Figure 5.6. Preparing the artificial bones

Left: Artificial femur *Right: Artificial acetabulum*

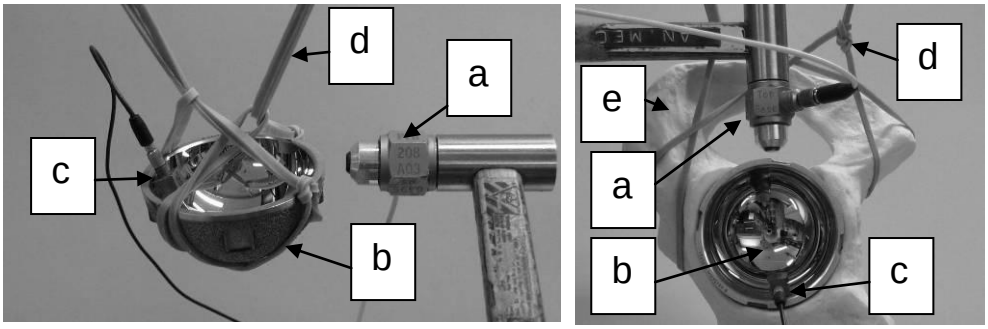

Figure 5.7. Experimental setup (acetabular implant)

Left: "free-free" implant
Right: implant inserted in acetabulum

a. Instrumented hammer
b. Acetabular implant (cup)
c. Accelerometer
d. Elastic bands
e. Artificial acetabulum

The experimental protocol consisted in three categories of experiments:

- The resonance frequencies of the acetabular implants were measured in "free-free" conditions (figure 5.7 left). The corresponding FRFs could be used as references.
- While the implants were being inserted in artificial acetabula, the FRFs were measured on the implants at different insertion stages (figure 5.7 right).
- While the implants were being inserted in artificial acetabula, the FRFs were measured on the impactor, in transversal (figure 5.8 left) and axial direction (figure 5.8 right), at different insertion stages. This measuring method seems to be more adapted to the real conditions existing in the surgical theatre where is no direct access to the implant.

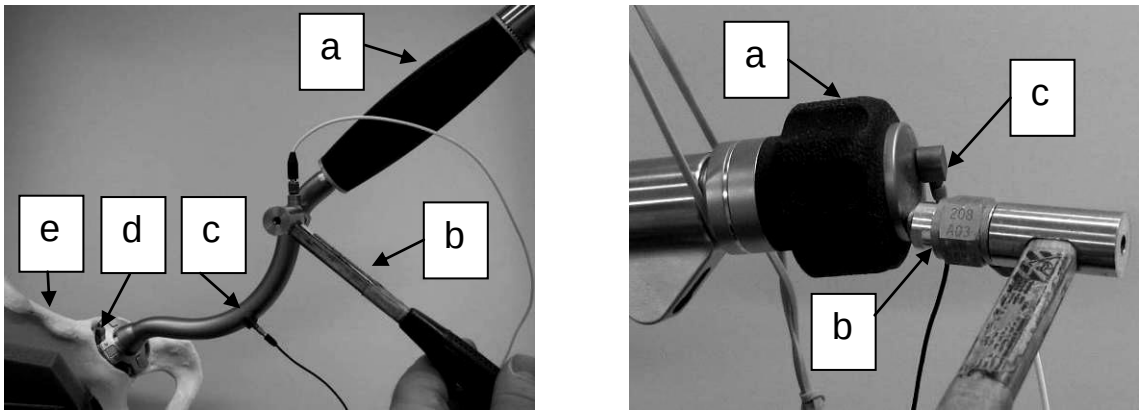

Figure 5.8. Experimental setup (acetabulum, implant, and impactor)
Left: Transversal excitation
Right: Axial excitation

a. Impactor
b. Instrumented hammer
c. Accelerometer
d. Acetabular implant
e. Artificial acetabulum

5.1.3. Results and discussion

5.1.3.1. Femoral implants

The FRF graphs corresponding to femoral implants in "free-free" conditions are represented in figure 5.9. As expected, smaller implants have higher resonance frequencies.

At the beginning of the insertion of the implants in human femora the FRF graph shifted to the right, but during the next steps the FRF graph had an oscillatory behaviour. However, at the end of the insertion the FRF graph was stable and the average coherence

reached a maximum. Lower coherence resulted after extra hammer blows. The FRF had a similar behaviour in the case of the insertion in artificial femora.

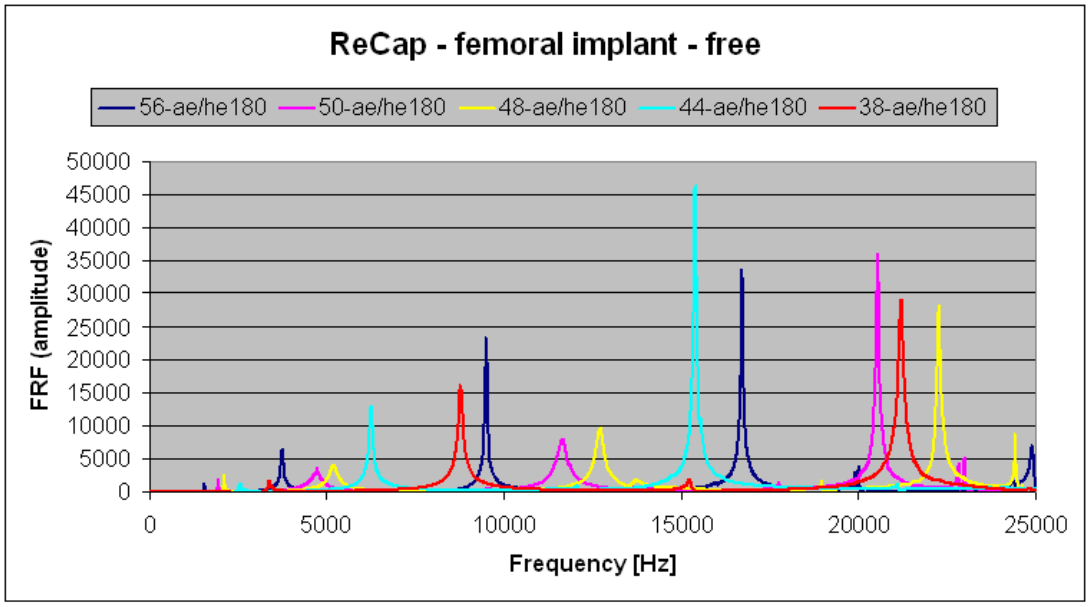

Figure 5.9. FRF graphs corresponding to femoral implants in "free-free" conditions (dark blue-56mm, pink-50mm, yellow-48mm, light blue-44mm, red-38mm)

An example of final FRF graphs corresponding to a 38 mm implant is presented in figure 5.10a and the evolution of the average coherence during the insertion is shown in figure 5.10b. The end point of insertion process was reached after the 10th hammer blow.

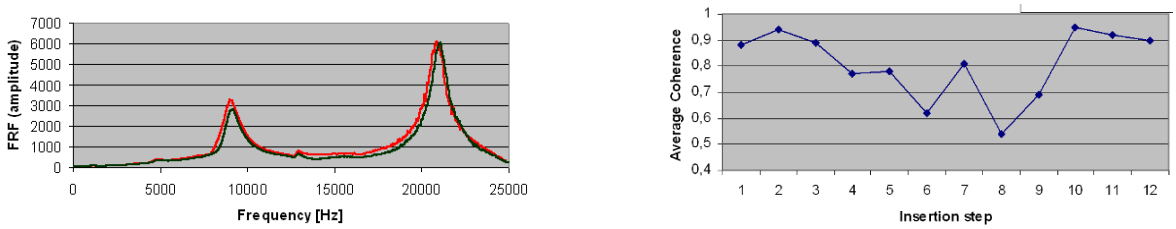

Figure 5.10. Graphs corresponding to a 38 mm femoral implant
Left: FRF graphs corresponding to the 10th (red) and 11th (dark green) insertion steps
Right: The evolution of the average coherence during the insertion

The FRF graphs corresponding to the implant in "free-free" conditions, fully inserted in human femora, and fully inserted in artificial femora have a similar shape but they are shifted and the height of the peaks are different indicating a different stability and a different damping. The FRF graphs obtained for a Ø56 mm implant are presented in figure 5.11.

It can be observed that the system implant-human femur is more damped and seems to be more stable than the system implant-artificial femur.

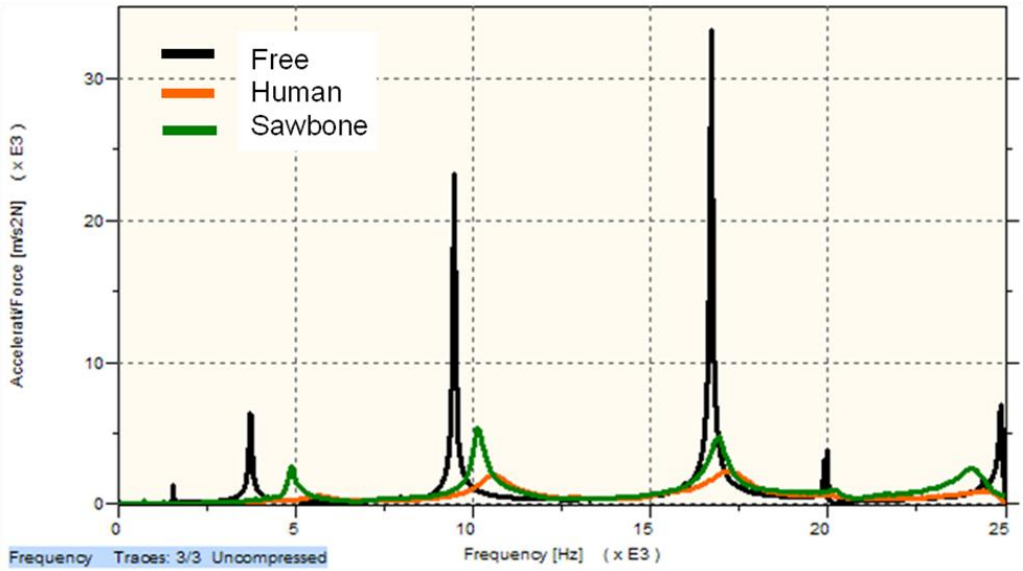

Figure 5.11. FRF graphs corresponding to a 56 mm femoral implant
Black: implant in free-free conditions
Orange: implant fully inserted in human femur
Green: implant fully inserted in artificial femur

The relationship between the FRF shift and the implant fixation was tested by extracting and reinserting the implants installed on artificial femora. After reinsertion, the FRFs were measured and compared with the corresponding FRFs measured before extraction. Obviously, the implant is less stable after extraction and reinsertion, due to the supplementary damage supported by the surface of the femoral head. In all cases the resonance frequencies decreased and, as a consequence, FRF shifted to the left. An example is presented in figure 5.12.

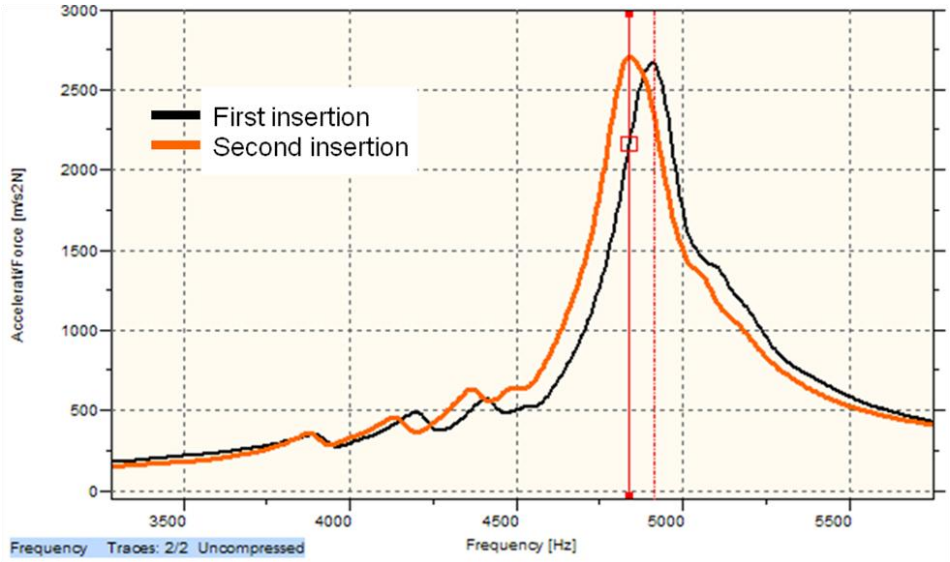

Figure 5.12. FRF graphs corresponding to the first and second insertion of a 56 mm implant (a shift to the left can be observed after reinsertion)

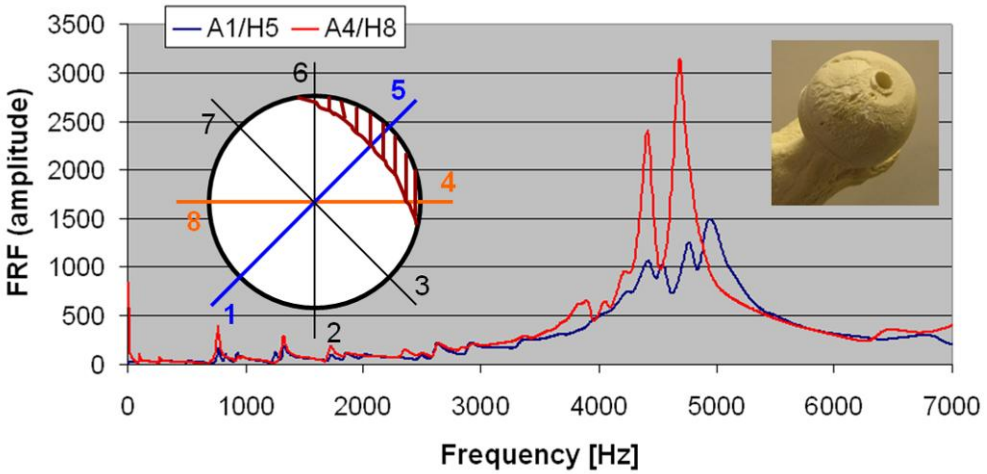

Figure 5.13. Asymmetric contact detection
(the hatched region indicates lack of contact)

Blue FRF graph: accelerometer at point 1 and hammer hit at point 5
Red FRF graph: accelerometer at point 4 and hammer hit at point 8

Changing the position of the accelerometer along the "equator" of the implant, it was observed that FRF graph changes if irregularities of the contact between the implant and the femoral head were present. An example is shown in figure 5.13. An important defect of the spherical surface can be observed in the picture of the femoral head resulting in lack of contact in that region.

A typical FRF evolution during the insertion of the femoral resurfacing implant (Ø44) on the polyurethane cylinder (Ø37.2) is presented in figure 5.14.

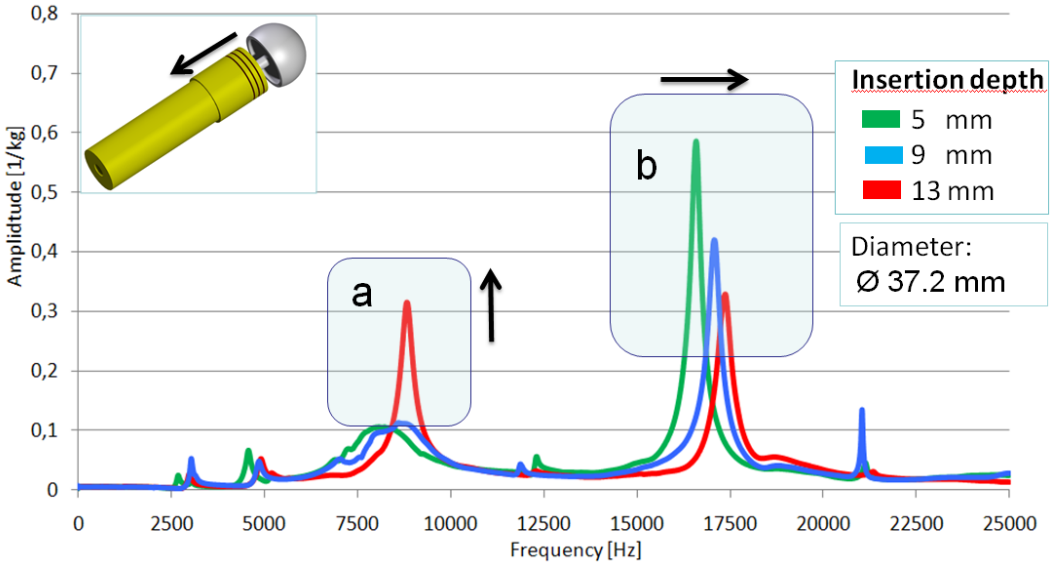

Figure 5.14. The FRF graph evolution during the insertion of a femoral resurfacing implant

The peak “a” becomes very well defined at the end of the insertion, while the peak “b” shifts continuously to the right indicating an increasing stability. The behaviour of peak “a” could be used as a warning signal indicating the end point of the insertion process.

The FRF graphs corresponding to the femoral implant (Ø44) fully inserted on polyurethane cylinders with different diameters are presented in figure 5.15.

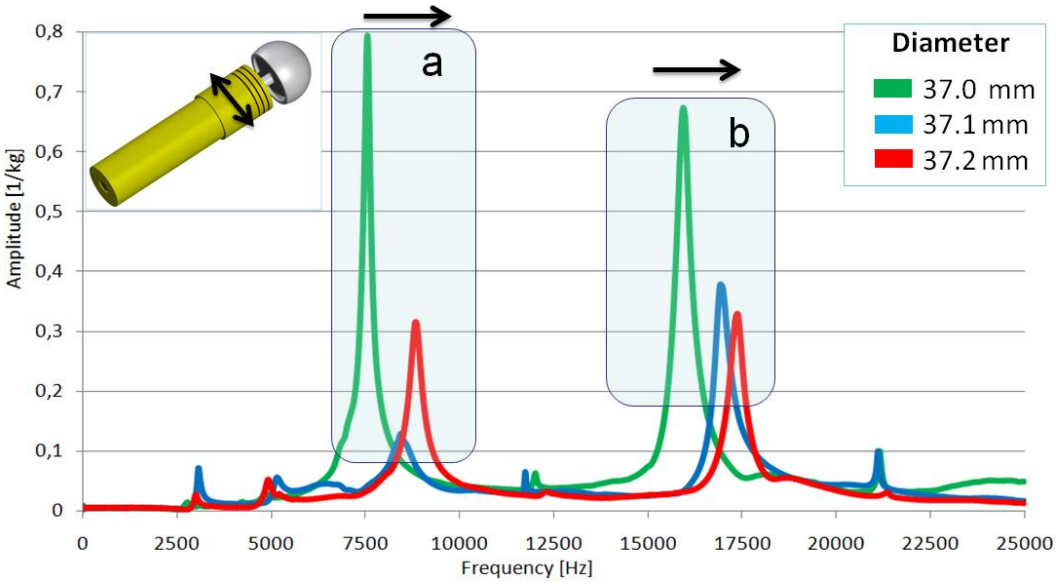

Figure 5.15. FRF graphs corresponding to the femoral resurfacing implant fully inserted on polyurethane cylinders with different diameters

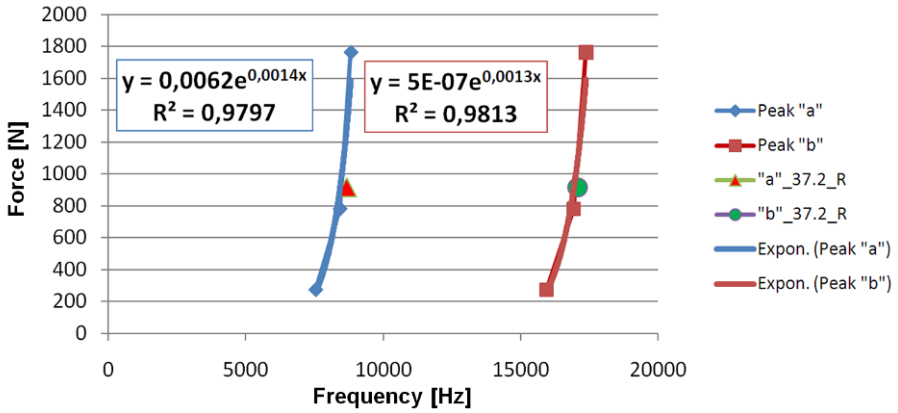

Figure 5.16. Extraction force represented as a function of resonance frequency

Increasing the diameter of the cylinder results in an increasing interference between the cylinder and the implant surfaces and in a resonance frequency increase. The main peaks “a” and “b” shift to the right.

Table 5.1 presents the extraction forces and the corresponding resonance frequencies for peaks “a” and “b”. The correlation between the extraction forces and the corresponding

resonance frequencies is represented in figure 5.16 and the points corresponding to the femoral implant reinserted on the polyurethane cylinder (37.2 R) are very close to the curves corresponding to peaks “a” and “b”.

Table 5.1. Extraction forces, corresponding interferences and resonance frequencies.

Cylinder diameter	Theoretical interference	Extraction force	Resonance frequency	
			Peak “a”	Peak “b”
mm	µm	N	Hz	Hz
Free implant	0	0	6226	15393
37.0	10	273	7544	15936
37.1	110	781	8429	16925
37.2	210	1763	8826	17380
37.2 reinserted	x	916	8675	17079

The Pearson’s correlation coefficient between the interference series and the corresponding extraction force series was 0.98 and the same coefficient calculated for the two resonance frequency series corresponding to peaks “a” and “b” was 0.99.

5.1.3.2 Acetabular implants

The FRF graphs corresponding to the acetabular implants in “free-free” conditions are presented in figure 5.17. As expected, the bigger implant has lower resonance frequencies.

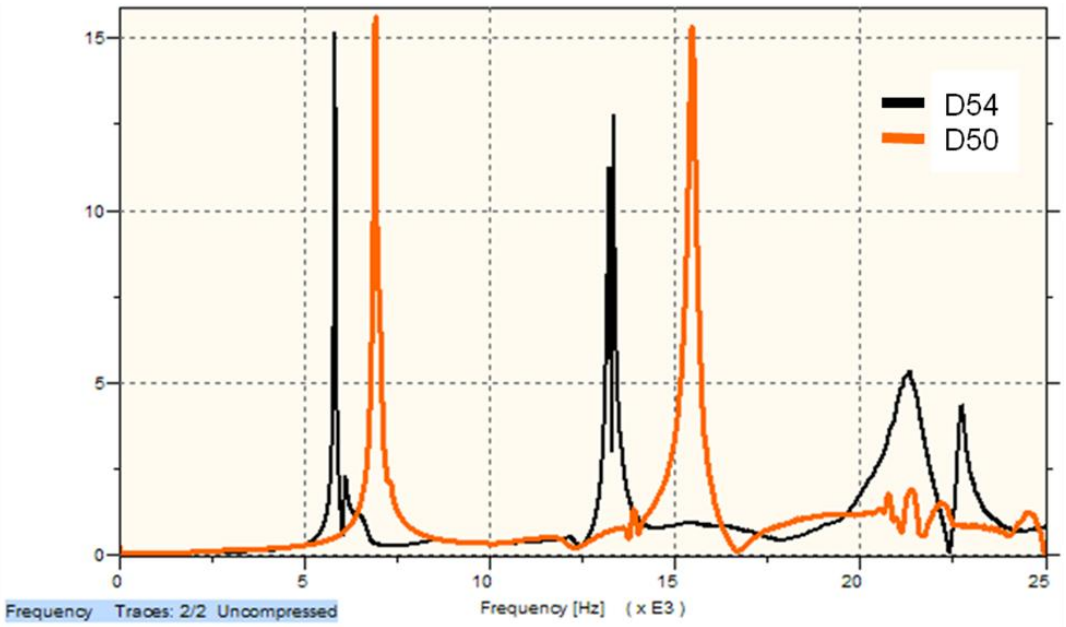

Figure 5.17. FRF graphs corresponding to the acetabular implants in “free-free” conditions

Black: implant with 54 mm diameter
Orange: implant with 50 mm diameter

Measuring the FRF directly on the acetabular implant during its insertion, the best coherence was obtained in the range 0-2500 Hz, thus the obtained graphs were analysed in this interval. The FRF graph shifted to the right after every insertion step (figure 5.18 left). Surprisingly, when the implant reached the end point of the insertion, the FRF graph shifted to the left (figure 5.18 right). The explanation could be the important change in contact distribution after the implant passed the rim existing at the edge of the acetabular cavity (figure 5.19) and not necessarily a stability decrease. This phenomenon could be used to detect the end point of the insertion process.

A similar behaviour exists for a simple beam. The resonance frequencies of a one end pinned beam are higher than the resonance frequencies of a cantilever beam corresponding to the same vibration modes even the latter is more rigidly fixed. This is the result of the boundary condition influence (see appendix A4.4, table A4.1).

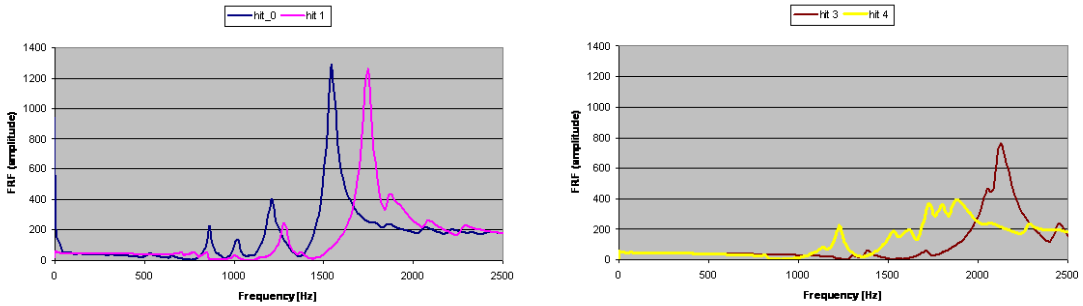

Figure 5.18. FRF graph change during the insertion of an acetabular implant
Left: FRF graph shifts to the right at the beginning of the insertion
Right: FRF graph shifts to the left when the end point of insertion is reached

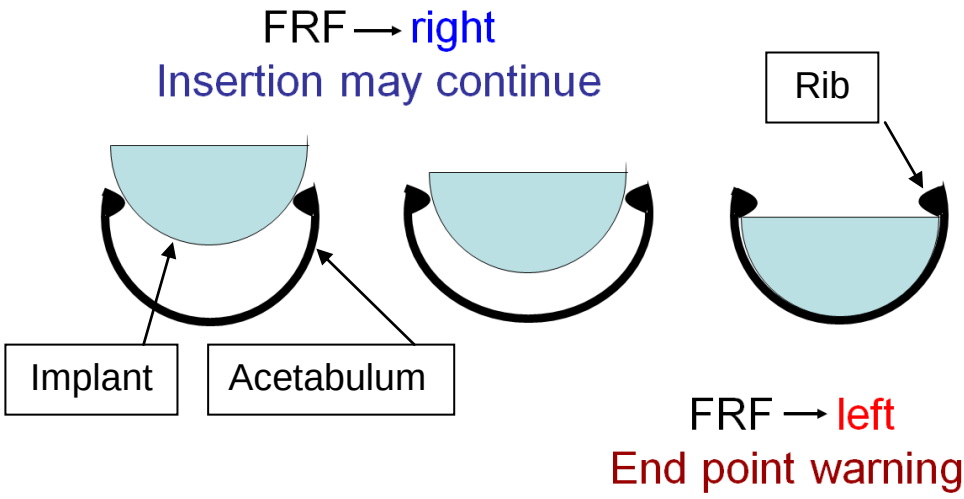

Figure 5.19. Schematic representation of the acetabular insertion process

In order to reproduce the conditions existing in the surgical theatre during the insertion, the FRF was measured on the impactor attached to the implant. In this case the FRF evolution reflected the vibrational behaviour of the structure composed by artificial acetabulum, acetabular implant, and impactor. The only variables were the contact and stress distributions at the interface between the implant and the bone. Some noise was introduced in the structure due to the less rigidly fixed parts composing the impactor assembly. To eliminate the noise influence, the FRF evolution was analysed in the frequency intervals where the coherence was considered acceptable, i.e. 0-700 Hz and 5-7.5 kHz. (Figure 5.20).

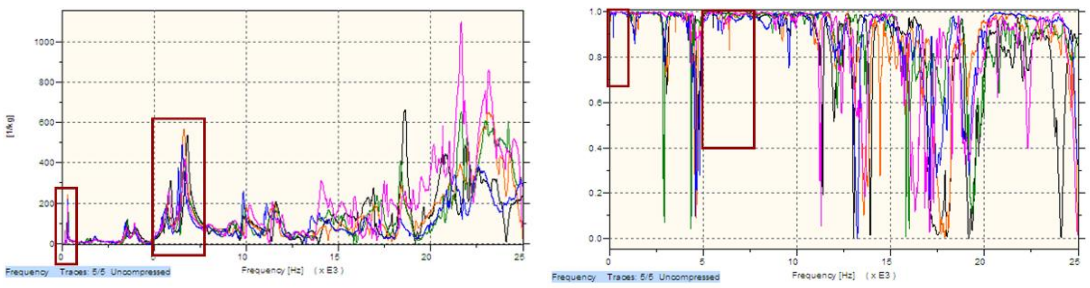

Figure 5.20. Graphs corresponding to the structure composed by artificial acetabulum, acetabular implant, and impactor
Left: FRF graph measured on the impactor in transversal direction
Right: The coherence corresponding to the FRF graphs presented in the left image
(The rectangles indicate the intervals where the coherence was considered acceptable)

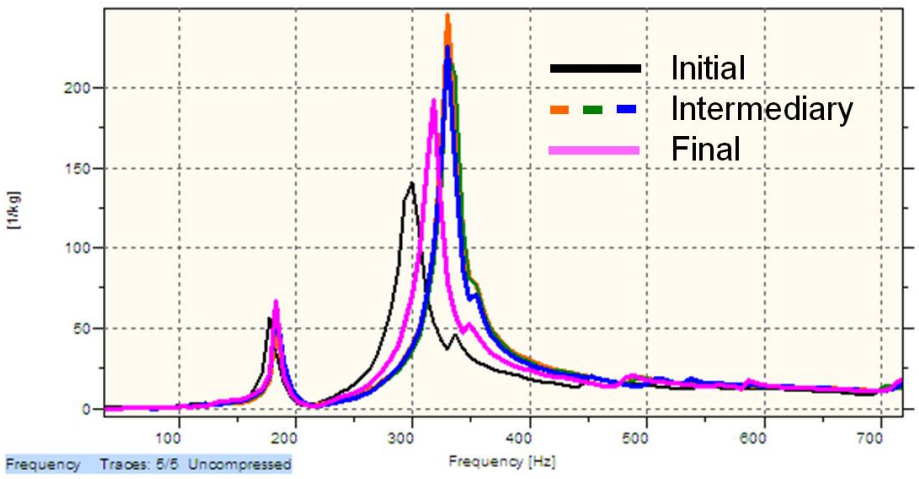

Figure 5.21. FRF graphs corresponding to the structure composed by artificial acetabulum, acetabular implant, and impactor (range 0 – 700 Hz)

The evolution of the FRF in the range 0-700 Hz is presented in figure 5.21. At the beginning of the insertion process the FRF shifted to the right, from the black graph to the orange graph. During the next two steps (green and blue graphs) the FRF was mostly stationary. When the end point of the insertion process was reached, the FRF shifted to the

left (pink graph). The vibrational behaviour is similar to the case when the measurements were performed directly to the acetabular implant.

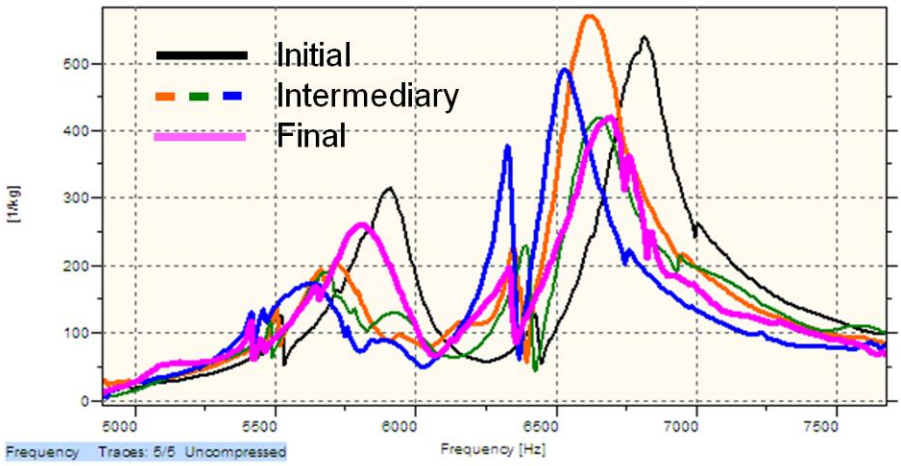

Figure 5.22. FRF graphs corresponding to the structure composed by artificial acetabulum, acetabular implant, and impactor (range 5 – 7.5 kHz)

Analysing the FRF graphs obtained for the range 5-7.5 kHz, a different evolution was found (figure 5.22). At the beginning of the insertion process, the FRF shifted to the left, from the black graph to the orange graph. During the next two steps (green and blue graphs) the FRF had a less important shift to the left. At the final step, the FRF had an opposite change, shifting to the right (pink graph). This could be the normal influence of the evolution of the boundary conditions on specific vibrational modes.

5.2. Reverse shoulder implant

5.2.1. Introduction

The reverse shoulder artificial joint, presented in figure 5.23, is composed by a humeral stem provided with a polyethylene humeral concavity insert, a spherically convex glenoid articular surface (glenosphere), and a base-plate (metaglene). The humeral stem is cemented in the medular cavity of the humerus, while the metaglene is fixed to a prepared glenoid using four screws and a press-fit hydroxyapatite-coated central peg. The glenosphere, is fitted to the metaglene and held in position with use of a Morse taper and it is secured with a central screw.

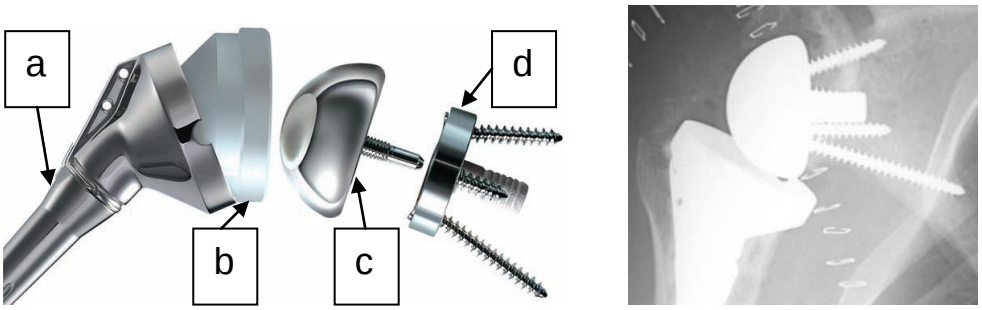

Figure 5.23. Reverse shoulder artificial joint (Matsen et al. 2007)[5]

Left: Exploded view
Right: Radiography of a reverse shoulder prosthesis implanted in a patient

a. Humeral stem
b. Polyethylene humeral concavity insert
c. Glenosphere
d. Metaglene (Morse taper)

This design is the "reverse" configuration of that seen with a conventional shoulder arthroplasty, in which the convex spherical surface is part of the humeral component (figure 1.2.c).

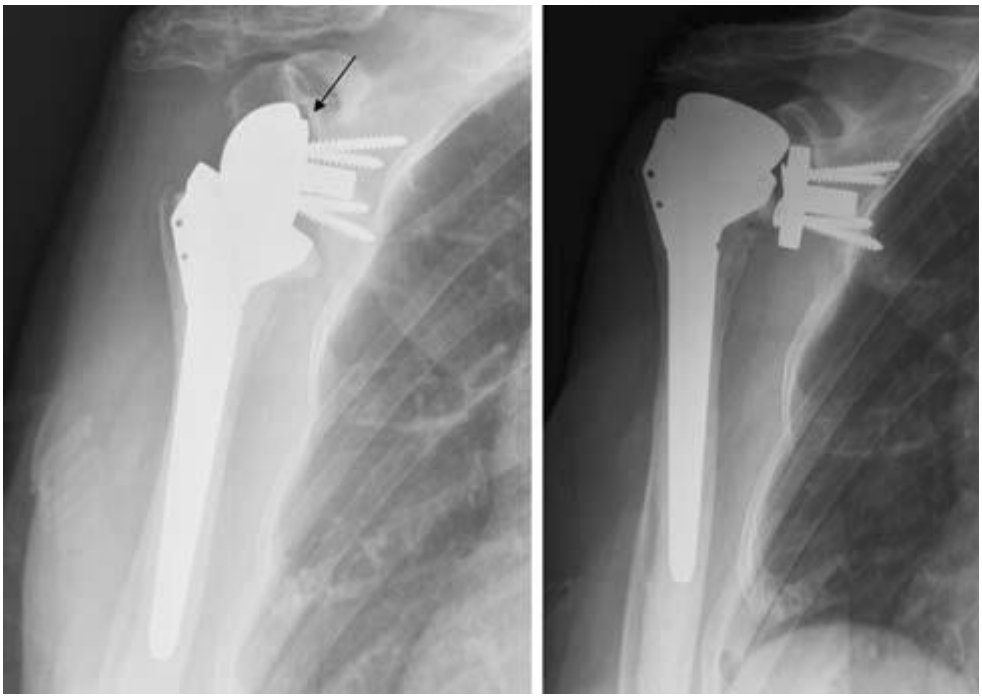

Figure 5.24. Failure of reverse shoulder prosthesis (Middernacht et al. 2008)[6]

Left: Partial disengagement of the glenosphere (arrow)
Right: Total disengagement of the glenosphere with fracture of the central screw

[5] Reprinted from Matsen F. A. III, Boileau P., Walch G., Gerber C., Bicknell R.T., 2007. The Reverse Total Shoulder Arthroplasty. J Bone Joint Surg [Am] 89: 660-667 with permission.
[6] With kind permission from Springer Science+Business Media: Middernacht B., De Wilde L., Mole D., Favard L., Debeer P., 2008. Glenosphere disengagement. Clinical Orthopaedics and Related Research 4, 892-898.

Due to the surgical complexity of the implantation, the reverse shoulder prosthesis is recommended in cases associated with irreparable rotator cuff tears or other reconstructions of shoulder joint in which the conventional techniques would be inefficient (Gerber et al. 2009, Guery et al. 2006, Katz et al. 2007, Matsen et al. 2007, McFarland et al. 2006).

In a recent article (Middernacht et al. 2008) glenophere disengagement is described as a possible failure with sometimes need to revision (figure 5.24).

The problem could be generated by some imperfections in the primary fixation of the glenosphere on to the metaglene. The stability of the Morse-type connection might be compromised if there is a suboptimal contact at the conical interface (Friedman et al. 1993, Pennock et al. 2002). As a result, relative movements between the components occur during the daily activities and the central screw breaks due to metal fatigue.

One of the causes for the imperfect fixation could be soft tissue, bone debris and/or blood accidentally inserted between glenosphere and metaglene during surgery.

This preliminary experimental study tries to find if a method based on vibration analysis could detect a suboptimal contact in the Morse-type assembly composed by metaglene and glenosphere.

5.2.2. Materials and methods

A glenoid component of a Delta III^{TM} reverse shoulder prosthesis (DePuy International Ltd, Leeds, UK) was used for this study. It was composed by a base-plate (metaglene), a glenosphere, and a central screw which was retained inside the glenosphere by a disk (figure 5.25)

The experimental protocol consisted in measuring the FRF of the glenoid assembly and the corresponding coherence in four situations:

- Optimal contact between the conical surfaces, glenosphere and metaglene well fixed to each other, tightened screw. This represents the optimal fixation for the glenoid assembly.
- Optimal contact between the conical surfaces, glenosphere and metaglene well fixed to each other, released screw.
- Suboptimal contact between the conical surfaces, glenosphere and metaglene well fixed to each other, tightened screw. This represents a bad fixation for the glenoid assembly that might be possible during surgery.

- Suboptimal contact between the conical surfaces, glenosphere and metaglene well fixed to each other, released screw. This represents the worst fixation for the glenoid assembly.

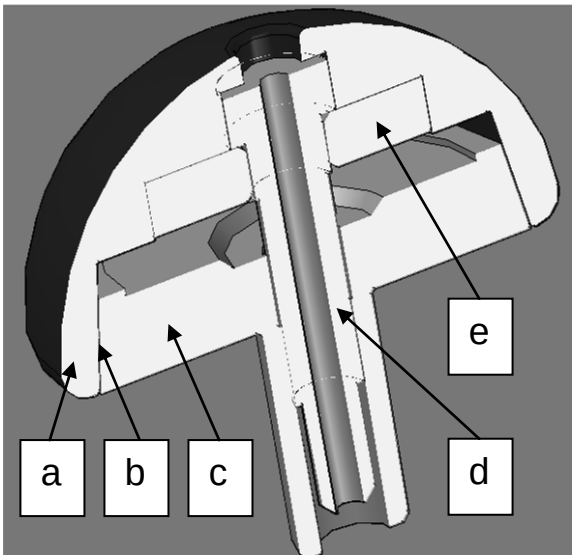

Figure 5.25. Schematic drawing of a Delta III™ glenoid component

a. Glenosphere
b. Morse-type connection
c. Metaglene (base-plate)
d. Central screw
e. Disk

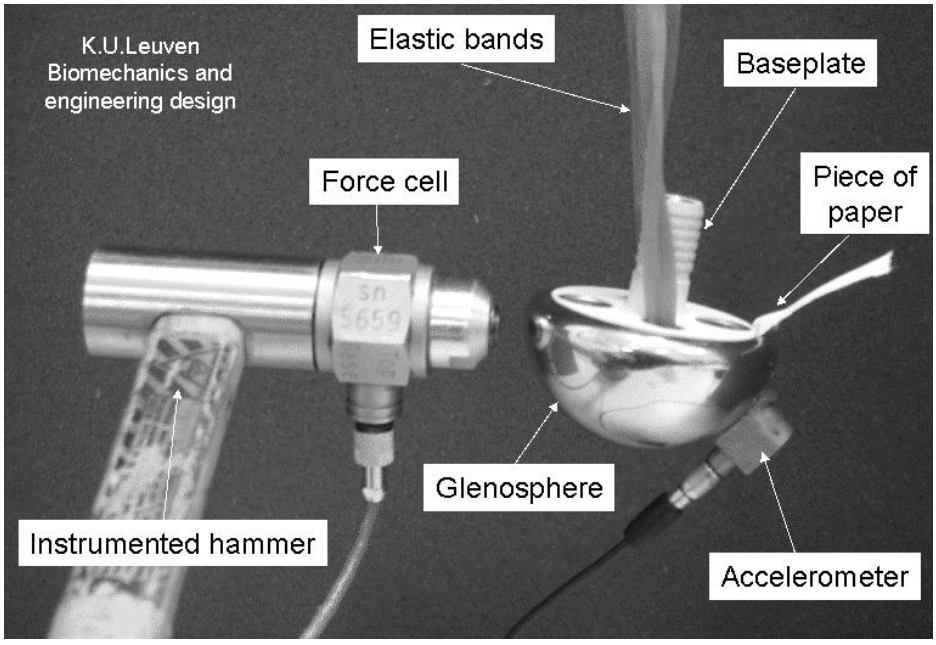

Figure 5.26. Vibration analysis on glenoid assembly - experimental setup

The suboptimal contact, as the result of the presence of an unwanted body in the assembly, was simulated by inserting a small piece of paper (80 g/m2) between the conical surfaces. In all four situations no difference in fixation could be detected by hand.

The structure was excited by a hammer instrumented with a force cell (PCB Piezotronics) and the response was measured using an accelerometer (PCB Piezotronics) attached to the glenosphere (Figures 5.26).

A Pimento vibration analyser (LMS International) and a portable computer were used to analyse the input-output signals and to calculate the FRFs between 0 and 20 kHz.

5.2.3. Results and discussion

The most sensitive band was comprised between 12 and 15 kHz and a typical vibrational behaviour is represented in figure 5.27.

The results can be summarised as follows:

- When the contact between the conical surfaces is optimal and the screw is well tightened, the FRF graph presents two main peaks at 13488±6 and 13630±6 Hz. The coherence is good (blue graphs in figure 5.27).
- After releasing the screw, the FRF graph shifted around 500 Hz to the right. The explanation could be an important change in vibrational modes after removing the connection between glenosphere and metaglene represented by the tightened screw. The corresponding coherence became very bad, probably due to the noise introduced by the quasi-free screw and a certain instability at the conical interface (yellow graphs in figure 5.27).
- In the case of the suboptimal contact resulted after inserting a small piece of paper between the conical surfaces and tightening the screw, the FRF graph presented only a main peak below 13450 Hz. The FRF graph shift to the left could be explained by a reduced stiffness due to the change of contact conditions at the conical interface. The coherence was good, but slightly below the coherence corresponding to the optimal fixation (green graphs in figure 5.27).
- Releasing the screw resulted in a dramatic decrease of the FRF amplitude and a very bad coherence. Practically, in this situation, the assembly did not behave as a linear system (red graphs in figure 5.27).

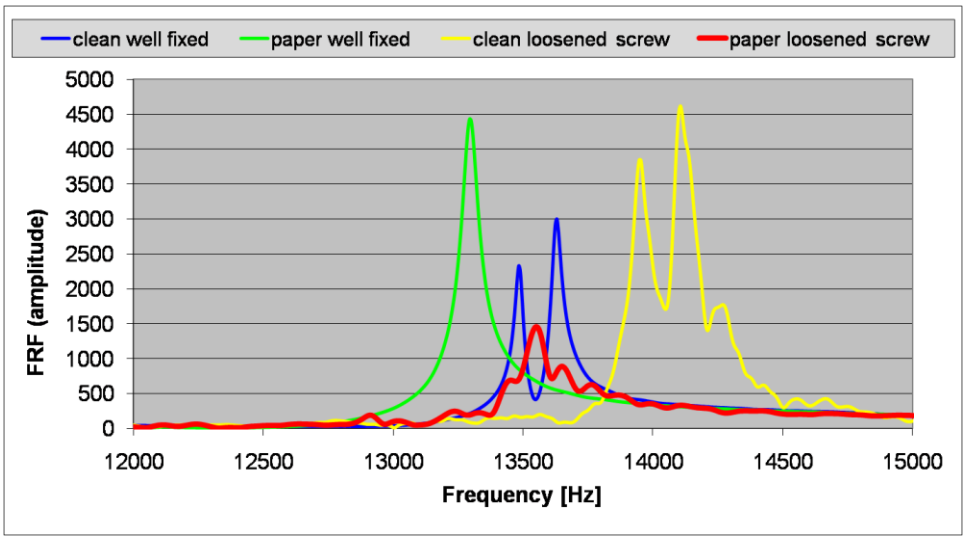

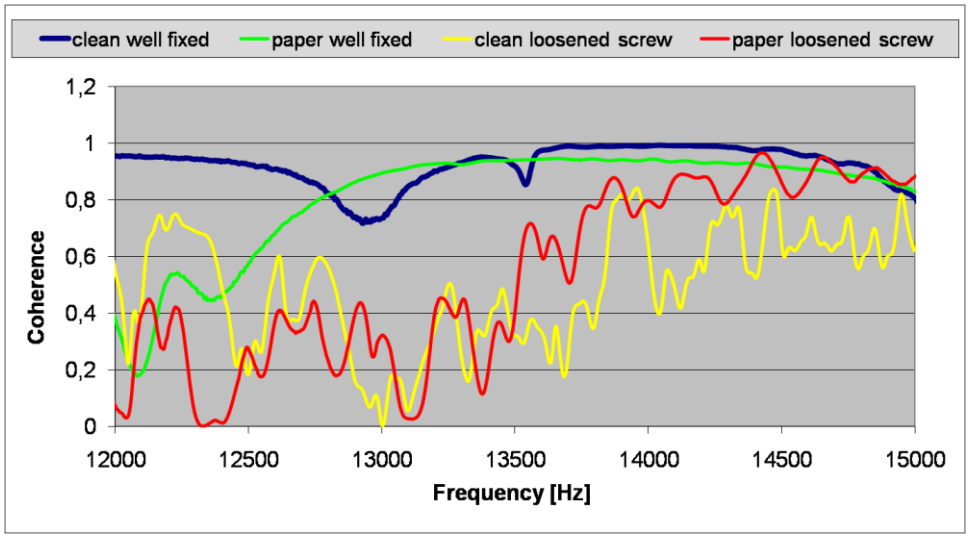

Figure 5.27. Vibrational behaviour of the glenoid assembly

Up: Frequency response function graphs
Down: Coherence graphs

Blue: Optimal contact between the conical surfaces, glenosphere and metaglene well fixed to each other, tighten screw.

Yellow: Optimal contact between the conical surfaces, glenosphere and metaglene well fixed to each other, released screw.

Green: Suboptimal contact between the conical surfaces, glenosphere and metaglene well fixed to each other, tighten screw.

Red: Suboptimal contact between the conical surfaces, glenosphere and metaglene well fixed to each other, released screw.

5.3. Conclusions and future work

5.3.1. Femoral implants

At the beginning of the insertion of the femoral implants on artificial or human femora (one or two steps) the FRF graph shifted to the right, but during the next steps the FRF graph could have an oscillatory behaviour. However, at the end of the insertion the FRF graph was stable and the coherence reached a maximum. When extra hammer hits were applied, the coherence slightly decreased.

The differences between the FRFs corresponding to the free implants, implants inserted in human femora, implants inserted and reinserted in Sawbones are visible, less stable implants having lower resonance frequencies.

Asymmetrical contact distribution at the interface between the implant and the femoral head has been detected.

The FRF has shown a more regular and coherent behaviour when the femoral implant was inserted on polyurethane cylinders probably due to the more strictly controlled geometry.

In this case, a quantitative correlation has been established between the resistance against the relative motion (extraction force), the interference at the contact surface, and the resonant frequencies.

5.3.2. Acetabular implants

Depending on specific vibrational modes and measurement methods, the FRF graph shifted to the right or to the left during the insertion of acetabular implants. The FRF shift was more important at the beginning of the insertion. At the end of the insertion the FRF graph shifted to the opposite direction, probably due to the important change in contact distribution after the rim of the acetabular implant passed over the rib existing at the edge of the acetabular cavity. This behaviour could be used to detect the end point of the insertion process.

The FRF graph shift was more visible in the range 0-2500 Hz if the FRF was measured directly on the implant without the impactor.

It was also possible to measure FRF directly on the impactor in two ways, transversal and axial. In this case, the FRF evolution was better observed in the ranges 0-700 Hz and 5-7.5 kHz.

5.3.3. Reverse shoulder implant

The results have proven that the analyses of FRF and coherence are sensitive enough to assess the quality of the contact in a Morse-type connection. In this way, the experiments performed on the glenoid component of a reverse shoulder prosthesis extend the applicability of vibration analysis in orthopaedy from the assessment of the stability of an implant inserted in a bone (like in the studies presented in previous chapters) to the detection of different degrees of fixation existing between the components of an orthopaedic implant.

Comparing the reference graphs corresponding to the optimal fixation to the graphs obtained during surgery, it is possible to detect dangerous situations and correct them.

5.3.4. Future work

Measurements have to be performed for both, femoral and acetabular, implants in various controlled situations to understand exactly the relationship between the contact conditions at the bone-implant interface and the vibrational behaviour, i.e. FRF, coherence, and vibration modes. In this way, quantitative correlation between the vibrational parameters (i.e. resonance frequencies) and the resistance against bone-implant relative movement, due to external loads, i.e. traction or torsion, will be derived.

It would be also interesting to realize a comparison between the FRFs corresponding to the cemented and uncemented femoral implants. Sawbones models with better mechanical properties and structure must be used in future experiments.

Finite element analyses (FEA) must be performed to simulate a larger variety of fixation situations and to predict the vibrational behaviour of the implant-bone structure.

If the in vitro experiments and FEA are promising, then per-operative protocols should be designed and, after testing and validating in cadavers, they could be applied during surgery as valuable methods to assess the implant primary stability and to detect the end point of insertion process.

In the case of the reverse shoulder implant, before obtaining a valuable tool for the surgeon, this study must be completed with an extensive analysis of the vibrational behaviour of the glenoid implant in more realistic conditions.

The per-operative protocol should take into account the influence of the human tissues on the vibrational properties of the analysed implant and an interesting extension might be obtained by the assessment of the stability of the metaglene on the glenoid. Shaker excitation, combined with the use of an impedance head instead the couple accelerometer-force cell, might be a solution for a user-friendly device.

6. Conclusions and further considerations

6.1. Hypotheses and questions

The study presented in this paper focused on a particular type of femoral component used in THR, the intra-operatively manufactured prosthesis. Two hypotheses guided the research work:

- Excepting the beginning, during the insertion process, the implant-bone structure behaves as a quasi-linear system, therefore the measuring method should be rather based on FRF analysis than on harmonic distortion.
- In the case of lower bending modes, the implant acts more like an added mass and the degree of fixation has no significant influence on the corresponding resonance frequencies. Exciting the more complicated modes, at higher frequencies, would increase the sensitivity of measurements because these modes are more influenced by the stress and contact conditions at the bone-implant interface.

The mechanical linearity predicted by the first hypothesis was confirmed by the good coherence obtained during the *in vitro* and *in vivo* measurements, therefore the per-operative monitoring of the fixation of implant-bone structures by FRF analysis is justified.

FEA confirmed the higher sensitivity of complicated modes to contact changes at the stem-femur interface and the experimental results have validated the second hypothesis.

The research work tried to find the correct answers for two questions:

- Can vibration analysis provide an objective measure for the increase in stability during the insertion in the case of cementless THR stems and by cement curing in the case of cemented THR stems?
- Can vibration analysis provide an objective criterion to detect the insertion endpoint of a cementless THR stem?

The measuring method has a good sensitivity between 5 and 10 kHz, the FRF graph evolution being a reliable indication of the fixation change in vitro and in vivo as well.

In normal conditions, an FRF graph shift to the right, between two successive insertion steps, indicates a normal increase of implant fixation. Closer to the end point of the insertion process, the FRF shift to the right becomes smaller despite the fact that the hammer blows have approximately the same magnitude, indicating an increase of fixation stability. When the FRF graph does not shift anymore, the implant is stable and the maximum fixation level

is reached. Further hammering could only increase the fracture risk. An implant is considered stable when the Pearson's coefficient of correlation between two consecutive FRF graphs is at least 0.99.

Another application of the presented vibrational method is the monitoring of cement curing. In this way it is possible to assess the fixation increase between the initial and the final stage of cement solidification. It is also possible to detect the moment when the curing process is complete.

6.2. Relevance and limitations

When this paper has been published the protocol described in this study was being the only known vibrational method successfully applied several times in real surgical conditions to assess the initial stability of femoral stems.

The monitoring process can be summarised as follows:

- After one or several orthopaedic hammer blows applied by the surgeon, the implant has reached a degree of fixation that is reflected by the corresponding FRF graph.
- To verify if the fixation is stable enough, another hammer blow is applied. In a normal situation there are two possibilities:
    - The FRF graph shifts to the right indicating a new degree of fixation superior to the previous one which was not stable enough.
    - The FRF graph does not change noticeably (Pearson's correlation coefficient higher than 0.99) indicating a stable fixation. Hammering must stop.

This method has two main advantages:

- The stability is tested by using normal hammer blows that generally result in increasing the degree of fixation.
- Since the load induced by an average hammer blow has at least a magnitude of 7000 N (Crisman et al. 2007) and the physiological load has a magnitude lower than 3000 N (Bergmann 2001), it is logical to assume that an implant stable to hammer blows will be stable to physiological load as well.

Sometimes abnormal situations may occur:

- The FRF does not change, but visibly the implant did not reach the end point of insertion. In this case the implant is jammed; it has to be pulled out and, after correcting the cavity, it may be reinserted.

- An FRF shift to the left indicates a loss of fixation, probably due to plastic deformations of the bone. This is a warning; the next hammer blow could fracture the bone.
- The FRF aspect changes dramatically and the coherence drops. This may indicate a bone fracture or a failure in the measurement system.

Although few non-typical cases were encountered during the experiments on cementles CMPs, the vibrational method has been proven to be useful in the prevention of intra-operative fractures.

The per-operative experimental study is currently completed and validated by post-operative follow-up of the patients that includes:

- Clinical examination, radiographies and standardised questionnaires.
- RSA (follow-up of migration of the stems).
- DXA (follow-up of bone remodelling).

(Claassen et al. 2007)

Due to the large geometrical variability of the CMP stems, this method is limited to a qualitative assessment of the fixation, indicating whether the insertion process unfolds correctly and resulting in the best possible fixation for the implant and the patient.

However, in the case of standardised stems, calibration tests can be performed to correlate the magnitude of implant micromotions to FRF shifts or to resonance frequency values. The resistance to sinking, tilting or rotating could be also correlated to the FRF graph evolution.

Applying a torque of a specific magnitude to quantitatively evaluate the stability of a femoral stem (as described in section 2.4) is not recommendable because of its destructive potential. If a quantitative assessment of the stability is really needed, it would be better to measure the impact force at each insertion stage by using an instrumented orthopaedic hammer.

However, the method based on a torque test might be useful during the revisions of the acetabular components. A torque equivalent to the load supported for climbing stairs could be applied to the femoral component. A method based on axial load, similar to the method used during surgery, could be applied as well. If the FRF graphs measured before and after applying the torque or the axial load are nearly identical, then the femoral implant is stable. Otherwise, it must be replaced.

6.3. Suggestions for future developments

The evaluation of the primary fixation of spherical orthopaedic implants by vibration analysis was a domain unexplored until now. The glenoidal assembly of reverse shoulder prostheses, hip resurfacing femoral and acetabular implants were studied during an in vitro series of exploratory experiments.

The preliminary study on shoulder prostheses, focused on metal-on-metal fixation, has shown the capacity of the vibrational method to detect a suboptimal contact due to the unwanted presence of soft tissues between the glenoidal components.

In the case of acetabular implants, the lack of visibility during surgery makes difficult the detection of end point of insertion. The vibrational method presented in section 5.1 could help in solving this problem.

In the case of HRA, the femoral and acetabular implants are standardised, thus the FRF graphs obtained during surgery could be easily compared to a reference graph obtained in satisfactory conditions of fixation.

Moreover, the results presented in section 5.1. show that it is possible to obtain quantitative relations between vibrational parameters (i.e. resonance frequency) and the resistance against the relative motion at the implant/bone interface (i.e. extraction force). These results also indicate that vibrational methods could be more easily derived and implemented for the assessment of the stability of standardised orthopaedic implants. Various criteria could be defined to decide if the implant fixation is satisfactory or if corrections must be applied.

The per-operative vibrational measurement protocol designed for CMP was easily integrated in the THR procedure. The surgical team manipulated the equipment without difficulties and the inherent changes introduced by the vibrational measurements did not disturb the surgical process. The total time for the surgical procedure was extended with 5-10 minutes only. However, for operating the measuring software and for interpreting the obtained results the presence of a trained technician was required.

Obviously, for a regular basis use, the measuring protocols described in chapters 2 and 4 and the corresponding equipment must be improved:

- Where possible, the components of the measuring equipment should be wireless interconnected.
- The components should be better adapted to the use in surgical theatre:
    - Repeated sterilisation capability;

    - Resistance against corrosion;
    - Biologically inert.
- Different connection devices are necessary for different types of implants.
- A software dedicated to the vibration analysis of orthopaedic implants must be written.
    - An extendible modular structure is preferable (each module would correspond to a specific type of implant).
    - An user-friendly interface should allow the surgical team to operate the whole measuring system without any technical assistance.
    - A database including the technical characteristics of different implants and the corresponding fixation requirements from the vibrational point of view must be part of such a software.

Certainly, vibration analysis is a promising tool for the orthopaedic implant domain, giving complementary information that helps the surgeon in taking the optimal decisions. Such a tool would be very useful especially for young, unexperimented surgeons.

Due to the Osstell system, the fixation and the osseointegration of dental implants can be easily evaluated by a vibrational technique, but a similar instrument, adapted for orthopaedic implants, does not exist yet. Probably, it is the moment for universities, medical and vibrational equipment manufacturers, software specialists, and orthopaedic surgeons to unite their efforts and produce such a tool that would introduce the non-invasive and efficient vibration analysis in the surgical theatres.

Another direction of development is represented by the vibrational instruments able to assess the osseointegration and the stability of orthopaedic implants after the surgery, during the follow-up procedures. Due to the fact that there is no possible direct contact to the orthopaedic implant, like in the case of dental and other Brånemark implants, such instruments should be based on telemetry systems (Puers et al. 2000) or indirect measurement methods (Rowlands et al. 2008). Methods based on harmonic distortion could be used to detect severe loosening, while methods based on resonance frequency shift seem to be more appropriate for detecting early loosening.

Accurate FEMs based on patient-specific anatomy and bone quality could predict the vibrational behaviour and this information might be used as an alternative reference for the assessment of the stability of orthopaedic implants.

Appendices

A1. Elements of anatomy

A1.1. Shoulder joint

The shoulder girdle (pectoral girdle) contains four bones: two clavicles and two scapulae. It supports the arms and serves as a place of attachment for muscles that move the arms. The bones of this girdle are weakly attached and held in place by ligaments and muscles. Each clavicle articulates medially with the sternum and laterally with the corresponding scapula.

The generic term "shoulder joint" usually refers to the glenohumeral joint. It is a ball and socket joint formed by the articulation between the head of the humerus and the glenoid fossa of the scapula. The "ball" of the joint is the rounded, medial anterior surface of the humerus and the "socket" is formed by the glenoid fossa, the concave portion of the lateral scapula (figure A1.1). The shallowness of the fossa and relatively loose connections between the shoulder and the rest of the body allows the arm to have tremendous mobility, but the shoulder joint is much easier to dislocate than most other joints in the body.

(Gray 1918, Mader 2005)

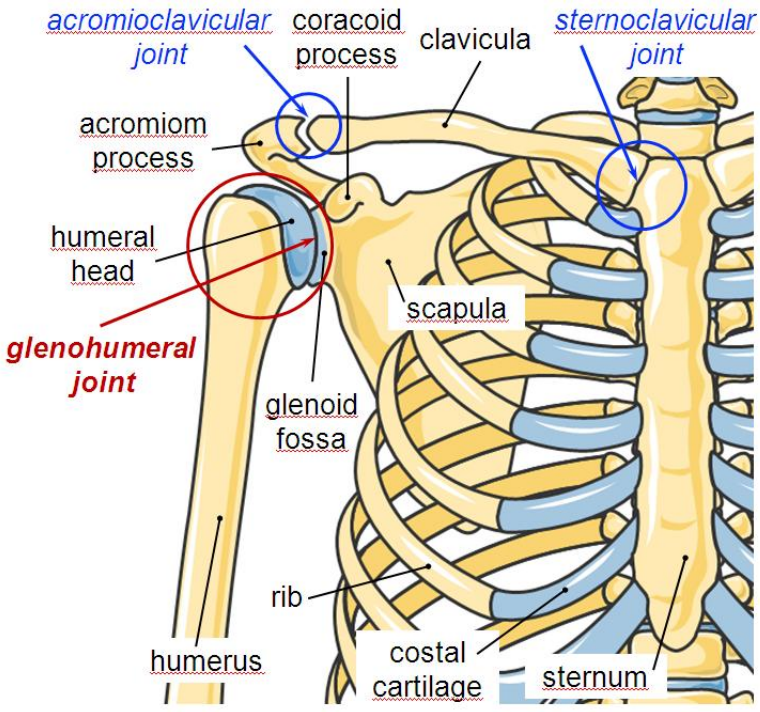

Figure A1.1. Frontal view of the shoulder girdle (right side) with the humerus attached (Figure produced using Servier Medical Art)

A1.2. Hip joint

The hip joint is a ball and socket joint formed by the articulation of the rounded head of the femur and the cup-shaped cavity of the acetabulum. It forms the primary connection between the bones of the lower limb and the axial skeleton of the trunk and pelvis. The pelvic girdle contains two coxal bones (hipbones), as well as the sacrum and coccyx. The cup-like acetabulum is situated at the union of the three parts of the coxal bone — the ilium, pubis, and ischium (figure A1.2).

Both joint surfaces are covered with a strong and lubricated layer called articular hyaline cartilage. The articular cartilage on the head of the femur is thicker at the center than at the circumference and covers the entire surface with the exception of the fovea capitis femoris, to which the ligamentum teres is attached. The articular cartilage on the acetabulum forms an incomplete marginal ring, the lunate surface. Within the lunate surface there is a circular depression without cartilage, occupied by a mass of fat, covered by synovial membrane.

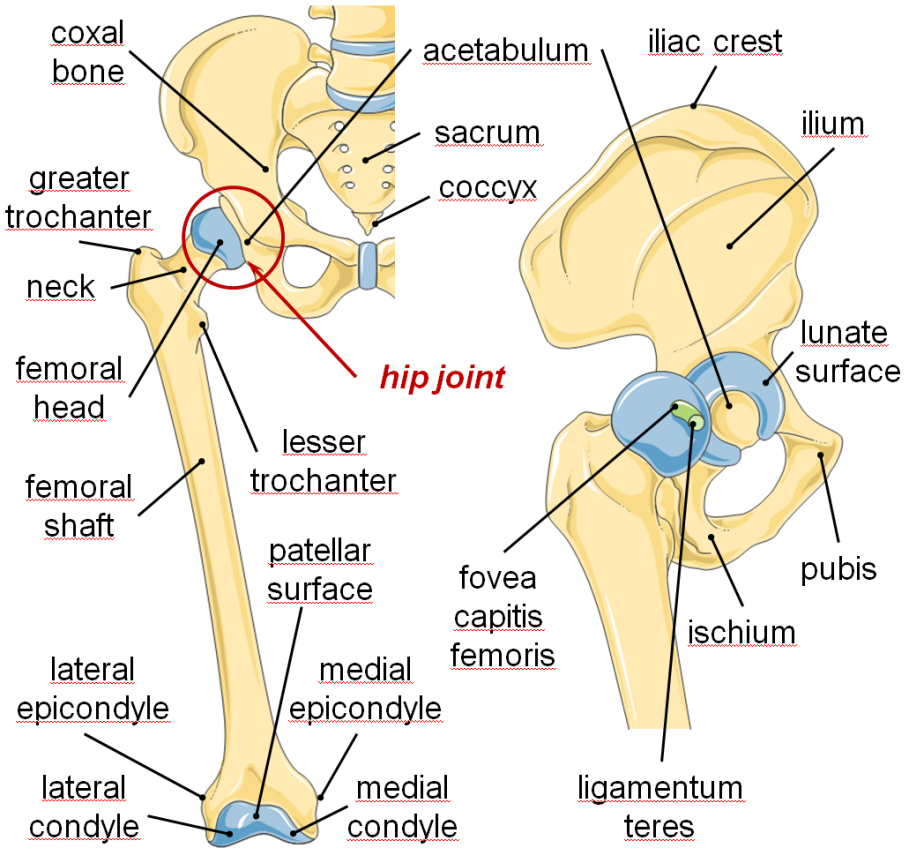

Figure A1.2. Pelvic girdle

Left: Frontal view with the right femur attached
Right: Lateral view of the hip joint. The femur is detached and rotated 90°
(Figures were produced using Servier Medical Art)

The hip joint is characterised by the fact that the approximate spherical femoral head is largely contained within the acetabulum and has an average radius of curvature of 2.5 cm. The acetabulum grasps almost half the femoral ball, a grip augmented by a the acetabular labrum, ring-shaped fibrocartilaginous lip, which extends the joint beyond the equator. The head of the femur is attached to the shaft by a neck that is often prone to fracture in the elderly, which is mainly due to the degenerative effects of osteoporosis.

(Gray 1918, Mader 2005)

A2. Custom made prosthesis

A2.1. Introduction

An infinite variety of femoral cavities have to be fitted with a very limited range of available prostheses. The characteristics of every prosthesis concern not only the size of the stem, which must be stabilised in the femoral cavity, but also the shape, location and the orientation of the acetabular part of the joint. Numerous other position factors are important: the offset of the head, the anteversion or retroversion of the neck, and the varus or valgus position of the prosthesis.

With an artificial prosthesis stem, the transfer of the load to the tubular structure of the femoral canal creates forces and stresses quite different from those encountered in normal physiological and anatomical conditions. The result of these mechanical influences on the bone tissue can be resorption, new bone formation or a stable situation. In these conditions a better “fit and fill” of the prosthesis in the femoral cavity might prevent the mechanical problems of subsidence and breakdown of the interface, with loosening and bone destruction as consequence.

Because custom prostheses pre-operatively manufactured from information obtained by radiographs or computer tomography scans were very often unsatisfactory, a system was developed to produce an individual prosthetic stem during the surgical procedure by using the measurements of the mould of the properly prepared femoral cavity.

A2.2. Manufacturing the implant

After preparing the femoral shaft by removing all very soft or very loose cancellous bone tissue and after compression of the walls of the cavity by means of a series of conical shaped compactors, a mould is taken of the cavity by injecting an elastomer into a very thin rubber bag (figure A2.1)

The mould is introduced in a specially designed measuring machine with a rotating axis and a laser beam that moves along a vertical axis (figure A2.2). Because the mould is somewhat flexible, it is measured without physical contact. Approximately 1600 points of the surface of the mould are registered in about 90 seconds with an accuracy of +/-0.05 mm. These coordinates are sent to a CAD-CAM system that reconstructs the femoral cavity.

An engineer-designer will take into account the instructions of the surgeon in order to adjust, in a computer-aided system, the offset, the stem length, the degree of anteversion of the neck, and the varus or valgus position. The mould is slightly flexible and can be

withdrawn from the femoral cavity even when there are interlocking contours within the bone. The final metal prosthesis, however, is rigid and interlocking features must be eliminated. The system is programmed to achieve this with minimal loss of bone contact.

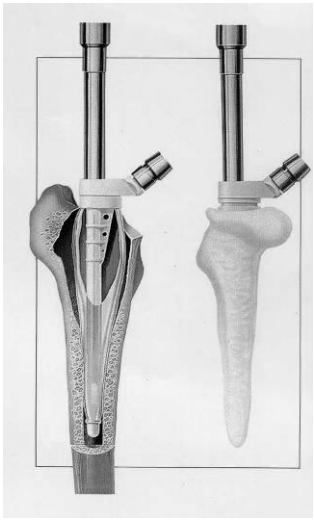

Figure A2.1. The mould (Courtesy of Advanced Custom Made Implants SA/NV, Belgium)

Figure A2.2. Measuring the mould (Courtesy of Advanced Custom Made Implants SA/NV, Belgium)

After designing the final prosthesis following the surgeon's requirements, the geometrical data are treated by the proprietary CAM software that generates a program for a particular NC milling machine. This program will ensure that the prosthesis is safely milled from a forged annealed preform in titanium alloy (TiA16V4), in the shortest possible time. From a variety of preforms, of which the geometrical data are stored in the database, the most suitable one is chosen for manufacturing the prosthesis. The machining is carried out with specialised cutting tools and under the right cooling conditions to avoid transformation of the metallurgical structure. (Figure A2.3).

After NC machining, some manual finishing operations follow, such as the removal of burrs and sharp edges. Thorough decontamination and passivation then dispose of all external inclusions on the surface of the prosthesis. To improve the osseointegration of the stem, the proximal part of the prosthetic surface is coated with hydroxyapatite (HA). After a final inspection of the surface by a microscope, the prosthesis is sterilised, as required. Figure A2.4 shows a mould and the corresponding prosthesis.

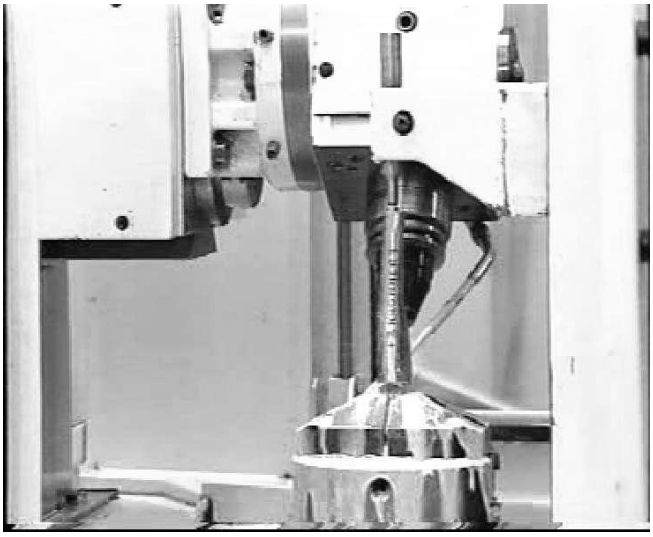

Figure A2.3. Milling the stem (Courtesy of Advanced Custom Made Implants SA/NV, Belgium)

Figure A2.4. The mould and the prosthesis

The CMP system allows accomplishing the following objectives:

- To produce maximal initial stability by obtaining a better "fit and fill" of the prosthesis in the femoral cavity;
- To avoid localized stress at any given area of the prepared cavity;
- To vary at will the characteristics of the femoral neck:
    - Length of the neck (offset);
    - Anteversion-retroversion of the neck.
- To vary the characteristics of the stem :
    - Valgus or varus position in the cavity (axis of the stem);
    - Length.

Hybrid fixation of the IMP stem is also possible. In this fixation system, the distal part of the stem is thinner than the corresponding mould and it is cemented, providing better initial stability of the implant, which should favour osseointegration of the proximal femur with the HA coating on the proximal part of the IMP stem.

(Eggars 1993, Mulier et al. 1989, Mulier et al. 2010, Salvi 1992)

A3. Gruen zones

The proximal femur was divided into 14 zones around the femoral component of a THR prosthesis for zonal evaluation of bone-implant contact, bone quality, and loosening (Breusch et al. 2001, Gruen et al. 1979). In the literature related to THR this zones are widely used as topographic references (figure A3.1). Zone 7 is also known as the calcar region.

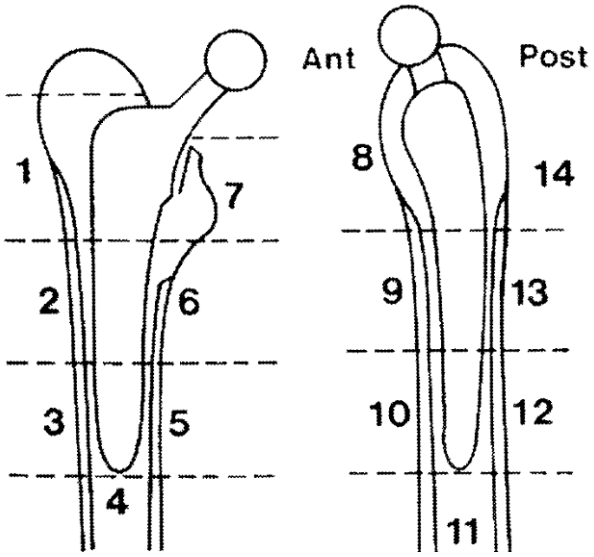

Figure A3.1 Gruen zones in anteroposterior (left) and lateral (right) planes (Breusch et al. 2001)[7]

[7] Reprinted from Breusch S.J., Lukoschek M., Kreutzer J., Brocai D., Gruen T.A., 2001. Dependency of cement mantle thickness on femoral stem design and centralizer. Journal of Arthroplasty 16 (5), 648-657 with permission from Elsevier.

A4. Elements of vibration analysis

A4.1. Harmonic motion

An oscillatory motion repeated in equal intervals of time *T* is called periodic motion. The repetition time *T* is called the *period* of the oscillation and its reciprocal, *f = 1/T*, is called the *frequency*. Any periodic motion described by the time function *x(t)* satisfies the equation:

$$x(t) = x(t+T) \tag{A4.1}$$

The harmonic motion is the simplest form of periodic motion and can be expressed by the equation:

$$x = X \sin \omega t \tag{A4.2}$$

where:

- x = displacement from the equilibrium position;
- X = displacement amplitude (single-peak amplitude) of the oscillation, x travels between the limits ± X;
- ω = so called angular frequency expressed in rad/s;
- t = time.

The period of function sine is 2π, hence:

$$T = \frac{2\pi}{\omega}, \qquad f = \frac{\omega}{2\pi} \tag{A4.3}$$

The velocity is obtained by differentiating the equation (A4.2):

$$\dot{x} = \omega X \cos \omega t = \omega X \sin\left(\omega t + \frac{\pi}{2}\right) \tag{A4.4}$$

and the corresponding acceleration is obtained by differentiating the equation (A4.4):

$$\ddot{x} = -\omega^2 X \sin \omega t = \omega^2 X \sin(\omega t + \pi) \tag{A4.5}$$

From (A4.2) and (A4.5) results:

$$\ddot{x} = -\omega^2 x \tag{A4.6}$$

therefore, in harmonic motion, the acceleration is proportional to the displacement and is directed toward the origin. Since the acceleration is proportional to the force, harmonic motion can be expected for systems with linear springs with force varying as *kx*.

The trigonometric functions of *sine* and *cosine* are related to the exponential functions by Euler's equation:

$$e^{i\theta} = \cos\theta + i \sin\theta \tag{A4.7}$$

where *e* is an irrational constant number, the base of natural logarithms $(e \cong 2{,}718281)$, the angle θ is expressed in radians, and $i = \sqrt{-1}$.

A vector of amplitude X rotating at constant angular speed ω can be represented as a complex quantity x in an Argand diagram (figure A4.1).

$$x = Xe^{i\omega t} = X\cos\omega t + iX\sin\omega t = Re(x) + iIm(x) \quad \text{(A4.8)}$$

The quantity $x = Xe^{i\omega t}$ also satisfies the differential equation (A4.6) for harmonic motion. *Re* stands for the real part of the complex number *x*, while *Im* stands for the imaginary part.

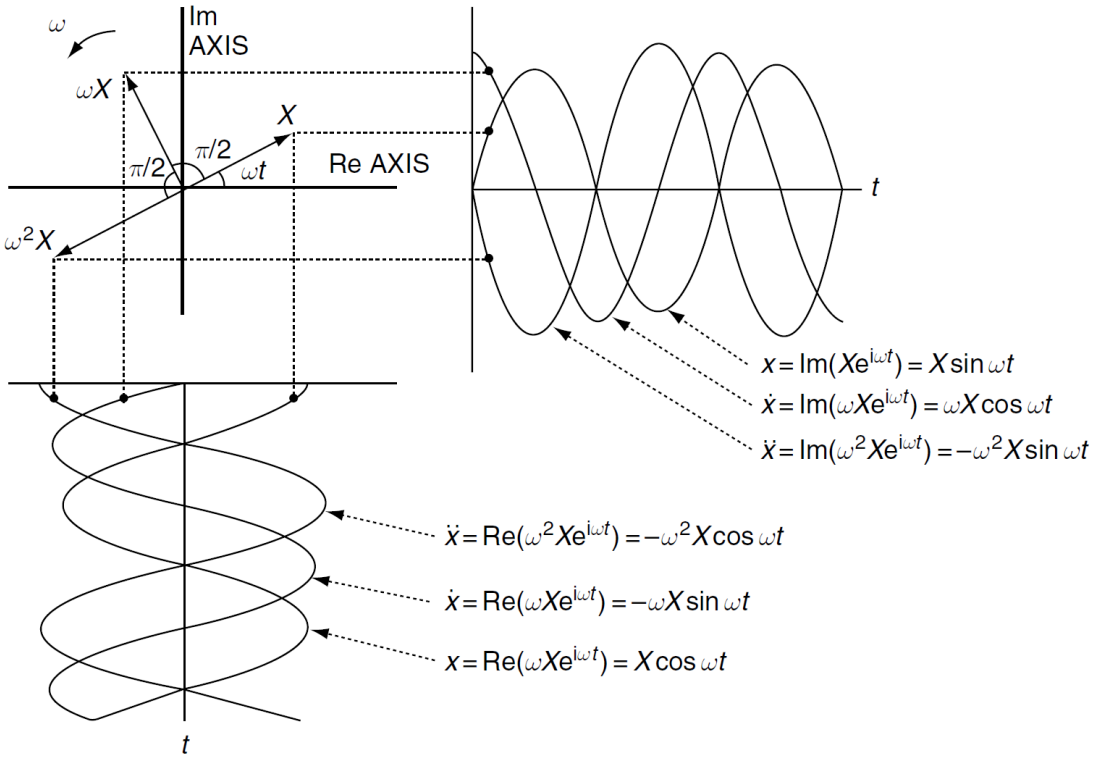

Figure A4.1. Harmonic motion represented by a rotating vector

The exponential form of the harmonic motion often offers mathematical advantages over the trigonometric form.

(Thomson 1998, Thorby 2008)

A4.2. Response to harmonic excitation

In this section, the response of single degree of freedom (SDOF) systems to simple harmonic excitation is discussed (figure A4.2).

The following notation is used:

- m = total moving mass;
- k = spring stiffness;
- ωn = undamped natural frequency, rad/s,

$$\omega_n = \sqrt{\frac{k}{m}} \quad \text{(A4.9)}$$

- fn = undamped natural frequency in Hz, where fn = ωn/2π;
- c = viscous damping coefficient;
- cc = critical damping coefficient;

$$c_c = 2m\sqrt{\frac{k}{m}} = 2m\omega_n = 2\sqrt{km} \quad \text{(A4.10)}$$

- γ = damping ratio;

$$\gamma = \frac{c}{c_c} \quad \text{(A4.11)}$$

- ωd = damped natural frequency, rad/s:

$$\omega_d = \omega_n\sqrt{1-\gamma^2} \quad \text{(A4.12)}$$

- ω = forcing frequency, rad/s;
- Ω = frequency ratio;

$$\Omega = \frac{\omega}{\omega_n} \quad \text{(A4.13)}$$

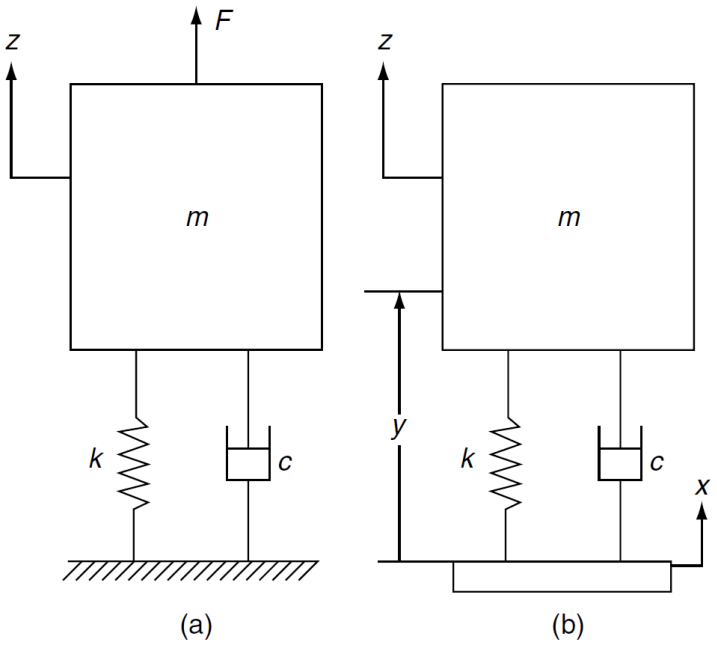

Figure A4.2. Single degree of freedom vibrating system

(a) direct force excitation, (b) base motion excitation

The differential equation of motion for the linear system shown in the figure A4.2.a is:

$$m\ddot{z} + c\dot{z} + kz = F \quad \text{(A4.14)}$$

where the force *F* is defined as:

$$F = P\sin\omega t \quad \text{(A4.15)}$$

The solution of the equation (A4.14), representing the total response of the SDOF system, is:

$$z = e^{-\gamma\omega_n t}(A\cos\omega_d t + B\sin\omega_d t) + C\cos\omega t + D\sin\omega t \qquad \text{(A4.16)}$$

where the first two terms (those including $e^{-\gamma\omega_n t}$) are the *transient* terms that will disappear soon if damping is present. Therefore, the *steady-state* displacement response to the sinusoidal force F is:

$$z = C\cos\omega t + D\sin\omega t \qquad \text{(A4.17)}$$

where:

$$C = \frac{P}{k}\cdot\frac{-2\gamma\Omega}{(1-\Omega^2)^2+(2\gamma\Omega)^2} \qquad \text{(A4.18)}$$

$$D = \frac{P}{k}\cdot\frac{1-\Omega^2}{(1-\Omega^2)^2+(2\gamma\Omega)^2} \qquad \text{(A4.19)}$$

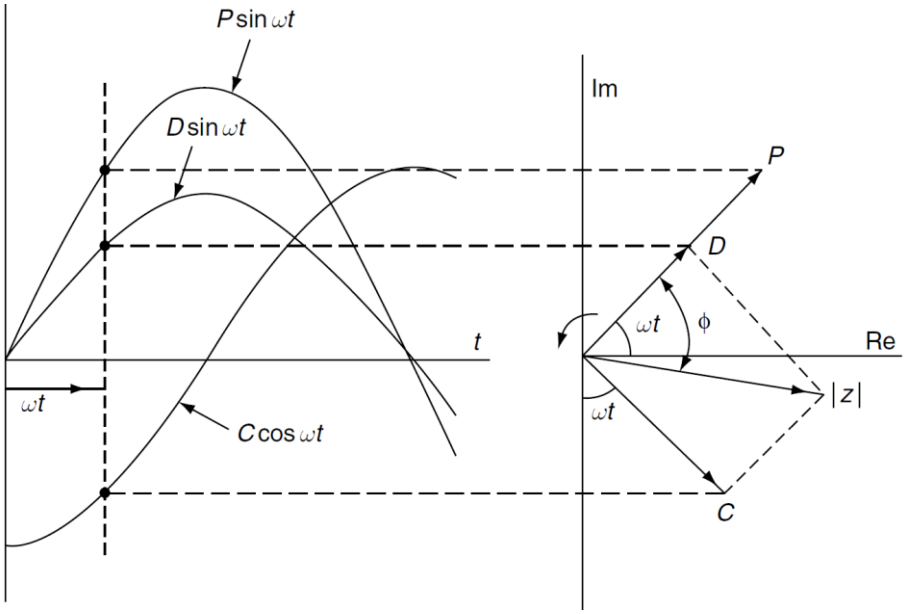

Figure A4.3. Excitation force and corresponding steady-state response
(a) trigonometric representation, (b) complex representation

From figure A4.3 can be seen that the modulus (magnitude) of *z*, say |*z*|, and the phase angle ϕ by which the displacement vector |*z*| lags the force *P* are given by:

$$|z| = \sqrt{C^2 + D^2} = \frac{P}{k}\cdot\frac{1}{\sqrt{(1-\Omega^2)^2+(2\gamma\Omega)^2}} \qquad \text{(A4.20)}$$

$$\tan\phi = \frac{-C}{D} = \frac{2\gamma\Omega}{1-\Omega^2} \qquad \text{(A4.21)}$$

For the configuration shown in the figure A4.2.b, the differential equation of the relative motion between the mass and the base is:

$$m\ddot{y} + c\dot{y} + ky = -m\ddot{x} \tag{A4.22}$$

The solution, expressed in amplitude and phase form, is:

$$\frac{|y|}{|x|} = \frac{\Omega^2}{\sqrt{(1-\Omega^2)^2+(2\gamma\Omega)^2}} \tag{A4.23}$$

$$\tan\phi = \frac{2\gamma\Omega}{1-\Omega^2} \tag{A4.24}$$

The differential equation relating the absolute motion of the mass, shown as z in figure A4.2.b, to the base motion is:

$$m\ddot{z} + c\dot{z} + kz = c\dot{x} + kx \tag{A4.25}$$

The amplitude ratio and the corresponding phase lag are:

$$\frac{|z|}{|x|} = \sqrt{\frac{1+(2\gamma\Omega)^2}{(1-\Omega^2)^2+(2\gamma\Omega)^2}} \tag{A4.26}$$

$$\tan\phi = \frac{2\gamma\Omega^3}{1-\Omega^2+(2\gamma\Omega)^2} \tag{A4.27}$$

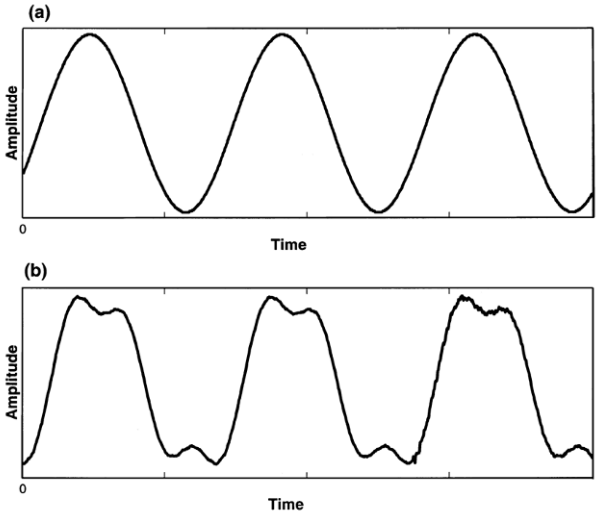

Figure A4.4. Response signal to harmonic excitation (time domain)

(a) Linear system, non-distorted sine wave

(b) Non-linear system, distorted sine wave

If a linear mechanical system is harmonically excited, the response will be a harmonic motion described by a sinusoidal graph. If the excited system is non-linear, supplementary content is added to the harmonic input signal resulting in a distorted output signal (figure A4.4). An intermittent contact between two components of a mechanical structure may introduce nonlinearities.

(Puers 2000, Thomson 1998, Thorby 2008)

A4.3. Frequency response function

The frequency response function (FRF) is a transfer function that describes the input-output relationship between two points on a mechanical system as a function of frequency. An FRF is a measure of the dynamic properties of a structure by indicating the displacement, velocity, or acceleration response at an output point, per unit of excitation force at an input point. Since both, force and motion, are vectors, an FRF is actually defined between an SDOF input (point and direction) and an SDOF output.

The FRF is also defined as the ratio of the Fourier transform of an output response ($X(\omega)$) divided by the Fourier transform of the input force ($F(\omega)$) that caused the output (figure A4.5 and equation (A4.28)).

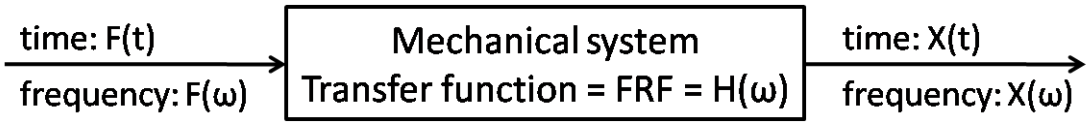

Figure A4.5. Block diagram of an FRF

$$H(\omega) = \frac{X(\omega)}{F(\omega)} \qquad \text{(A4.28)}$$

$$X(\omega) = H(\omega)F(\omega) \qquad \text{(A4.29)}$$

$F(\omega)$ is the input force as a function of the angular frequency ω, $H(\omega)$ is the transfer function, and $X(\omega)$ is the displacement response function. Each function is a complex function, which can be represented in terms of magnitude and phase. Similar transfer functions can be developed for the velocity and acceleration responses. There are six basic transfer functions:

- Compliance, receptance or admittance (displacement / force)
- Mobility (velocity / force)
- Inertance or accelerance (acceleration / force)
- Dynamic stiffness (1 / compliance)
- Mechanical impedance (1 / mobility)
- Dynamic mass (1 / inertance)

The compliance function is:

$$\frac{X(\omega)}{F(\omega)} = \frac{1}{k} \cdot \frac{\omega_n^2}{\omega_n^2 - \omega^2 + i(2\gamma\omega\omega_n)} \qquad \text{(A4.30)}$$

The compliance function can be represented in terms of magnitude and phase angle ϕ as:

$$\left|\frac{X(\omega)}{F(\omega)}\right| = \frac{1}{k} \cdot \frac{\omega_n^2}{\sqrt{\left(\omega_n^2-\omega^2\right)^2+(2\gamma\omega\omega_n)^2}} = \frac{1}{m} \cdot \frac{1}{\sqrt{\left(\omega_n^2-\omega^2\right)^2+(2\gamma\omega\omega_n)^2}} \quad \text{(A4.31)}$$

$$\phi = \tan^{-1}\left(\frac{2\gamma\omega\omega_n}{\omega_n^2-\omega^2}\right) \quad \text{(A4.32)}$$

The mobility function is:

$$\frac{V(\omega)}{F(\omega)} = \frac{1}{k} \cdot \frac{i\omega\omega_n^2}{\omega_n^2-\omega^2+i(2\gamma\omega\omega_n)} \quad \text{(A4.33)}$$

The mobility function can be represented in terms of magnitude and phase angle θ as:

$$\left|\frac{V(\omega)}{F(\omega)}\right| = \frac{1}{k} \cdot \frac{\omega\omega_n^2}{\sqrt{\left(\omega_n^2-\omega^2\right)^2+(2\gamma\omega\omega_n)^2}} = \frac{1}{m} \cdot \frac{\omega}{\sqrt{\left(\omega_n^2-\omega^2\right)^2+(2\gamma\omega\omega_n)^2}} \quad \text{(A4.34)}$$

$$\theta = \tan^{-1}\left(\frac{-\omega_n^2+\omega^2}{2\gamma\omega_n}\right) \quad \text{(A4.35)}$$

The accelerance function is:

$$\frac{A(\omega)}{F(\omega)} = \frac{1}{k} \cdot \frac{-\omega^2\omega_n^2}{\omega_n^2-\omega^2+i(2\gamma\omega\omega_n)} \quad \text{(A4.36)}$$

The accelerance function can be represented in terms of magnitude and phase angle α as:

$$\left|\frac{A(\omega)}{F(\omega)}\right| = \frac{1}{k} \cdot \frac{-\omega^2\omega_n^2}{\sqrt{\left(\omega_n^2-\omega^2\right)^2+(2\gamma\omega\omega_n)^2}} = \frac{1}{m} \cdot \frac{-\omega^2}{\sqrt{\left(\omega_n^2-\omega^2\right)^2+(2\gamma\omega\omega_n)^2}} \quad \text{(A4.37)}$$

$$\alpha = -\pi + \tan^{-1}\left(\frac{2\gamma\omega_n}{\omega_n^2-\omega^2}\right) \quad \text{(A4.38)}$$

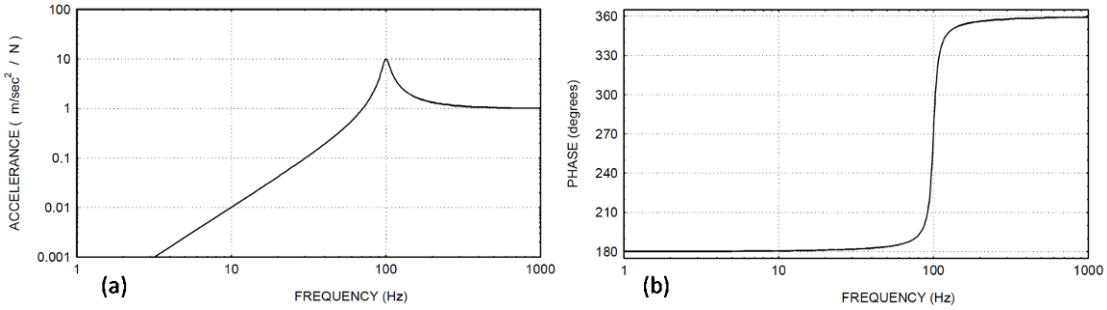

Figure A4.6. FRF (Accelerance) for an SDOF system

(a) Amplitude, (b) Phase

Figure A4.6 presents an example of accelerance function plotted in terms of amplitude and phase. If the linear system is excited by a sinusoidal force (harmonic excitation), the frequency corresponding to the maximum of the accelerance function (figure A4.6a) is the

excitation frequency, otherwise, if the system is excited by impulse or noise, that is the resonance frequency of the vibrating system.

In most cases a real mechanical structure cannot be described as an SDOF system because it is composed by a large number of masses, stiffnesses, and dampings. Such structures requiring two or more coordinates to describe their motion are defined as multi degree of freedom (MDOF) systems.

The dynamic behaviour of an MDOF system is described by the equation:

$$[M]\{\ddot{x}\} + [C]\{\dot{x}\} + [K]\{x\} = \{f\} \quad \text{(A4.39)}$$

where:

- $[M]$ = mass matrix;
- $[C]$ = damping matrix;
- $[K]$ = stiffness matrix;
- $\{f(t)\}$ = forcing vector;
- $\{x(t)\}$ = displacement response vector;

The transfer function (FRF) matrix is given by the equation:

$$\{X(\omega)\} = [H(\omega)]\{F(\omega)\} \quad \text{(A4.39)}$$

which can be also written as:

$$\begin{bmatrix} X_1(\omega) \\ X_2(\omega) \\ \dots \\ X_p(\omega) \end{bmatrix} = \begin{bmatrix} H_{11}(\omega) & \dots & H_{1q}(\omega) \\ H_{21}(\omega) & \dots & H_{2q}(\omega) \\ \dots & \dots & \dots \\ H_{p1}(\omega) & \dots & H_{pq}(\omega) \end{bmatrix} \begin{bmatrix} F_1(\omega) \\ F_2(\omega) \\ \dots \\ F_q(\omega) \end{bmatrix} \quad \text{(A4.40)}$$

$F_q(\omega)$ is the input force at point q as a function of the angular frequency ω, $X_p(\omega)$ is the displacement response function at point p, and $H_{pq}(\omega)$ is the transfer function (FRF) between the input at point q and the output at point p.

An example of FRF graph corresponding to a system with three degrees of freedom is presented in figure A4.7.

Resonance frequencies are inherent properties of a structure and they are determined by the material properties (mass, stiffness, damping), and boundary conditions. The number of resonance frequencies is equal to the number of degrees of freedom.

A stiffness increase results in a higher resonance frequencies while a damping increase causes a slight decrease in resonance frequencies. The main influence of damping increase is a decrease in the amplitude of the FRF at resonances. Also the phase change more smoothly. An increasing mass shifts the resonance frequencies to lower values.

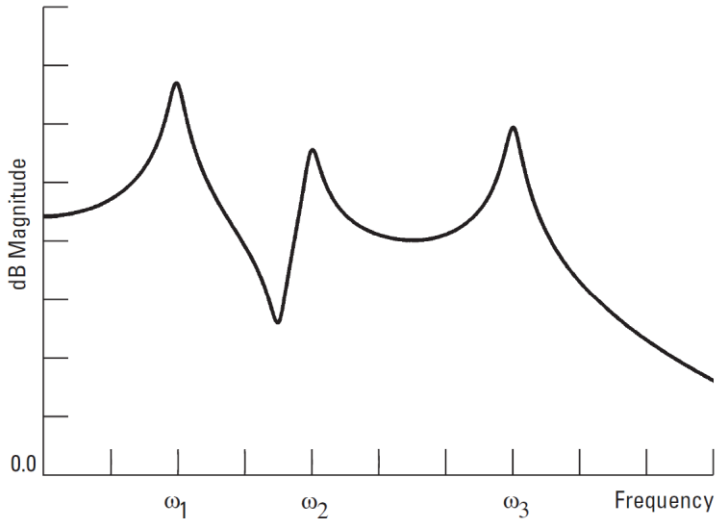

Figure A4.7. Frequency response function – MDOF system

(Ewins 2000, Heylen et al. 1997, Schwarz, Richardson 1999, Thomson 1998, Thorby 2008)

A4.4. Modal analysis

Modal analysis is defined as the study of the dynamic characteristics of a mechanical structure. It is based on two major assumptions:

- The studied system is linear;
- The system is stationary.

Vibrational modes are inherent properties of mechanical structures; each mode being defined by three parameters: a modal (natural or resonant) frequency, a modal damping, and a modal shape. If either the material properties or the boundary conditions of a structure change, its modes will change. If a structure vibrates at or near the natural frequency of a mode, the overall vibration shape will tend to be dominated by the mode shape of the resonance.

The modal parameters can be obtained analytically and experimentally. Figure A4.8 shows a schematic representation of both methods.

Numerical methods can also be used to extract the modal parameters from finite element models.

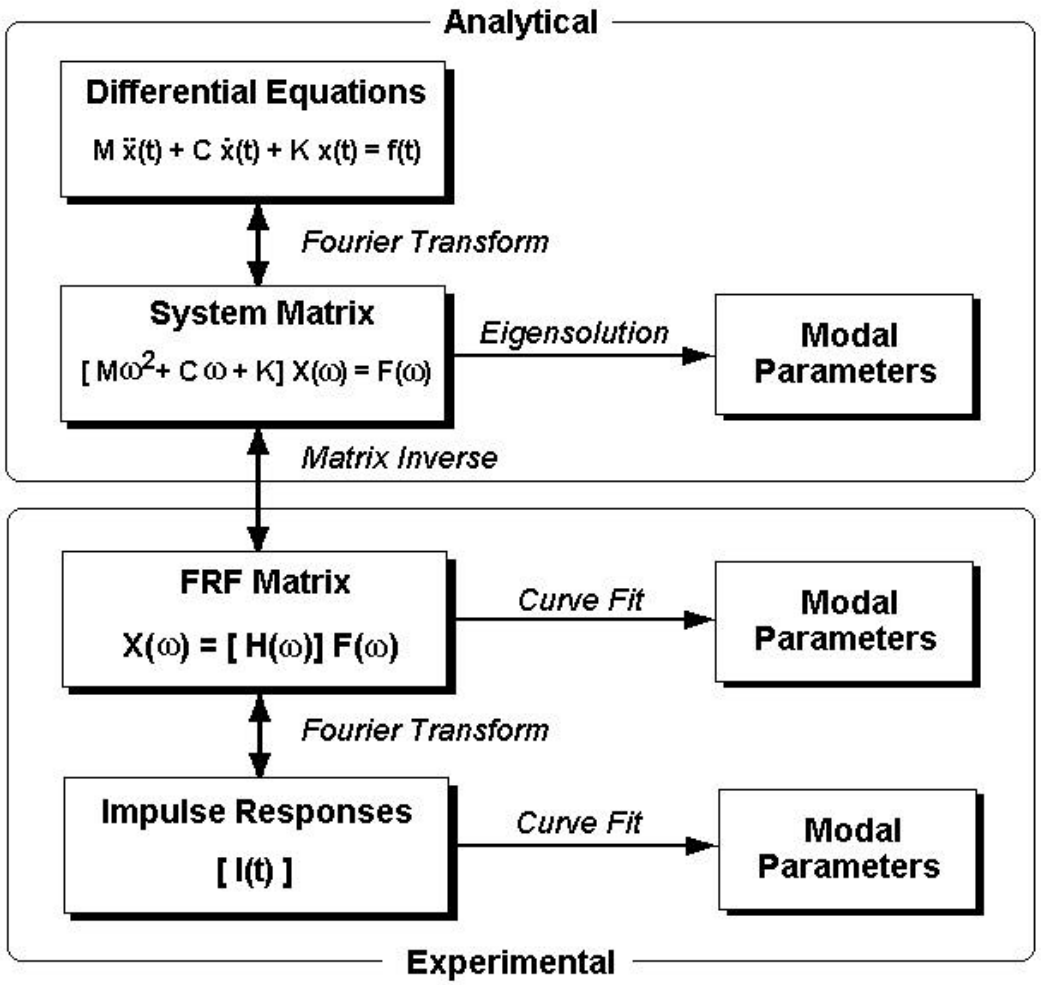

Figure A4.8. Analytical and experimental sources of modal parameters (Schwarz, Richardson 1999)[8]

In the FRF matrix from equation (A4.40), columns correspond to inputs, and rows correspond to outputs. Modal analysis requires FRFs from at least one row or column of the FRF matrix. The resonance frequencies and modal damping can be estimated from any or all of the FRFs in a row or column, while each mode shape is obtained by assembling together the FRF numerator terms (residues) from at least one row or column of the FRF matrix.

The FRFs are measured under controlled conditions. The analysed structure is excited at the input points by either using an impact hammer, or one or more shakers, instrumented with load transducers. The vibrational response is measured using one or several accelerometers positioned at the output points. A vibration analyser records the input and output signals in time domain, applies FFT, and calculates the corresponding FRFs. Finally, during a post-processing phase, the modal parameters are extracted and the mode shapes are

[8] Reprinted from Schwarz B. J., Richardson M. K. 1999, Experimental modal analysis, CSI Reliability Week, Orlando, FL, USA with permission.

visualised. The input-output structural response problem for the first four modes of a plate is schematically illustrated in figure A4.9.

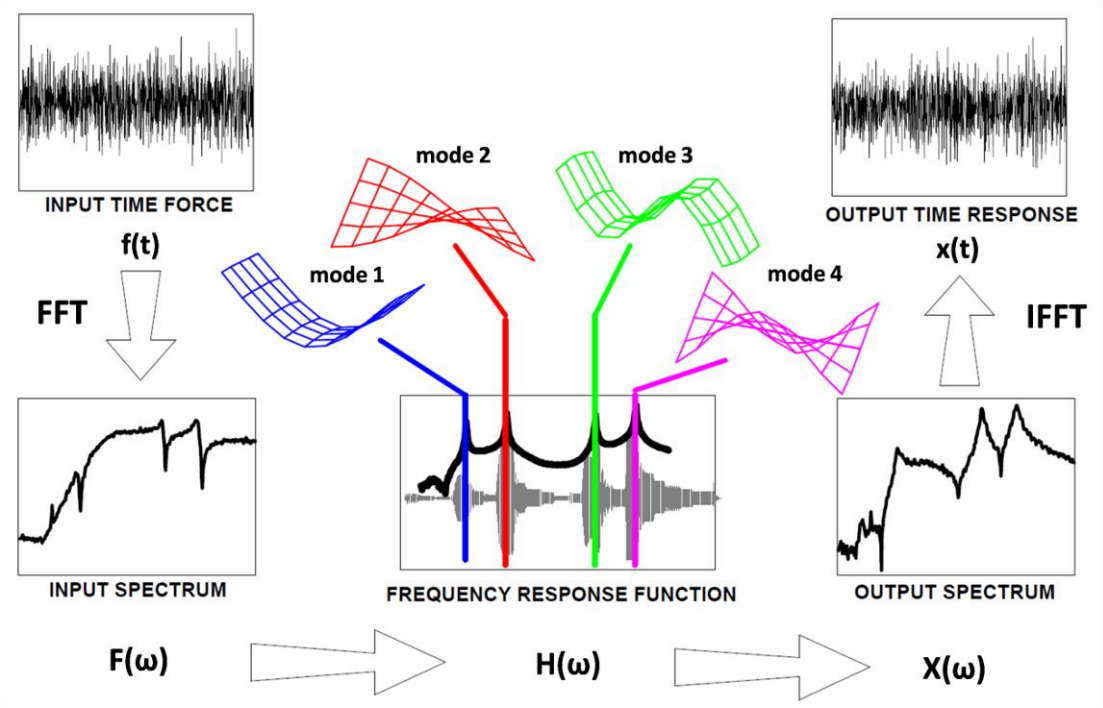

Figure A4.9. Input-output structural response problem. Schematic overview. (Avitabile 2001)[9]

Experimental modal analysis can be realised by single or multiple reference testing.

The single reference method that uses a single fixed input (the reference) is called single-input-multiple-output (SIMO) testing. A single column of the FRF matrix is obtained, and the equation (A4.39) becomes:

$$\begin{bmatrix} X_1(\omega) \\ X_2(\omega) \\ \dots \\ X_p(\omega) \end{bmatrix} = \begin{bmatrix} H_1(\omega) \\ H_2(\omega) \\ \dots \\ H_p(\omega) \end{bmatrix} F(\omega) \qquad \text{(A4.41)}$$

The single reference method that uses a single fixed output (the reference) is called multiple-input-single-output (MISO) testing.

By this method a single row of the FRF matrix is obtained and the equation (A4.39) becomes:

$$X(\omega) = [H_1(\omega) \quad \dots \quad H_q(\omega)] \begin{bmatrix} F_1(\omega) \\ F_2(\omega) \\ \dots \\ F_q(\omega) \end{bmatrix} \qquad \text{(A4.42)}$$

[9] Reprinted from Avitabile P., 2001. Experimental modal analysis - a simple non-mathematical presentation, Sound and Vibration, 11 pp. with permission.

The method that uses several references is called multiple-input-multiple-output (MIMO) testing. In this case multiple rows and columns from the FRF matrix are obtained and the equation (A4.40) is applicable.

MIMO testing is used if:

- All modes of interest cannot be adequately excited from a single reference;
- The vibrational responses cannot be adequately measured from a single reference;
- Some modes are so closely coupled that more than one reference is needed to identify them correctly.

Experimental modal parameters are obtained from a set of FRF measurements by applying different curve fitting methods:

- Local SDOF
- Local MDOF
- Global
- Multi-reference (Poly-reference)

SDOF methods obtain modal parameters for one mode at a time, while the other methods can simultaneously estimate modal parameters for several modes. Local methods are applied to one FRF at a time. Global and multi-reference methods are applied to a whole set of FRFs at once.

SDOF methods can be mostly applied to FRF data sets with light modal coupling (density). The cases with high modal coupling should be analysed using MDOF methods.

Global methods are recommended for structures with local modes. Multi-reference methods can find very closed coupled modes where the other methods are inefficient.

The frequency of a resonance peak in the FRF is considered as the modal frequency. A resonance peak should appear at the same frequency in all FRF measurements, excepting those corresponding to nodal points (zero magnitude).

The width of the resonance peak at the half power point is a measure of modal damping. Since the modal damping is constant for a specific mode, the resonance peak width should be the same in every measured FRF.

The peak values of the imaginary part of the displacement/force or acceleration/force FRFs are taken as components of the modal shape. If velocity/force FRFs are measured, then the peak values of the real part are used as modal shape components.

As an example, the estimation of the first three modes of a simple beam is presented in figure A4.10.

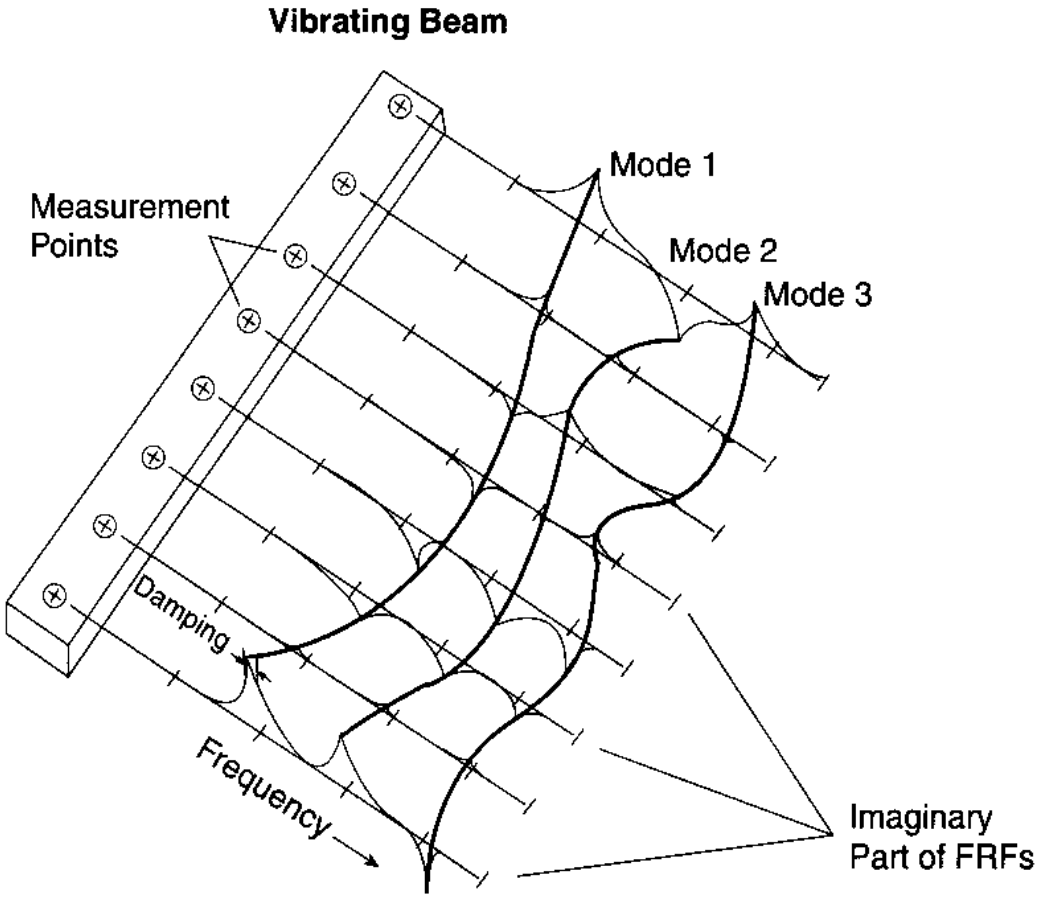

Figure A4.10. First three bending modes of a simple beam. Curve fitting FRF measurements. (Schwarz, Richardson 1999)[10]

The natural frequencies and the vibration modes can be also obtained analytically for relative simple structures (uniform beams, plates, cables, membranes etc.).

For example, in the case of a simple beam, the modal shapes for the bending mode number *n* (*n= 1, 2, 3* ...) can be calculated using the equation:

$$y_n(x) = A \sin \beta_n x + B \cos \beta_n x + C \sinh \beta_n x + D \cosh \beta_n x \quad \text{(A4.43)}$$

where:

$$\beta_n^2 = \frac{\omega_n}{\sqrt{EI/\mu}} \quad \text{(A4.43)}$$

- $y_n(x)$ = bending mode shape factor corresponding to a point situated at distance *x* from the end of the beam (modal characteristic function);

[10] Reprinted from Schwarz B. J., Richardson M. K. 1999, Experimental modal analysis, CSI Reliability Week, Orlando, FL, USA with permission

- A, B, C, D = constants depending upon the boundary conditions (fixed, pinned, or free end, etc.);
- E = Young's modulus;
- I = the second moment of area about bending axis;
- μ = linear mass density of the beam, $\mu=m/L$;
- m = mass of the beam;
- L = length of the beam;
- ω_n = resonance frequency.

The resonance frequencies can be calculated using the equation:

$$\omega_n = \alpha_n \sqrt{\frac{EI}{mL^3}} \qquad \text{(A4.44)}$$

where the value of constant α_n depends upon the mode complexity and the boundary conditions. From equation (A4.44) can be observed that a stiffness increase will result in a resonance frequency increase, while a mass increase will determine a resonance frequency decrease.

Table A4.1. The first four bending modes of a beam (after Broch 1984)

Clamped - Free (Cantilever)	α = 3.52	0.774 α = 22.4	0.500 0.868 α = 61.7	0.356 0.644 0.906 α = 121
Hinged - Hinged (Simple)	α = 9.87	0.500 α = 39.5	0.333 0.667 α = 88.9	0.25 0.50 0.75 α = 158
Clamped - - Clamped (Built-in)	α = 22.4	0.500 α = 61.7	0.359 0.641 α = 121	0.278 0.500 0.722 α = 200
Free - Free	0.224 0.776 α = 22.4	0.132 0.500 0.868 α = 61.7	0.094 0.644 0.356 0.906 α = 121	0.277 0.723 0.073 0.500 0.927 α = 200
Clamped - - Hinged	α = 15.4	0.560 α = 50.0	0.384 0.692 α = 104	0.529 0.294 0.765 α = 178
Hinged - Free	0.736 α = 15.4	0.446 0.853 α = 50.0	0.308 0.616 0.898 α = 104	0.471 0.922 0.235 0.707 α = 178

The characteristic functions $y_n(x)$ and their coefficients have been calculated and tabulated for different boundary conditions (Young, Felgar 1949). An abbreviated summary is presented in table A4.1.

(Heylen et al. 1997, Schwarz, Richardson 1999, Thomson 1998, Thorby 2008)

A5. Elements of Fourier analysis

A5.1. Fourier series

A periodic function of time $x(t) = x(t \pm T)$ can be represented as an infinite series of sinusoids:

$$x(t) = \frac{1}{2}a_0 + \sum_{n=1}^{\infty}(a_n \cos\omega_n t + \sin\omega_n t) \quad \text{(A5.1)}$$

where

$$\omega_n = \frac{2\pi n}{T} \quad \text{(A5.2)}$$

and the coefficients are given by

$$a_0 = \frac{2}{T}\int_0^T x(t)dt \quad \text{(A5.3)}$$

$$a_n = \frac{2}{T}\int_0^T x(t)\cos\omega_n t\, dt \quad \text{(A5.4)}$$

$$b_n = \frac{2}{T}\int_0^T x(t)\sin\omega_n t\, dt \quad \text{(A5.5)}$$

Equation (A5.1) can be represented in alternative forms.

$$x(t) = c_0 + \sum_{n=1}^{\infty} c_n \cos(\omega_n t + \phi_n) \quad \text{(A5.6)}$$

where

$$c_n = \sqrt{a_n^2 + b_n^2} \quad \text{(A5.7)}$$

$$\phi_n = \tan^{-1}\left(-\frac{b_n}{a_n}\right) \quad \text{(A5.8)}$$

or

$$x(t) = \sum_{-\infty}^{\infty} X_n e^{i\omega_n t} \quad \text{(A5.9)}$$

where

$$X_n = \frac{1}{T}\int_0^T x(t)e^{-i\omega_n t}dt \quad \text{(A5.10)}$$

$$X_{-n} = X_n^*\,; \quad X_n^* = complex\ conjugate\ of\ X_n \quad \text{(A5.11)}$$

$$Re(X_n) = \frac{a_n}{2} \quad \text{(A5.12)}$$

$$Im(X_n) = -\frac{b_n}{2} \quad \text{(A5.13)}$$

$$|X_n| = \frac{c_n}{2} \tag{A5.14}$$

(Ewins 2000, Thorby 2008)

A5.2. Fourier transform

A nonperiodic function *x(t)* satisfying the condition

$$\int_{-\infty}^{\infty} x(t)\,dt < \infty \tag{A5.15}$$

can be represented by the integral:

$$x(t) = \int_{-\infty}^{\infty} (A(\omega)\cos\omega t + B(\omega)\sin\omega t)dt \tag{A5.16}$$

where

$$A(\omega) = \frac{1}{\pi}\int_{-\infty}^{\infty} x(t)\cos\omega t\,dt \tag{A5.17}$$

$$B(\omega) = \frac{1}{\pi}\int_{-\infty}^{\infty} x(t)\sin\omega t\,dt \tag{A5.18}$$

The alternative complex form is more convenient:

$$x(t) = \int_{-\infty}^{\infty} X(\omega)\,e^{i\omega t}d\omega \tag{A5.19}$$

where

$$X(\omega) = \frac{1}{2\pi}\int_{-\infty}^{\infty} x(t)e^{-i\omega t}dt \tag{A5.20}$$

$$Re\big(X(\omega)\big) = \frac{A(\omega)}{2} \tag{A5.21}$$

$$Im\big(X(\omega)\big) = \frac{B(\omega)}{2} \tag{A5.22}$$

$$X(-\omega) = X^*(\omega) \tag{A5.23}$$

Equation (A5.19) is known as the Fourier integral, and equations (A5.19) and (A5.20), taken together, are a Fourier transform pair. The quantity *X(ω)* is the Fourier transform of *x(t)*, and *x(t)* is the inverse Fourier transform of *X(ω)*.

If the frequency is expressed as *f*, in Hz, instead as *ω*, in rad/sec, the Fourier transform pair becomes:

$$x(t) = \int_{-\infty}^{\infty} X(f)e^{i2\pi ft}df \tag{A5.24}$$

and

$$X(f) = \int_{-\infty}^{\infty} x(t)\, e^{-i2\pi ft}\, dt \qquad \text{(A5.25)}$$

where

$$\omega = 2\pi f \qquad \text{(A5.26)}$$

These equations are used in the derivation of many of the expressions encountered in vibration analysis. The Fourier transform is a special case of the Laplace transform.

(Ewins 2000, Thorby 2008)

A5.3. The discrete Fourier transform

Equations (A5.24) and (A5.25) can only be used when *x(t)* or *X(f)* is known analytically. In practical vibration analysis a discrete series of data points is obtained by digitising the analogue outputs of transducers at constant time intervals.

The discrete Fourier transform (DFT) is a way to implement numerically the equation (A5.24), while the inverse discrete Fourier transform (IDFT) is a similar way to solve numerically the equation (A5.25).

A function defined only at *N* discrete points ($t = t_k$, $k = 1, 2, \ldots N$) can be represented by a finite series:

$$x(t_k) \equiv (x_k) = \frac{1}{2} a_0 + \sum_{n=1}^{\frac{N}{2}\ or\ \frac{N-1}{2}} \left(a_n \cos \frac{2\pi nk}{N} + b_n \sin \frac{2\pi nk}{N} \right) \qquad \text{A5.27}$$

where

$$a_0 = \frac{2}{N} \sum_{k=1}^{N} x_k \qquad \text{A5.28}$$

$$a_n = \frac{1}{N} \sum_{k=1}^{N} x_k \cos \frac{2\pi nk}{N} \qquad \text{A5.29}$$

$$b_n = \frac{1}{N} \sum_{k=1}^{N} x_k \sin \frac{2\pi nk}{N} \qquad \text{A5.30}$$

Alternative complex form:

$$x(t_k) \equiv (x_k) = \sum_{n=0}^{N-1} X_n e^{\frac{2\pi ink}{N}} \qquad \text{A5.31}$$

where

$$X_n = \frac{1}{N}\sum_{k=1}^{N} x_k e^{\frac{-2\pi i n k}{N}},\ n = 1, 2, \ldots N \qquad \text{A5.32}$$

$$X_{N-r} = X_r^* \qquad \text{A5.33}$$

The DFT necessarily assumes that the function *x(t)* is periodic and the DFT representation is only valid for the specific values x_k (*x(t)* at $t = t_k$) used in the discretised description of *x(t)*. There are just *N* values x_k and, correspondingly, the Fourier series is described by just *N* values.

(Ewins 2000, Thorby 2008)

A5.4. The fast Fourier transform

In 1965 an algorithm, known as the fast Fourier transform (FFT), has been created. It is able to calculate the DFT and IDFT many times faster than it was possible before (Cooley, Tukey 1965). This is a "divide and conquer" algorithm that recursively breaks down a DFT into many smaller DFTs. The most well-known use of the Cooley–Tukey algorithm is to divide the DFT into two pieces of size $N/2$ at each step, and is therefore limited to power-of-two sizes, but any factorization can be used in general. Nowadays every computer program for evaluating the DFT incorporates a version of the FFT algorithm.

(Ewins 2000, Thorby 2008)

A6. Elements of statistical analysis

A6.1. Correlation coefficient

Pearson's product moment correlation coefficient, *r*, is a dimensionless index that ranges from -1.0 to 1.0 inclusive and reflects the extent of a linear relationship between two data sets (i.e. two variables x_i, y_i, where i = 0, 1, 2...N-1).

The equation for the correlation coefficient is:

$$r = \frac{\sum(x-\bar{x})(y-\bar{y})}{\sqrt{\sum(x-\bar{x})^2 \sum(y-\bar{y})^2}} \qquad \text{(A6.1)}$$

Where x and y are the two variables and $\bar{x}$, $\bar{y}$ are the corresponding arithmetic means (Spiegel 1972).

An alternative equation that uses only the raw data is:

$$r = \frac{N\sum xy - (\sum x)(\sum y)}{\sqrt{N\sum x^2 - (\sum x)^2}\sqrt{N\sum y^2 - (\sum y)^2}} \qquad \text{(A6.2)}$$

Where x and y are the two variables and N is the number of (x_i, y_i) pairs (Brase, Brase 2007).

A.6.2. Cross correlation function

Cross correlation is a standard method of estimating the degree to which two series are correlated. Consider two series x_i and y_i where i = 0, 1, 2...N-1. The cross correlation r at delay (shift) d is defined as:

$$r(d) = \frac{\sum_i (x_i-\bar{x})(y_{i-d}-\bar{y})}{\sqrt{\sum_i (x_i-\bar{x})^2 \sum_i (y_{i-d}-\bar{y})^2}} \qquad \text{(A6.3)}$$

Where $\bar{x}$ and $\bar{y}$ are the arithmetic means of the corresponding series.

If the cross correlation is computed for all delays d = 0, ±1, ±2,...±(N-1) then it results in a cross correlation series with the length equal to 2N-1. The range of delays d can be less than N, for example the aim may be to test correlation at short delays only. The denominator in the expression A6.3 serves to normalise the correlation coefficients such that -1 <= $r(d)$ <= 1, the bounds indicating maximum correlation and 0 indicating no correlation. A high negative correlation indicates a high correlation but of the inverse of one of the series (Orfanidis S.J., 1996).

Remark: if d becomes 0 in the equation A6.3 then the formula for calculating the Pearson's coefficient of correlation is obtained (equation A6.1).

References

Albrektsson T., Brånemark, P.-I., Hansson H.-A., Lindström J., 1981. Osseointegrated titanium implants: Requirements for ensuring a long-lasting, direct bone-to-implant anchorage in man. Acta Orthopaedica, 52(2):155 — 170.

Amstutz H.C., Beaulé P.E., Dorey F.J., Le Duff M.J., Campbell P.A., Gruen T.A., 2004. Metal-on-metal hybrid surface arthroplasty: two to six-year follow-up study. J. Bone Joint Surg. [Am] 86 (1): 28-39

Amstutz H.C., Beaulé P.E., Dorey F.J., Le Duff M.J., Campbell P.A., Gruen T.A., 2006. Metal-on-metal hybrid surface arthroplasty. Surgical technique. J. Bone Joint Surg. [Am] 88 Suppl 1 Pt 2:234-49

Asiminei A., Pastrav C., Jaecques S., Mulier M., Van der Perre G., 2007. Intraoperative manufactured hip prosthesis insertion - a finite element simulation. In: Jonkers I., Jaecques S., Mulier M., Van der Perre G. (Eds.) Prediction and evaluation of total hip replacement performance: can we plan success? K.U.Leuven, Leuven, Belgium, pp. 28-30.

Avitabile P., 2001. Experimental modal analysis - a simple non-mathematical presentation, Sound and Vibration, 11 pp.

Bathe K.J., 1996. Finite element procedures. Prentice-Hall, Upper Saddle River, New Jersey, USA.

Bauer T.W., Schils J., 1999. The pathology of total joint arthroplasty I. Mechanisms of implant fixation. Skeletal Radiol 28:423–432.

Bauer T.W., Schils J., 1999. The pathology of total joint arthroplasty II. Mechanisms of implant failure. Skeletal Radiol 28:483–497.

Bellemans J., 1999. Osseointegration in porous coated knee arthroplasty - The influence of component coating type in sheep. Acta Orthop. Scand. Suppl. 288, 70:1-35.

Bergmann G., Deuretzbacher G., Heller M., Graichen F., Rohlmann A., Strauss J., Duda G.N., 2001. Hip contact forces and gait patterns from routine activities. Journal of Biomechanics, 34: 859-871.

Brånemark P.-I., Hansson B.O., Adell R., Breine U., Lindström J., Hallán O., Öhman A., 1977. Osseointegrated implants in the treatment of the edentulous jaw. Stockholm: Almqvist and Wiksell. p. 132

Brånemark P.-I., 1983. Osseointegration and its experimental studies. J Prosthetic Dentistry. 50:399–410.

Brase C.H., Brase C.P., 2007. Understanding basic statistics. Houghton Mifflin Company, Boston, USA.

Breusch S.J., Lukoschek M., Kreutzer J., Brocai D., Gruen T.A., 2001. Dependency of cement mantle thickness on femoral stem design and centralizer. Journal of Arthroplasty 16 (5), 648-657

Britton A.R., Murray D.W., Bulstrode C.J., McPherson K., Denham R.A., 1996. Long-term comparison of Charnley and Stanmore design total hip replacements. J. Bone Joint Surg. [Br] 78, 802-808.

Broch J.T., 1984. Mechanical vibration and shock measurements, Bruel & Kjaer, Naerum, Denmark.

Burny F., Donkerwolcke M., Moulart F., Borgwardt A., Vryzakis P., Pichon D., Collier R., Louridas S., Van der Perre G., Denayer I., Jaecques S., Catrysse M., Puers R, 2000. STIMuLus: Smart Total Implant for the Monitoring of Loosening. Medical Physics, 27, 1406.

Claassen W., Nijs J., Jaecques S., Van der Perre G., Mulier M., 2007a. Early periprosthetic bone remodelling around cemented and uncemented custom-made femoral components and their uncemented acetabular cups. In: Jonkers I., Jaecques S., Mulier M., Van der Perre G. (Eds.) Prediction and evaluation of total hip replacement performance: can we plan success? K.U.Leuven, Leuven, Belgium, pp. 6-8

Claassen W., Nijs J., Mulier M., Jaecques S., Van der Perre G., 2007b. Follow-up of implant performance using RSA. In: Jonkers I., Jaecques S., Mulier M., Van der Perre G. (Eds.) Prediction and evaluation of total hip replacement performance: can we plan success? K.U.Leuven, Leuven, Belgium, pp. 2-5.

Clarke IC, Campbell P, Kossovsky N (1992) Debrismediated osteolysis-A cascade phenomenom involving motion, wear, particulates, macrophage induction, and bone lysis. In: St. John KR (ed). Particulate debris from medical implants: mechanisms of formation and biological consequences, ASTM STP 1144. Philadelphia, American Society for Testing and materials, 7-26.

Collier J., Donarski J., Worley J., Lay A., 1993. The use of externally applied mechanical vibrations to assess both fractures and hip prosthesis. In: R. Turner-Smith (Ed.), Micromovement in Orthopaedics, Oxford Univ. Press, pp. 151–163.

Cook R.D., Malkus D.S., Plesha M.E., 1989. Concepts and applications of finite element analysis. John Wiley & Sons, New York, USA.

Cooley J.W., Tukey J.W., 1965. An algorithm for the machine calculation of complex Fourier Coefficients. Mathematics of Computation, 19, 297–301.

Couteau B., Hobatho MC., Darmana R., Brignola JC., Arlaud JY., 1998. Finite element modelling of the vibrational behaviour of the human femur using CT-based individualized geometrical and material properties, Journal of Biomechanics, 31:383-386

Crisman, A., McCuskey M., Yoder N., Meneghini R.M., Cornwell P.J., 2007. Femoral component insertion monitoring using human cadaveric specimens. Proceedings of the 25th IMAC Conference on Structural Dynamics, Orlando, FL, USA.

Cristofolini, L., Varini E., Pelgreffi I., Cappello A., Toni A., 2006. Device to measure intra-operatively the primary stability of cementless hip stems. Medical Engineering & Physics. 28(5): pp. 475-82.

Denayer I., Jaecques S.V.N., Burny F., Puers R., Borgwardt A., Van der Perre G., 2000. Measurement of implant stability and osseointegration: non-linearities and resonance frequencies. Proc. 12th Conf. Eur. Soc. Biomech. P. J. Prendergast, T. C. Lee, A. J. Carr, eds., Dublin, 151.

Denis K., Van Ham G., Bellemans J., Labey L., Vander Sloten J., Van Audekercke R., Van der Perre G., De Schutter J., 2002. How correctly does an intramedullary rod represent the longitudinal tibial axes? Clin. Orthop. Rel. Res. 397:424-433.

Devos J., Jaecques S., Pastrav C., Van der Perre G., 2007. The influence of contact conditions on resonance frequencies of a hip stem-femur system: a finite element analysis. In: Jonkers I., Jaecques S., Mulier M., Van der Perre G. (Eds.) Prediction and evaluation of total hip replacement performance: can we plan success? K.U.Leuven, Leuven, Belgium, pp. 35-36.

Doebling, S. W., Farrar, C. R., Prime, M. B., and Shevitz, D. W., 1996. Damage identification and health monitoring of structural and mechanical systems from changes in their vibration characteristics: A literature review. Los Alamos National Laboratory report LA-13070-MS.

Eggars E. A., 1993. Future of custom hip prosthetics. Joint Implant Surgery and Research Foundation, Update News, 2:9.

El'Sheikh H.F., MacDonald B.J., Hashmi M.S.J., 2003. Finite element simulation of the hip joint during stumbling: a comparison between static and dynamic loading, Journal of Materials Processing Technology, pp. 143–144, 249–255.

Ewins D.J., 2000. Modal testing: theory, practice and application. Research Studies Press, Baldock, Hertfordshire, England.

Fahlgren A., Bostrom M.P.G., Yang X., Johansson L., Edlund U., Agholme F., Aspenberg P., 2010. Fluid pressure and flow as a cause of bone resorption. Acta Orthopaedica, 81 (4), 508-516.

Freeman M.A.R., Plante-Bordeneuve P., 1994. Early migration and late aseptic failure of proximal femoral prostheses. J. Bone Joint Surg. 76 [Br]:432-438.

Friedman R.J., Black J., Galante J.O., Jacobs J.J., Skinner H.B., 1993. Current concepts in orthopaedic biomaterials and implant fixation. J Bone Joint Surg [Am] 75-A: 1086- 1008

Georgiou A.P., Cunningham J.L., 2001. Accurate diagnosis of hip prosthesis loosening using a vibrational technique. Clin. Biomech. 16, 315-323.

Gerber C., Pennington S. D., Nyffeler R. W., 2009. Reverse total shoulder arthroplasty. J Am Acad Orthop Surg. 17:5, 284-295.

Goodman S., Aspenberg P., 1992. Effect of amplitude of micromotion on bone ingrowth into titanium chambers implanted in the rabbit tibia. Biomaterials 13:944-948.

Goodman S.B., Barrena E.G., Takagi M., Konttinen Y.T., 2008. Biocompatibility of total joint replacements: A review. J Biomed Mater Res 90A: 603-618.

Gray H., 1918. Anatomy of the human body. Lea & Febiger, Philadelphia, USA.

Gross T.P., Liu F., 2008. Metal-on-metal hip resurfacing with an uncemented femoral component: a seven year follow-up study. The Journal of Bone and Joint Surgery [Am]. 90:32-37.

Gruen TA., McNeice GM., Amstutz HC., 1979. Modes of failure of stem-type femoral components. Clinical Orthopaedics and Related Research. 141:17-27.

Gruen T.A., 1987. Radiographic criteria for the clinical performance of uncemented total joint replacements, p. 207-218. In Lemons JE (ed): Quantitative characterization and performance of porous implants for hard tissue applications. ASTM STP 953. American Society for Testing Materials, Philadelphia, USA.

Guery J., Favard L., Sirveaux F., Oudet D., Mole D., Walch G., 2006. Reverse total shoulder arthroplasty - survivorship analysis of eighty replacements followed for five to ten years . The Journal of Bone and Joint Surgery (American). 88:1742-1747.

Harris W.H., 1991. Aseptic loosening in total hip arthroplasty secondary to osteolysis induced by wear debris from titanium-alloy modular femoral heads, J Bone Joint Surg [Am] 73:470-472.

Havermans L., Daenen B., 2002. Ontwikkeling van een intelligente heupprothese: trillingsanalyse als detectiemethode voor vroegtijdig loskomen van een heupprothese, MSc Eng Thesis, K.U.Leuven

Heiner, A.D. and Brown, T.D., 2001. Structural properties of a new design of composite replicate femurs and tibias. J. Biomechanics, 34, 773-781

Heisel C., Kleinhans J.A., Menge M., Kretzer J.P., 2008. Ten different hip resurfacing systems: biomechanical analysis of design and material properties. International Orthopaedics (SICOT). 5pp, DOI 10.1007/s00264-008-0607-y

Heo S. J., Sennerby L., Odersjö M., Granström G., Tjellström A., Meredith N., 1998. Stability measurements of craniofacial implants by means of resonance frequency analysis. A clinical pilot study. The Journal of Laryngology & Otology, 112:537-542.

Heylen W., Lammens S., Sas P., 1997. Modal Analysis Theory and Testing, K.U. Leuven, Leuven, Belgium.

Horikoshi M., Macaulay W., Booth R.E., Crossett L.S., Rubash H.E., 1994. Comparison of interface membranes obtained from failed cemented and cementless hip and knee prostheses. Clin Orthop Relat Res 309:69-87.

Huang H.M., Chiu C.L., Yeh C.Y., Lee S.Y., 2003. Factors influencing the resonance frequency of dental implants. Journal of Oral and Maxillofacial Surgery. 61 (10): 1184-1188

Huiskes, R., 1993. Failed innovation in total hip replacement. Acta Orthop. Scand. 64:699-716.

Jaecques S., Pastrav C., Mulier M., Van der Perre G., 2005. Determination of THR stem insertion endpoint by vibrational analysis. In: Cabral R., Cassiano Neves M., Camilo C., (Eds.), Transactions of the EORS, Soc Portugesa de Ortopedia e Traumatologia, pp. 92.

Jaecques S.V.N., Pastrav L.C., Mulier M., Van der Perre G., 2006. Vibration analysis on partially cemented custom hip stems: a per-operative study. In: Baldini N., Savarino L., (Eds.), Transactions of the EORS, Italian Orthopaedic Research Society, Vol. 16, p. O67,

Jaecques S., Pastrav C., Zahariuc A., Van der Perre G., 2004. Analysis of the fixation quality of cementless hip prostheses using a vibrational technique. In: Sas P., De Munck M. (Eds.), ISMA 2004, International Conference on Noise and vibration engineering. K.U.Leuven, Leuven, Belgium, pp. 443-456.

Kärrholm J., 1989. Roentgen stereophotogrammetry. Review of orthopaedic applications. Acta Orthop. Scand. 60:491-503.

Kärrholm J., Borssen B., Lowenhielm G., Snorrason F., 1994. Does early micromotion of femoral stem prostheses matter? 4-7-year stereoradiographic follow-up of 84 cemented prostheses. J Bone Joint Surg [Br] 76:912-917.

Kassi J.-P., Heller M.O., Stoeckle U., Perka C., Duda G.N., 2005. Stair climbing is more critical than walking in pre-clinical assessment of primary stability in cementless THA in vitro. Journal of Biomechanics 38: 1143–1154.

Katz D., O'Toole G., Cogswell L, Sauzières P., Valenti P., 2007. A history of the reverse shoulder prosthesis. Int J Shoulder Surg, 1:4, 108-13.

Kavanagh B.F., Ilstrup D.M., Fitzgerald Jr., R.H., 1985. Revision total hip arthroplasty. J. Bone Joint Surg. [Am] 67, 517-526.

Khalil TB., Viano DC., Taber LA., 1981. Vibrational characteristics of the embalmed human femur. Journal of Sound and Vibration, 75, 417-436.

Kiratli B.J., Checovich M.M., McBeath A.A., Wilson M.A., Heiner J.P., 1996. Measurement of bone mineral density by dual-energy x-ray absorptiometry in patients with the Wisconsin hip, an uncemented femoral stem. Journal of Arthroplasty, 11:2, 184-193.

Kobayashi S., Takaoka K., Saito N., Hisa K., 1997. Factors affecting aseptic failure of fixation after primary Charnley total hip arthroplasty. Multivariate survival analysis. J Bone Joint Surg [Am] 79:1618-1627.

Kuiper J.H., Huiskes R., 1996. Friction and stem stiffness affect dynamic interface motion in total hip replacement. J. Orthop. Res. 14:36-43.

Labey L., Bellemans J., Vander Sloten J., Van Audekercke R., Van der Perre G., Fabry G., 2000. Roentgen stereophotogrammetric analysis of total knee prostheses using inherent features of the implant: accuracy and early follow-up results. 12th Conference of the European Society of Biomechanics, Dublin, August 27 - 30, 2000, Book of abstracts, p. 376.

Labey L., Gross U., Boyde A., Hahn M., Merolli A., Meunier A., Revell P., Tanner K., Thomsen P., Van der Perre G., Vogel M., 1996. Mechanical evaluation of explanted hip prostheses: technique and first results. 5th World Biomaterials Conference, Toronto, May 29 - June 2, 1996, Book of abstracts, p. II-81.

Lannocca M., Varini E., Cappello A., Cristofolini L., Bialoblocka E., 2007. Intra-operative evaluation of cementless hip implant stability: A prototype device based on vibration analysis. Med. Eng. Phys. 29(8), 886-894.

Learmonth I.D., Young C., Rorabeck C., 2007. The operation of the century: total hip replacement. The Lancet, 370 (9597), 1508-1519.

Li P.L.S., Jones N.B., Gregg P.J., 1995. Loosening of total hip arthroplasty; diagnosis by vibration analysis. J Bone Joint Surg. 77-B: 640-644.

Li P.L.S., Jones N. B., Gregg P.J., 1996. Vibration analysis in the detection of total hip prosthetic loosening. Med. Eng. Phys. 18 (7), 596-600.

Lindhal H., 2007. Epidemiology of periprosthetic femur fracture around a total hip arthroplasty. Injury, Int. J. Care Injured. 38, 651-654.

Lippmann R.K., 1932. The use of auscultatory percussion for the examination of fractures. J. Bone Jt Surg. [Am]14, 118-126.

Liu X.C., Fabry G., Labey L., Van Den Berghe L., Van Audekercke R., Molenaers G., Moens P., 1997. A new technique for the three-dimensional study of the spine in vitro and in vivo by using a motion-analysis system. Journal of Spinal Disorders 10: 329-338.

Lowet G., Buelens W., Goossens S., Van der Perre G., 1993. Measuring resonant frequencies: Practical recommendations. In: Van der Perre, G., Lowet, G., Borgwardt Christensen, A., Eds. In vivo assessment of bone quality by vibration and wave propagation techniques. Part III, Belgium, Leuven, 57-66.

Lowet G., Van Audekercke R., Van der Perre G., Geusens P., Dequeker J., Lammens J., 1993. The relation between resonant frequencies and torsional stiffness of long bones in vitro. Validation of a simple beam model. J. Biomech. 26, 689-696.

Lombardi A.V., Mallory T.H., Vaughn B.K., Drouillard P., 1989. Aseptic loosening in total hip arthroplasty secondary to osteolysis induced by wear debris from titanium-alloy modular femoral heads, J Bone Joint Surg [Am] 71:1337-1342.

Lowet G., Van der Perre G., 1996. Ultrasound velocity measurement in long bones: measurement method and simulation of ultrasound wave propagation. J. Biomech. 29, 1255-1262.

Lucht U., 2000. The Danish Hip Arthroplasty Register. Acta Orthop. Scand. 71, 433-439.

Mader S.S., 2005. Understanding human anatomy & physiology. McGraw Hill, New York, USA.

Malchau, H., Kärrholm, J., Wang, Y.X., and Herberts, P. (1995): Accuracy of migration analysis in hip arthroplasty. Acta Orthop. Scand. 66:418-424.

Maloney W.J., Jasty M., Burke D.W., O'Connor D.O., Zalenski E.B., Bragdon C., 1989. Biomechanical and histological investigation of cemented total hip arthroplasties. A study of autopsy-retrieved femurs after in vivo cycling. Clin Orthop. 249: 129-140.

Mandell J.A., Carter D.R., Goodman S.B., Schurman D.J., Beaupre G.S., 2004. A conical-collared intramedullary stem can improve stress transfer and limit micromotion. Clin Biomech (Bristol, Avon) 19:695-703.

Matsen F. A. III, Boileau P., Walch G., Gerber C., Bicknell R.T., 2007. The Reverse Total Shoulder Arthroplasty. J Bone Joint Surg Am 89: 660-667.

McFarland E.G., Sanguanjit P., Tasaki A., Keyurapan E., Fishman E.K., Fayad L.M., 2006. The reverse shoulder prosthesis: a review of imaging features and complications. Skeletal Radiol. 35: 488-496

Meek R.M., Garbuz D.S., Masri B.A., Greidanus N.V., Duncan C.P., 2004. Intraoperative fracture of the femur in revision total hip arthroplasty with a diaphyseal fitting stem. J. Bone Joint Surg. [Am] 86-A, 480-485.

Meredith N., Book K., Friberg B., Jemt T., Sennerby L., 1997. Resonance frequency measurements of implant stability in vivo. A cross-sectional and longitudinal study of resonance frequency measurements on implants in the edentulous and partially dentate maxilla. Clin. Oral Implants Res. 8, 226-233.

Middernacht B., De Wilde L., Mole D., Favard L., Debeer P., 2008. Glenosphere disengagement. Clinical Orthopaedics and Related Research 4, 892-898.

Mjöberg B., 1997. The theory of early loosening of hip prostheses. Orthopedics 20, 1169-1175.

Monti L., Cristofolini L., Viceconti M., 1999. Methods for quantitative analysis of the primary stability in uncemented hip prostheses. Artificial Organs 23(9):851-859.

Mulier, J.C. et al, 1989, Intraoperative production of femoral prostheses, Joint replacement – State of the Art, (eds. R. Coombs, A. Gristina, D. Hungerford), Orthotext, 163-169.

Mulier J.C., Mulier M., Brady L.P., Steenhoudt H., Cauwe Y., Goossens M., Elloy M., 1989. A new system to produce intraoperatively custom femoral prosthesis from measurements taken during the surgical procedure. Clin. Orthop. Relat. Res., 97-112.

Mulier M., Pastrav C., Van der Perre G., 2008. Per-operative vibration analysis: a valuable tool for defining correct stem insertion: preliminary report. Ortopedia Traumatologia Rehabilitacja. 10(6): 576-582.

Mulier M., Raaijmaakers M., Van den Bekerom M., 2010. Technical pearls in total hip arthroplasty. Minerva Ortop. Traumatol. 61: 27-41.

Nakatsuchi Y., Tsuchikane A., Nomura A., 1996. Assessment of fracture healing in the tibia using the impulse response method. J. Orthop. Trauma 10, 50-62.

Nikiforidis G., Bezerianos A., Dimarogonas A., Sutherland C., 1990. Monitoring of fracture healing by lateral and axial vibration analysis. J. Biomech. 23, 323-330.

Njeh C.F., Fuerst T., Hans D., Blake G.M., Genant H.K., 1999. Radiation exposure in bone mineral density assessment. Applied Radiation and Isotopes 50:1, 215-236

Nokes L.D.M., 1999. The use of low-frequency vibration measurement in orthopaedics. Proc. Instn. Mech. Engrs. 213H: 271-290.

Orfanidis S.J., 1996. Optimum Signal Processing. An Introduction, Prentice-Hall, Englewood Cliffs, NJ.

Oyen W.J.G., Lemmens J.A.M., Claessens R.A.M.J., Van Horn J.R., Slooff T.J.J.H., Corstens F.H.M., 1996. Nuclear arthrography: combined scintigraphic and radiographic

procedure for diagnosis of total hip prosthesis loosening. The Journal of Nuclear Medicine. 37(1):62-70.

Pastrav C., Jaecques S., Deloge G,. Mulier M., Van der Perre G., 2005. A system for intra operative manufacturing and stability testing of hip prostheses. In: Dumitru I. (Ed.) XIIIth International conference on New technologies and products in machines manufacturing and technologies (TEHNOMUS XIII). University of Suceava, Suceava, Romania, pp. 505-510.

Pastrav L.C., Asiminei A.G., Devos J., Van der Perre G., Jaecques S.V.N., 2008. A finite element study on the relationship between the vibrational behaviour of the hip stem-femur system and the contact area change at the implant-bone interface. In: Sas P., Bergen B. (Eds.), Proceedings of ISMA2008 International Conference on Noise and Vibration Engineering, Leuven, Belgium, [CD-ROM]: 2085-2095.

Pastrav L.C., Devos J., Van der Perre G., Jaecques S.V.N., 2009a. A finite element analysis of the vibrational behaviour of the intra-operatively manufactured prosthesis – femur system, Journal of Medical Engineering & Physics, 31(4):489-94.

Pastrav L.C., Jaecques S.V.N., Asiminei A.G.. Devos J., Mulier M., Van der Perre G., 2007. Per-operative stability measures for total hip replacement. In: Jonkers I., Jaecques S., Mulier M., Van der Perre G. (Eds.) Prediction and evaluation of total hip replacement performance: can we plan success? K.U.Leuven, Leuven, Belgium, pp. 48-51.

Pastrav L.C., Jaecques S.V.N., Jonkers I., Van der Perre G., Mulier M., 2009b. In vivo evaluation of a vibration analysis technique for the per-operative monitoring of the fixation of hip prostheses, Journal of Orthopaedic Surgery and Research, 4:10.

Pastrav L.C., Jaecques S.V.N., Mulier M., Van der Perre G., 2008. Detection of the insertion end point of cementless hip prostheses using the comparison between successive frequency response functions. Journal of Applied Biomaterials & Biomechanics, 6(1), 23-29.

Pastrav L., Jaecques S., Mulier M., Van der Perre G., 2006. Determination of total hip replacement stem insertion endpoint and stability assessment by vibration analysis: first

experiences with per-operative measurements. In: Sas P., De Munck M. (Eds.), Proceedings of ISMA2006 International Conference on Noise and Vibration Engineering, Leuven, Belgium, [CD-ROM]: 897-908.

Pastrav L., Leuridan S., Denis K., Delport H., Debeer P., De Wilde L., Van der Perre G., Desmet W., Vander Sloten J. 2010. Vibrational techniques to assess the stability of spherical press-fitted implants : preliminary results. Paper accepted for oral presentation. Proceedings of ISMA2010 International Conference on Noise and Vibration Engineering, Leuven, Belgium,

Pattijn V., Van Lierde C., Van der Perre G., Naert I., Vander Sloten J., 2006. The resonance frequencies and mode shapes of dental implants: Rigid body behaviour versus bending behaviour. A numerical approach. Journal of Biomechanics. 39 (5): 939-947.

Pennock, A.T., Schmidt A.H., Bourgeault C.A., 2002. Morse-type tapers. Journal of Arthroplasty 17:6, 773-8 .

Pilliar R.M., Lee J.M., Maniatopoulos C., 1986. Observation on the effect of movement on bone ingrowth into porous-surfaced implants. Clin. Orthop. Rel. Res., 208:108-113

Prendergast P.J., 1997. Finite element models in tissue mechanics and orthopaedic implant design, Clinical Biomechanics, 12: 343-366.

Puers R., Catrysse M., Vandevoorde G., Collier R.J., Louridas E., Burny F., Donkerwolcke M., Moulart F., 2000. A telemetry system for the detection of hip prosthesis loosening by vibration analysis. Sensors and Actuators 85: 42–47.

Qi G., Mouchon W.P., Tan T.E., 2003. How much can a vibrational diagnostic tool reveal in total hip arthroplasty loosening? Clin. Biomech. (Bristol, Avon), 18, 444-458.

Ramamurti B.S., Orr T.E., Bragdon C.R., Lowenstein J.D., Jasty M., Harris W.H., 1997. Factors influencing stability at the interface between a porous surface and cancellous bone: a finite element analysis of a canine in vivo micromotion experiment, Journal of Biomedical Materials Research, 36(2):274-280.

Ramaniraka NA, Rakotomanana LR, Leyvraz PF, 2000. The fixation of the cemented femoral component. Effects of stem stiffness, cement thickness and roughness of the cement-bone surface. J Bone Joint Surg [Br] 82:297-303.

Reggiani B., Cristofolini L., Varini E., Viceconti M., 2007. Predicting the subject-specific primary stability of cementless implants during pre-operative planning: Preliminary validation of subject-specific finite-element models. J Biomech. 40(11):2552-8.

Roberts S.G., Hutchinson T.M., Arnaud S.B., Kiratli B.J., Martin R.B., Steele C.R., 1996. Noninvasive determination of bone mechanical properties using vibration response: A refined model and validation in vivo. Journal of Biomechanics. 29(1): 91-98.

Rowlands A., Duck F.A., Cunningham J.L., 2008. Bone vibration measurement using ultrasound: Application to detection of hip prosthesis loosening, Medical Engineering & Physics, 30(3), 278-284.

Rosenstein A.D., McCoy G.F., Bulstrode C.J., McLardy-Smith P.D., Cunningham J.L., Turner Smith A.R., 1989. The differentiation of loose and secure femoral implants in total hip replacement using a vibrational technique: an anatomical and pilot clinical study. Proc. Inst. Mech. Eng. [H] 203, 77-81.

Salvi V., 1992. Identifit: a silicone mould used to intraoperatively construct a cementless femoral stem. Chir Organi Mov. 77(4):443-445.

Saxena R., Kellers T.S., and Sullivan J.M., 1999. A three-dimensional finite element scheme to investigate the apparent mechanical properties of trabecular bone, Computer Methods in Biomechanics and Biomedical Engineering, 2: 4, 285 — 294

Schneider E., Kinast C., Eulenberger J., Wyder D., Eskilsson G., Perren S.M., 1989. A comparative study of the initial stability of cementless hip prostheses. Clin. Orthop., 248:200-209.

Schwarz B. J., Richardson M. K. 1999, Experimental modal analysis, CSI Reliability Week, Orlando, FL, USA.

Shao F., Xu W., Crocombe A., Ewins D. 2007, Natural frequency analysis of osseointegration for trans-femoral implant, Annals of Biomedical Engineering 35 (5), 817–824

Søballe K., Hansen E.S., B-Rassmussen H., Jorgensen P.H., Bunger C., 1992. Tissue ingrowth into titanium and hydroxyapatite-coated implants during stable and unstable mechanical conditions. J. Orthop. Res. 10, 285-299.

Sjöström M., Lundgren S., Nilson H., Sennerby L., 2005. Monitoring of implant stability in grafted bone using resonance frequency analysis A clinical study from implant placement to 6 months of loading. Int. J. Oral Maxillofac. Surg. 34: 45–51.

Spiegel M.R., 1972. Theory and Problems of Statistics. McGraw-Hill Publishing Co. Ltd., New York, USA.

Stadelmann V.A., Terrier A., Pioletti D.P., 2008. Microstimulation at the bone-implant interface upregulates osteoclast activation pathways. Bone 42:358—364.

Temmerman O.P., Raijmakers P.G., Deville W.L., Berkhof J., Hooft L., Heyligers I.C., 2007. The use of plain radiography, subtraction arthrography, nuclear arthrography, and bone scintigraphy in the diagnosis of a loose acetabular component of a total hip prosthesis: a systematic review. J. Arthroplasty. 22(6):818-27.

Thomson W.T., 1998. Theory of vibrations with applications. Stanley Thornes (Publishers) Ltd, Cheltenham, United Kingdom.

Thorby D., 2008. Structural dynamics and vibration in practice. Butterworth Heinemann, Oxford, United Kingdom.

Treacy R.B.C., McBryde C.W., Pynsent P.B., 2005. Birmingham hip resurfacing arthroplasty – a minimum follow-up of five years. J Bone Joint Surg [Br]. 87-B:167-70.

Valstar E.R., de Jong F.W., Vrooman H.A., Rozing P.M., Reiber J.H.C., 2001: Model-based roentgen stereophotogrammetry of orthopaedic implants. J. Biomech. 34:715-722.

Van der Perre G., 1984. Dynamic analysis of human bones. In: Functional Behaviour of Orthopaedic Biomaterials. Vol I: P. Ducheyne and G.W. Hastings, Eds., CRC Press, Boca Raton, 99-159.

Van der Perre G., Cornelissen P., 1983. On the mechanical resonance of a human tibia in vitro. J. Biomech. 16, 549.

Van der Perre G., Lowet G., 1996. In vivo assessment of bone mechanical properties by vibration and ultrasonic wave propagation analysis. Bone 18, 29S-35S.

Van der Perre G., Van Audekercke R., Martens M., Mulier J.C., 1983, Identification of in vivo vibration modes of human tibia by modal analysis, J. Biomech. 13, 134.

Vander Sloten J., Labey L., Van Audekercke R., Van der Perre G., 1994. Effectiveness of different fixation techniques for the tibial component of a total knee prosthesis (preliminary study)., in "Failure of joint replacement. A biological, mechanical or surgical problem?", ed. S. Downes and M. Dabestani, Institute of orthopaedics, pp 17-25.

Varini E. Lannocca M. Bialoblocka E. Cappello A. Cristofolini L., 2006. Primary stability assessment in hip arthroplasty — a device based on the vibrational technique, J. Biomech. 39 (S1):127.

Varini E., 2007. Primary stability in cementless total hip replacement: measurement techniques and aided-surgery (PhD thesis), Università degli Studi di Bologna, Bologna, Italy.

Viceconti M., Muccini R., Bernakiewicz M., Baleani M., Cristofolini L., 2000. Large-sliding contact elements accurately predict levels of bone-implant micromotion relevant to osseointegration. J Biomech. 33: 1611-1618.

Viceconti M., Monti L., Muccini R., Bernakiewics M., Toni A., 2001. Even a thin layer of soft tissue may compromise the primary stability of cementless hip stems, Clinical Biomechanics. 16: 765-775.

Vrooman H.A., Valstar E.R., Brand G.J., Admiraal D.R., Rozing P.M., Reiber J.H.C., 1998. Fast and accurate automated measurements in digitized stereophotogrammetric radiographs. J. Biomech. 31: 491-498.

Walker P., Mai S.F., Cobb A.G., Bentley G., Hua, J., 1995. Prediction of clinical outcome of THR from migration measurements on standard radiographs. J. Bone Joint Surg. 77-[Br]:705-714.

Wang F., Mechefske C., 2007. Modal analysis of a multilayered gradient coil insert in a 4-T MRI scanner. Concepts in Magnetic resonance, 31B (4), 237-254.

Williams D.F., 1999. Williams Dictionary of Biomaterials. Liverpool University Press, Liverpool, United Kingdom.

Wirtz DC., Schiffers N., Pandorf T., Radermacher K., Weichert D., Forst R., 2000. Critical evaluation of known bone material properties to realize anisotropic FE-simulation of the proximal femur, J. Biomech. 33:1325-1330

Worthington P., 1997. History, development, and current status of osseointegration as revealed by experience in craniomaxillofacial surgery. In: Brånemark P-I, Rydevik BL, Skalak R, editors. Osseointegration in skeletal reconstruction and joint replacement. Carol Stream, IL: Quintessence Publishing Co. p. 25–44.

Young D., Felgar Jr. R. P., 1949. Tables of characteristic function representing normal modes of vibration of a beam. The University of Texas Publication, 4913,

Zhang Y., Putnam A.W., Heiner A.D., Callaghan J.J., Brown T.D., 2002. Reliability of detecting prosthesis/cement interface radiolucencies in total hip arthroplasty. J. Orthop. Res. 20:683–687.

Curriculum Vitae

Personal information

Name **PASTRAV, Leonard Cezar**
Nationality: **Romanian**
Date of birth: **August 18th, 1957**

Work experience (in Belgium)

February, 2008 – present
Group T - Leuven engineering university college – department Energie
Visiting professor

January, 2004 – December 2008
Katholieke Universiteit Leuven, Belgium – Division of Biomechanics and Engineering Design
Researcher, PhD student (since April 2004)
Vibration analysis on orthopaedic implants - experiments in vitro and in vivo, finite element models, tutoring master students (K.U.Leuven project OT/03/31)

April, 2003 – Dec, 2003
Katholieke Universiteit Leuven, Belgium – Division of Biomechanics and Engineering Design
ICT manager (project **ICB-Dent**)
Designing and maintaining a website dedicated to the **ICB-Dent** international project. The website included an online course for dental technicians.

April, 2002 – March, 2003
Katholieke Universiteit Leuven, Belgium – EUROPACE
ICT manager (project **cEVU**)
Designing and maintaining a website dedicated to the **cEVU** international project. (A **c**ollaborative **E**uropean **V**irtual **U**niversity).

Education and training

April, 2004 – October, 2010
Katholieke Universiteit Leuven, Belgium
Arenberg Doctoral School
PhD student
Title of the doctorate:
Monitoring of the fixation of orthopaedic implants by vibration analysis

September, 1999 – June, 2001
University "A.I.Cuza" Iasi, Romania
Faculty of Computer Science
postgraduate course (2 years) – computers, information technology (IT), programming, teaching

September, 2000 – June, 2001
University “Stefan cel Mare” Suceava, Romania
The department for didactic training
postgraduate course (1 years) – psychology, pedagogy, ethics, teaching methods etc.

September, 1977 – June, 1982
Technical University “Gheorghe Asachi” Iasi, Romania
Faculty of Mechanics
Engineers (5 years) – engineering design, mechanical technology, tools, machines etc.

Personal skills and competences

Mother tongue: **Romanian**
Other languages: **English**, **French**

Patented inventions
Patent RO 100560 from November 28th, 1989, Installation for heating shrinkable plastic films that cover freights on pallets.

Publications

Papers in international journals

Pastrav L.C., Jaecques S.V.N., Jonkers I., Van der Perre G., Mulier M. In vivo evaluation of a vibration analysis technique for the per-operative monitoring of the fixation of hip prostheses, Journal of Orthopaedic Surgery and Research, 2009, 4:10.

Pastrav L.C., Devos J., Van der Perre G., Jaecques S.V.N. A finite element analysis of the vibrational behaviour of the intra-operatively manufactured prosthesis – femur system, Journal of Medical Engineering & Physics, 2009, 31(4):489-94.

Mulier M., Pastrav C., Van der Perre G. Per-operative vibration analysis: a valuable tool for defining correct stem insertion: preliminary report. Ortopedia Traumatologia Rehabilitacja, 2008, 10(6), 576-582.

Pastrav L.C., Jaecques S.V.N., Mulier M., Van der Perre G. Detection of the insertion end point of cementless hip prostheses using the comparison between successive frequency response functions. Journal of Applied Biomaterials & Biomechanics, 2008, 6(1), 23-29.

Papers at international conferences and symposia, published in full in proceedings

Pastrav L., Leuridan S., Denis K., Delport H., Debeer P., De Wilde L., Van der Perre G., Desmet W., Vander Sloten J. 2010. Vibrational techniques to assess the stability of spherical press-fitted implants : preliminary results. Paper accepted for oral presentation. Proceedings of ISMA2010 International Conference on Noise and Vibration Engineering, Leuven, Belgium.

Pastrav L.C., Asiminei A.G., Devos J., Van der Perre G., Jaecques S.V.N., A finite element study on the relationship between the vibrational behaviour of the hip stem-femur system and the contact area change at the implant-bone interface. Proceedings of the ISMA2008 conference, 15-17 September 2008, Leuven, Belgium.

Asiminei A., Pastrav L.C., Jaecques S.V.N., Van der Perre G., 3D dynamic finite element simulation of a cementless custom made prosthesis insertion into the femoral cavity. In: Proceedings of the 2007 Summer Workshop of the European Society of Biomechanics "Finite Element Modelling in Biomechanics and Mechanobiology", 26-28 August 2007, Trinity College, Dublin, Ireland. ISBN 0-9548583-1-X. Edited by A.B. Lennon, P.G. Prendergast, 72-73.

Devos J., Jaecques S.V.N., Pastrav L.C., Van der Perre G., Determining amount of contact and initial stability bay using vibration analysis. In: Proceedings of the 2007 Summer Workshop of the European Society of Biomechanics "Finite Element Modelling in Biomechanics and Mechanobiology", 26-28 August 2007, Trinity College, Dublin, Ireland. ISBN 0-9548583-1-X. Edited by A.B. Lennon, P.G. Prendergast, 78-79.

Asiminei A.G., Pastrav L.C, Jaecques S.V.N, Mulier M, Van der Perre G, Intraoperative manufactured hip prosthesis insertion – a finite element simulation. In: Proceedings of International Symposium "Prediction and evaluation of total hip replacement performance: can we plan success?", June 22nd – 23th, 2007, Leuven, Belgium. ISBN 978-90-5682-850-9. Edited by: I. Jonkers, S. Jaecques, M. Mulier and G. Van der Perre, 28-30.

Devos J, Jaecques S.V.N, Pastrav L.C, Van der Perre G, The influence of contact conditions on resonance frequencies of a hip stem_femur system: a finite element analysis. In: Proceedings of International Symposium "Prediction and evaluation of total hip replacement performance: can we plan success?", June 22nd – 23th, 2007, Leuven, Belgium. ISBN 978-90-5682-850-9. Edited by: I. Jonkers, S. Jaecques, M. Mulier and G. Van der Perre, 35-36.

Pastrav L.C, Jaecques S. V. N, Asiminei A.G, Devos J, Mulier M, Van der Perre G, Per-operative stability measures for total hip replacement. In: Proceedings of International Symposium "Prediction and evaluation of total hip replacement performance: can we plan success?", June 22nd – 23th, 2007, Leuven, Belgium. ISBN 978-90-5682-850-9. Edited by: I. Jonkers, S. Jaecques, M. Mulier and G. Van der Perre, 48-51.

Pastrav L.C, Jaecques S.V.N, Mulier M, Van der Perre G, The assessment of the stability of custom made hip stems in per-operative conditions using frequency response function analysis. In: Proceedings of International Symposium "Prediction and evaluation of total hip replacement performance: can we plan success?", June 22nd – 23th, 2007, Leuven, Belgium. ISBN 978-90-5682-850-9. Edited by: I. Jonkers, S. Jaecques, M. Mulier and G. Van der Perre, 52-53.

Pastrav L.C, Jaecques S.V.N, Mulier M, Van der Perre G, In vitro assessment of the stability of hip stems using frequency response function analysis. In: Proceedings of International Symposium "Prediction and evaluation of total hip replacement performance: can we plan success?", June 22nd – 23th, 2007, Leuven, Belgium. ISBN 978-90-5682-850-9. Edited by: I. Jonkers, S. Jaecques, M. Mulier and G. Van der Perre, 54-55.

Pastrav L., Jaecques S., Mulier M., Van der Perre G., Vibration analysis to asses the stability of custom made hip stems in per-operative conditions. Proceedings of IEEE/EMBS Benelux Symposium [CD-ROM], Brussels, Belgium, Dec 7-8, 2006: pp. 255-258.

Labey L., Jaecques S., Pastrav L., Gelaude F., Mulier M., Van der Perre G., Geometrical considerations relevant to the initial stability of hip prostheses. Proceedings of VAREHD13, 13th International Conference on EHD Lubrication and Traction, Suceava, Romania, October 6-7, 2006, 10 pp. paper ID VAREHD-13-29, ISBN-13 978-973-666-215-7.

Pastrav L., Jaecques S., Mulier M., Van der Perre G., The detection of insertion endpoint and stability assessment of cementless hip stems by vibration analysis: a per-operative pilot study. ", Proceedings of VAREHD13, 13th International Conference on EHD Lubrication and Traction, Suceava, Romania, October 6-7, 2006, 8 pp., paper ID VAREHD-13-27, ISBN-13 978-973-666-215-7.

Pastrav L., Jaecques S., Mulier M., Van der Perre G., A method based on vibration analysis to assess the stability of partially cemented hip stems: a clinical study. Proceedings of VAREHD13, 13th International Conference on EHD Lubrication and Traction, Suceava, Romania, October 6-7, 2006, 6 pp. paper ID VAREHD-13-28, ISBN-13 978-973-666-215-7.

Pastrav L., Jaecques S., Mulier M., Van der Perre G., Determination of total hip replacement stem insertion endpoint and stability assessment by vibration analysis: first experiences with per-operative measurements Proceedings of ISMA2006 International Conference on Noise and Vibration Engineering, September 18-20, 2006 [CD-ROM]. Eds. Sas P., De Munck M.: pp. 897-908.

Pastrav L., Jaecques S., Deloge G., Mulier M., Van der Perre G., A system for intra-operative manufacturing and stability testing of hip prostheses. Proceedings of TEHNOMUS XIII International Conference on New Technologies and Products in Machines Manufacturing and Technologies, Suceava, Romania, May 6-7, 2005: pp. 505-510.

Jaecques S., Pastrav L., Vegehan E., Van der Perre G., Analysis of the fixation quality of cementless hip prostheses using a vibrational technique. Proceedings of ISMA2004 International Conference on Noise and Vibration Engineering, Leuven, Belgium, Sep 20-22, 2004: pp. 443-456.

Papers at international conferences and symposia, published in abstract in proceedings

Leuridan S., Pastrav L.C., Mulier M., Delport H., Debeer P., Denis K., De Wilde L., Van der Perre G., Desmet W., Vander Sloten J. Vibrational techniques to assess the initial stability of spherical press-fitted implants: in vitro study. Proceedings of the EORS2010 conference, June 30-July 2, 2010, Davos, Switzerland.

Pastrav, L., Jaecques, S., Jonkers, I., Van der Perre, G., Mulier, M. (2009). Per-operative assessment of the primary stability of hip prostheses by vibration analysis, Journal of Bone and Joint Surgery. British Volume. Annual Meeting of the European Orthopaedic Research Society. Madrid, 24-26 April 2008 (475). Published for the British Editorial Society of Bone & Joint Surgery by Churchill Livingstone.

Pastrav L., Jaecques S., Mulier M., Van der Perre G., An intra-operative vibrational method for hip stem insertion endpoint detection and stability assessment - a pilot study. Proceedings of the 5th World Congress of Biomechanics, Münich, Jul 29 - Aug 4, 2006, Journal of Biomechanics 2006; Vol. 39 Suppl. 1, page S122.

Jaecques S.V.N, Pastrav L.C, Mulier M, Van der Perre G, Monitoring of cement curing by vibration analysis during total hip replacement: a per-operative pilot study, Proceedings of the 20th European Conference on Biomaterials (ESB 2006), September 27 - October 1, Nantes, France, CD-ROM, published by CYIM, Chantepie, France, T198, paper 480.

Jaecques S.V.N., Pastrav L.C., Mulier M., Van der Perre G., Vibration analysis on partially cemented custom hip stems: a per-operative study, 16th Annual Meeting of the European Orthopaedic Research Society (EORS 2006), Bologna, Italy, 7-9/06/2006, in: N. Baldini, L. Savarino, Eds., Transactions of the EORS, Vol. 16, 2006, p. O67, published by the Italian Orthopaedic Research Society.

Jaecques S., Pastrav L., Mulier M., Van der Perre G., Determination of THR stem insertion endpoint by vibrational analysis. Transactions of the EORS, 15th Annual Meeting of the European Orthopaedic Research Society, Lisbon, Portugal, Jun 2-4, 2005; vol. 15.

Jaecques S., Pastrav L., Van der Perre G., Analysis of the fixation quality of total hip replacements using a vibrational technique. Proceedings of ESDA 2004 [CD-ROM], Manchester, United Kingdom, Jul 19-22, 2004.

Papers at national conferences and symposia, published in abstract in proceedings

Pastrav L.C., Devos J., Van der Perre G., Jaecques S.V.N., Finite element analysis of the influence of the contact conditions on the resonance frequencies of a hip stem-femur system, Proceedings of Belgian Day on Biomedical Engineering, Brussels, Belgium, November 30, 2007.

Asiminei A, Pastrav L.C., Van der Perre G, Jaecques S.V.N., Custom made hip stem insertion – a dynamic finite element simulation, Proceedings of Belgian Day on Biomedical Engineering, Brussels, Belgium, November 30, 2007.

Pastrav L., Jaecques S., Mulier M., Van der Perre G., The vibrational behaviour of cementless hip implants during the insertion in the femur. Proceedings of the Fifth Belgian Day on Biomedical Engineering, Brussels, Belgium, Oct 28, 2005: p. 40.